Air entrainment by plunging water jets

PROEFSCHRIFT *ter verkrijging van de graad van doctor in de technische wetenschappen aan de Technische Hogeschool Delft, op gezag van de rector magnificus ir. H. B. Boerema, hoogleraar in de afdeling der elektrotechniek, voor een commissie aangewezen door het college van dekanen te verdedigen op woensdag 15 mei 1974 te 16.00 uur door*

EDUARD VAN DE SANDE

natuurkundig ingenieur, geboren te 's-Gravenhage

1974 / Delftse Universitaire Pers

SUMMARY

Gas entrainment caused by the impact of liquid jets upon liquid pool surfaces is a subject which has received too little attention. This well-known phenomenon,which occurs in nature and in numerous industrial operations, has only recently received interest from scientific workers. The influence on product quality and applications in waste water treatment have been the main stimuli for their investigations. This thesis is restricted to the study of water jets travelling through air. The results are generally applicable to low viscosity jet systems.

After a general introduction the observed entrainment mechanisms for turbulent waterjets are described. With increasing jet velocity the entrainment, which is at first erratic, becomes more continuous. This fact explains why a distinction must be made between low velocity ($v < 5$ m/s) and high velocity entrainment ($v > \sqrt{10\sigma/\rho_A D}$). At low velocities entrainment is determined by the presence of surface deformations upon the jet and the recovery processes of the target liquid. With high velocities air is mixed with the jet and together with an accompanying air boundary layer is brought under the receiving pool surface. From the study of these mechanisms it was concluded that jet surface deformation caused by destabilising factors and cavity formation in the pool liquid needed thorough investigation.

Although many publications have appeared describing jet disintegration, the influence of nozzle design, turbulence and air friction was unknown. Nozzle design and its effect upon the onset of turbulence,completely controls the surface distortions of the jet. Criteria have been established which define the issuing flow conditions.

Air friction forces cause a spreading of the waterjet and a correlation is presented which relates the increase of jet diameter to the variables used.

One chapter is entirely devoted to the cavity formation following the impact of drops upon liquid surfaces. A theoretical model is proposed which describes the cavity growth for single drop impact. Experimental verification fits the prediction. The impact of subsequent drops is also qualitatively examined.

The results of the measurements, combined with relevant data of other authors are compared with the fundamental analyses and a number of formulae are presented that permit calculation of the entrainment rate.

Mass transfer aspects, and in particular the transport of oxygen, are also treated. Mixing of the pool liquid as a result of the impact has been investigated and the size of the

bubbles in the bubble swarm determined. With these two studies in mind equations have been derived which relate the oxygen transfer rates to the jet parameters.
The penetration depth of the induced bubbles has also received attention. The remarkable result has been established that the simple measurement of this depth is sufficient to predict the amount of entrained air as well as the oxygen transfer rate.
The main conclusion of the work is that under certain conditions jet aeration is very efficient and its use for waste water treatment is attractive.

LIST OF SYMBOLS

A	Interfacial area	m^2
c	Concentration	kg/m^3
c_2	Concentration of oxygen in the pool liquid outside the bubble cone	kg/m^3
c_o	Concentration at t = 0	kg/m^3
c^*	Solubility	kg/m^3
D, d	Diameter	m
D_f	Diffusion coefficient of solute	m^2/s
D^*	Envelope diameter of high velocity jet	m
E	Kinetic energy	Nm
g	Gravitational acceleration	m/s^2
h	Height above water surface	m
H	Penetration depth of bubbles	m
K	Wavenumber of disturbance (= $2\pi/\lambda$)	1/m
K_b	Total buoyancy force of bubbles	N
K_j	Impact force of jet	N
K_l	Mass transfer coefficient	m/s
L	Length	m
L_B	Break-up length of jet	m
L_e	Entry length	m
l_b	Elongated bubble length in capillary	m
l	Nozzle length	m
m	Mass of droplet	kg
n	Total number of bubbles present in the pool	--
p	Pressure	N/m^2
R	Radius	m
r	Radial coordinate	m
S_b	Specific contact area	m^2/m^3
t	Time coordinate	s

t_b	Residence time of water in the circulation pipes etc.	s
t_c	Circulation time	s
U	Energy	Nm
u	Local time-mean axial velocity	m/s
u^*	Shear stress velocity	m/s
U_v	Output voltage of oxygen electrode	V
v	Velocity	m/s
V	Volume	m^3
V_1	Volume of bubble swarm or bubble cone	m^3
V_2	Volume of pool liquid excluding the bubble swarm	m^3
V_t	Total volume of pool liquid	m^3
V_b	Volume of water in circulation pipes etc.	m^3
x	Coordinate	m
y	Coordinate	m
z	Coordinate	m
α	Angle of impact (angle between jet and liquid surface)	rad
β	Coefficient in Sakiadis' velocity distribution	--
β^*	Coefficient in Rotte's velocity distribution	--
γ	Air boundary layer thickness	m
δ	Displacement of jet surface relative to the mean position	m
δ_o	Initial jet disturbance level	m
r	Dynamic viscosity	Ns/m^2
θ	Colatitude	rad
λ	Wavelength of jet disturbance	m
μ	Growthfactor of jet disturbance	1/s
ν	Kinematic viscosity	m^2/s
ρ	Density	kg/m^3

σ	Surface tension	N/m
τ	Interim time between subsequent drop impacts	s
τ_b	Signal time from detection of elongated bubble length	s
τ_{el}	Response time of oxygen electrode	s
τ_j	Shear stress at jet surface	N/m^2
τ_{wall}	Wall shear stress	N/m^2
ϕ	Flow rate	m^3/s
$\phi_{m/surf}$	Mass transfer rate by diffusion through pool surface	kg/s
Ψ	Velocity potential	m^2/s

Dimensionless groups

Re	Reynoldsnumber ($\rho vD/\eta$)
Re_L, Re_{length}	Reynoldsnumber ($\rho vL/\eta$)
We	Weber number ($\rho v^2 D/\sigma$)
Sh	Sherwood number ($K_l D/D_f$)

Indices

A	Air
b	Bubble
c	Cavity
j	Jet
l	Liquid
n	Nozzle
opt.	Optimum
S.M.	Sauter Mean
r	Radial direction
w	Water
x	x-direction
z	z-direction

CONTENTS

Chapter I

INTRODUCTION

Every schoolboy knows that a jet of liquid falling into a pool traps bubbles of the surrounding gas at the point of impact. Although the phenomenon is so familiar, there is little understanding of its origin.
The effects of entrainment are dependent on the fluid viscosity. With viscous materials (say $\eta > 50 \times 10^{-3} Nsm^{-2}$) the retention of the gas beneath the pool surface may be prolonged. This is an important problem in the industrial handling of many materials including molten glass, cosmetics, paints and food products. The entrainment with low viscosity liquids (say $\eta < 2 \times 10^{-3} Nsm^{-2}$) can also be a problem - as for example in the pouring of steel where local oxidation resulting from gas capture affects product quality adversely. These examples illustrate difficulties resulting from entrainment, but there are occasions when it can be exploited to advantage as a gas-liquid contacting mechanism. *Mertes* (1938) patented a two-phase chemical reactor which was based on this principle. The reactor simply contains a pool of liquid and an impinging jet which falls through a reacting gas. He claimed a contacting efficiency which is as much as five times that of a conventional spraytower. A similar reactor was patented by the *Badische Anilin und Soda Fabrik A.G.* (Ludwigshaven) in 1970. In their proposal the bubble swarm is contained within an open pipe which gives a degree of control over the reaction conditions.

Another important application is found in wateraeration. The influence of a waterfall upon the dissolved oxygen concentration and the resulting selfpurification of the water have been known for centuries. In the last few years at some power stations artificial waterfalls are created in the effluent stream of cooling water. The oxygen take-up produced by the fall can be further improved by division of the stream into seperate jets. This can be done with obstacles at the wier crest (*W. J. Kroon and Zehnan (1968)*).
There are also some surface aerators which use this contact principle. Water is pumped to some level above the water surface and then it is allowed to fall in sheets or jets. Various installations have adopted widely different impact water velocities and there is no clearly established guidance as to an optimum value.
An engineering office in East Germany (D.D.R.) has developed a waste water treatment system for large reservoirs which is slightly different. The jet is surrounded by an open pipe and

air is drawn in with the falling water stream so that a mixing shock effect occurs. The air-water mixture passes into the reservoir. The installation- and running costs are claimed to be superiour to those of other systems (*Jagusch and Schönherr (1972)*).

I.1 Purpose of the study

As stated above knowledge of the factors controlling and determining the physical process is almost nonexistent. Even the opinions of the few authors who have studied this phenomenon diverge at several points, particularly as regards the entrainment mechanism, the amount of entrained gas and the consequences for mass transfer.
This study is restricted to jets with low viscosities because the potential use for aeration is thought to be the most significant. For this and other obvious reasons water and air were the chosen fluids. The investigation will attempt to give an overall view of the phenomena associated with impacting liquid jets. In so considering the whole process, we have avoided an excessive concentration merely on one or two aspects of the phenomenon; the results are believed to be applicable to the whole class of low viscosity liquids.

I.2 Structure of the thesis

In chapter II the mechanisms which determine the gas entrainment are treated. The behaviour and irregularity of the jet and the energy transfer to the target liquid are found to be the controlling factors. Chapter III is devoted entirely to the disintegration and disruption of water jets and chapter IV quantitatively describes the cavity formation in drop collisions with water surfaces. The results of these two chapters are combined in chapter V when a quantitative model is proposed which predicts the amount of entrained air as a function of the jet parameters. Chapter VI compares the proposed models with experimental results.
The last chapter deals with various mass transfer aspects such as liquid mixing, bubble size distribution and mass transfer rates with its relation to the bubble penetration depth.
At the end of the thesis final conclusions are given together with recommandations for further investigation.

Chapter II

THE GAS ENTRAINMENT MECHANISMS OF IMPACTING LIQUID JETS

In this chapter a review is presented of the literature concerning plunging liquid jets. This concise chronological review reflects the different opinions about the mechanisms that control the volume of gas captured. Later an attempt will be made to explain the discrepancies. The paragraphs following give a detailed description of the observed entrainment mechanisms. These can be divided into several distinct phenomena which will be discussed in the last section of this chapter.

II.1 Literature review and general background

The first known publication concerning plunging liquid jets is a patent by *Mertens* registered in 1938. This patent dealt with a method of carrying out chemical reactions and was particularly applicable to the oxydation of ferrous iron in solutions of heavy metal salts. The method itself consists simply of a plunging jet system with recycling of the jet liquid. *Mertens* described the gas entrainment as follows. A film of gas is formed in the region immediately adjacent to the liquid jet. This film has the same velocity as the jet. After being brought below the surface of the receiving liquid the gas film is sheared from the jet. Gas bubbles are dispersed when the jet liquid loses its velocity after impact and distributes itself throughout the body of the liquid.

In 1950 *Shirley* measured the impact of turbulent waterjets but did not give any information about entrainment mechanisms. His concluding remarks state only that the entrainment is not simply a direct function of the velocity and diameter of the jet but is modified by the characteristics of the fluid. Although he varied a lot of parameters in the system he was not able to find a correlation for the entrainment rate. He also tried to determine the minimum velocity required for any air entrainment but he was only able to remark that both the roughness of the free surface of the jet and the degree of turbulence in the pool might have an influence upon that critical velocity.

Three years later *Ohyama, Takashima and Idemura* (1953) reported their experiments with a waterjet system. They observed that the jet surface became irregular above a jet

Reynoldsnumber (based upon jet diameter and velocity) of 2,000. They suggested that small water particles produced by this roughness and travelling with the jet would cause air to be entrained. The value of this Reynolds number suggests a transition from laminar to turbulent jet flow. However as will be pointed out in the next chapter such a transition does not necessarily occur at that Reynoldsnumber.
Lin and Donelly (1966) were the first who definitely distinguished between laminar and turbulent air entrainment. However their experiments deal mainly with the minimum velocity required for the entrainment of any air. The entrainment process itself was given minor consideration. Their laminar jets had a high viscosity and their experimental correlation of this minimum velocity is only valid for liquids having a viscosity exceeding 25×10^{-2} Ns/m^2.
Their description of the laminar entrainment process is similar to that of *Mertens* (1938). The entrainment is caused by the break-up of a gas film formed at the plunging point. The length of this thin film beneath the pool surface can, under certain circumstances, be 50 times the thickness of the film. In such cases it was observed that the upper portion of the film remained cylindrical in shape while the lower portion oscillated constantly; from that oscillation bubbles were generated. The entrainment at higher Reynoldsnumbers differs significantly from that of laminar high viscosity jets. No surrounding gas film was observed in any of the runs with a Reynoldsnumber above 2,000. This again suggests a turbulent flow situation. At very high Reynoldsnumbers the jet surface became ill-defined with air apparently mixed into the jet stream and vigorous bubble formation at the plunging point.
On the other hand *De Frate and Rush* (1969) observed water-jets having a Reynoldsnumber of 20,900 which had no gas entrainment at all, in contrast to the conclusions of the previous authors. Their description of entrainment only considered turbulent jets and according to their observations only deformations occurring on the jet surface were responsible for air entrainment. They distinguished three different mechanisms with increasing entrainment rates.
At low entrainment rates the bubbles are dispersed from the base of a depression in the poolsurface around the jet. Any dilation (or momentary expansion) of the jet momentarily deepens the depression whereupon air is trapped by the next disturbance. The second mode occurs when the jet becomes sinuous or disintegrates into drops. A cavity forms from the impact of a single drop or large dilation. The energy may be enough to make the depression several jet diameters deep. Air is trapped and dispersed into the pool when the following drop or dilated jet segment fills the contracting neck

of the cavity.
The third mode occurs when drops begin to scatter or jet segments twist away from the jet centre line. A broader cavity is formed which does not collapse. Under these last conditions the entrainment is maximal. Attemps were made to determine the transition from one mode to another. Although considering Reynolds, Weber and Rayleigh numbers they were unable to define transition points agreeing with their experiments.
The most recent publications in this field are by *McCarthy and his co-workers*. Their first publication (1969) concerned the entrainment process. An impacting smooth turbulent jet causes an indentation. They called this the 'induction trumpet'. This flow geometry resembles a venturi formed by the free liquid surface, and gas is entrained by a cavitating jet ejector action. The gasphase becomes discontinuous possibly by a mixing shock mechanism.
For plunging jets possessing irregular surfaces, entrainment is enhanced by direct bubble occlusion between the rough jet and the 'induction trumpet' surface. However this last mentioned phenomenon is another description of entrainment as given by the previous authors. In contrast to this when the jet is atomised into independent drops at high jet velocities their description (1970) agrees with those given by *De Frate and Rush* (1969).
Szekely (1969) does not distinguish between laminar and turbulent entrainment. He developed a theoretical prediction for entrainment rates of continuous molten metal streams by considering that the entrainment rate equals the total gaseous boundary layer volumetric flux associated with the liquid jet surface. Disturbances present on the jet do not influence the entrainment rate in his theory and he does not mention this phenomenon.
The last authors to be quoted are *Ciborowshi and Bin* (1972). They also conclude that disturbances on the jet might influence the air entrainment. They consider that the most important parameter is the kinetic energy of the impacting jet.

All authors known to have written about the entrainment mechanisms are cited above. As is clear from this literature review the opinions about entrainment differ from author to author. In general one might expect that a distinction must be made between laminar and turbulent jet flow. However the transition between these two situations is not made clear from the literature cited. This can further be illustrated by two examples.

The impacting jet having a Reynoldsnumber of 20,900 described by *De Frate and Rush* (1969) has no disturbances on the jet surface and therefore does not entrain air. Is this a situation of laminar of turbulent impact ? The authors do not give any information. Another example;the existence of a thin gas film around the liquid jet in the pool liquid can only occur for laminar plunging jets. However a simple experiment with a laminar waterjet (even in the kitchen !) shows no gas film at all.
Experiments from *Robertson and co-workers* (1973) indicate that the gas film inside the liquid pool only occurs when the impinging jet has a smooth surface and the viscosity of the jet is over 5 Nsm^{-2}. This process is independent of the viscosity of the liquid in the pool. Other examples could also be mentioned but it does not seem worthwhile to increase the confusion and disagreement over the entrainment mechanisms still further.

This thesis will focus its attention on the air entrainment caused by the impact of a turbulent waterjet on a water surface. The conclusion which can be drawn from the opinions of various authors who describe turbulent entrainment disturbances present on the jet surface must be of prime importance. This is true even though the direct effect of these disturbances has not been made clear. An attempt will therefore be made to explain the discrepancies. Our own observations will be described in detail and will be compared with the observations of others.

However before doing this some more information is needed. First we must give a clear definition of a turbulent jet in order to describe turbulent entrainment. This definition may appear very obvious but as will be shown in the next chapter it does restrict the possibilities.
Definition: When the flow issuing from the nozzle exit is turbulent, the jet itself is called a turbulent jet.
Another point that mustbe considered is that according to preliminary investigations the entrainment rate strongly depends on the flow configuration for both the turbulent jet and in the receiving pool. This can best be illustrated by showing the general trend of the entrainment rate as function of jet velocity (fig. II.1).
As is immediately clear from this figure distinct regimes must be considered. Anticipating what will be dealt within the next chapters, the value of v_1 is fixed (4,5 to 5 m/s) and v_2 is determined by a critical Webernumber. The entrainment mechanisms can therefore be divided into a low velocity region (1) and a high velocity region(2). Between these

there is of course a transition. Although *De Frate and Rush* also mention three different regions with increasing entrainment rate, in their lower velocity range they were concerned only with coherent jets, while their second and third regions described situations in which the jet is completely disrupted and drops strike the pool surface. These last two conditions will only briefly be considered in this thesis because they seldom occur and are energetically less valuable.

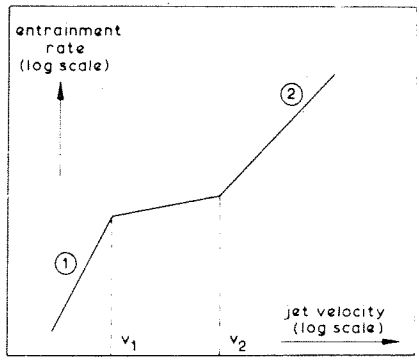

Fig. II.1 Typical entrainment/velocity curve

II.2 Impact of low velocity jets

Turbulent jets usually have disturbances on the free surface. High speed film (up to 10^4 frames/sec) showed that the interactions between these disturbances and the surface of the receiving liquid is of prime importance for the entrainment mechanism in the low velocity region. With the aid of the simplified sketches in fig. II.2 the entrainment can be explained. An impacting jet creates a flow pattern in the receiving bath. When no disturbances are present in the jet, no entrainment will occur. There will be a slight depression of the surface that is produced not only from the impact pressure of the associated boundary layer air but also from the flow field induced in the pool itself. In reality disturbances of the jet will amplify as the jet travels until they hit the water surface. Suppose only one irregularity is coming down the jet (fig. II.2a). The moment the disturbance reaches the water level, this surface will be deformed by forces acting on side walls E and F. The water particles start moving outwards (fig. II.2b). In the meantime the jet continues its movement downwards and the disrupted flow field in the receiving fluid will decrease and ultimately move back (fig. II.2c). After some time E and F reach the jet. Because the fluid particles below E and F start moving later an air filled toroidal hole is left in the liquid (fig. II.2d). Shear stresses cause break-up of the captured air and small bubbles appear in the receiving liquid.
With a real jet, before the sidewalls E and F have time to

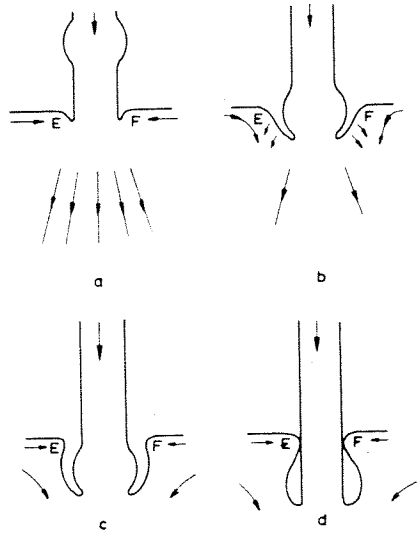

Fig. II.2 Air entrainment caused by a disturbance in the waterjet

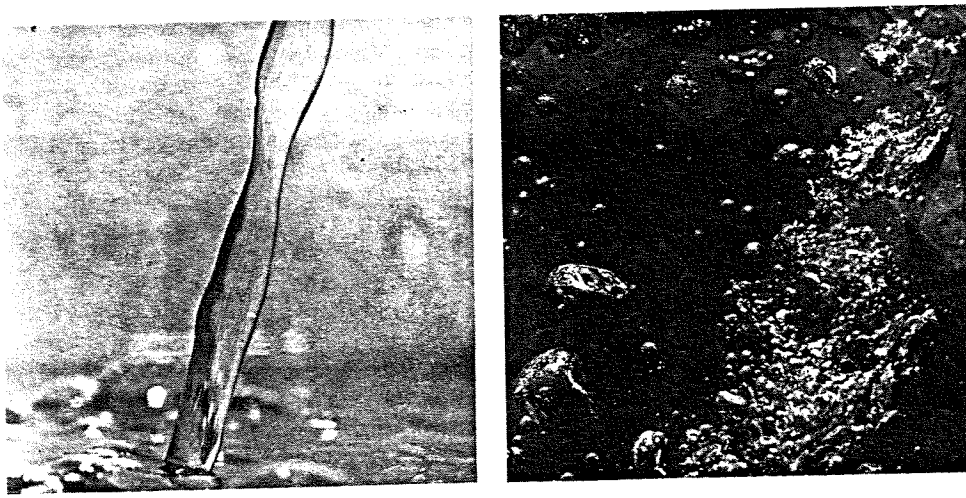

a b

Fig. II.3 Impact of water jet (jet velocity 3 m/s) and accompanying air entrainment

close it is possible that the following disturbance might have reached the receiving surface. This leads to an irregularity in the consequent entrainment. However the fundamental mechanisms remain the same at all low velocities. Fig. II.3 shows two pictures illustrating the entrainment. The pictures are taken with a Hasselblad camera type 500 C using a computerflash with a flashtime of 1/30,000 sec. Fig. II.3.a shows the impacting jet. The deformation of the jet can clearly be seen. These disturbances hit the water surface and fig. II.3b shows the seperate air filled cavities which are later dispersed as bubbles.
With increasing jet length the disturbances become larger (see chapter III). The impact of such a jet is shown in fig. II.4. The holes created in the free surface get larger. These holes or cavities can persist for a long enough time to allow secondary cavities to be produced in the bottom of the first cavity (see chapter IV).

If we compare our own observations with those which are given by the other authors we see that none of these authors mention the sideways movement of the fluid particles which is the basic entrainment mechanism for these turbulent jets at low speeds. That is one reason why disagreement exists even though the importance of the disturbances on the jet is recognized.

Burchard (1968) noticed an obliquely impacting jet entrains air although a vertical jet with the same velocity and length causes no air entrainment. With the suggested mechanisms this is easy to explain. The jet will entrain air only when disturbances are present. Sometimes these disturbances are small (with short jets we are still near the nozzle exit at the moment of impact) and not sufficient to cause sideways movement of the pool liquid. However when the jet impacts at an angle, a flow parallel to the watersurface is induced by the horizontal velocity component. This flow facilitates a displacement of the

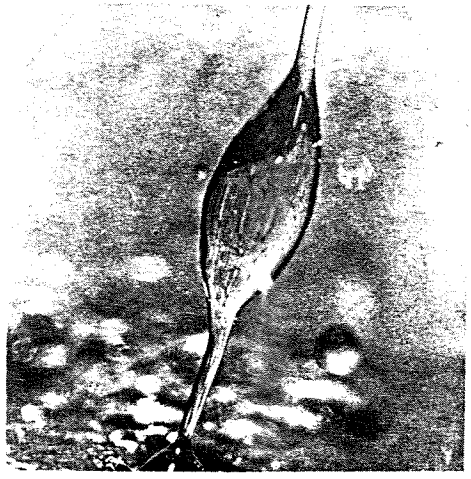

Fig. II.4 Jet near break-up point

fluid elements at one side of the plunging point and therefore air can entrain.
One final remark about the mechanism. A turbulent jet having no disturbances on the surface cannot entrain air. Deformations of the jet surface are dependent on the velocity, diameter, length of the jet, characteristics of the liquid and also on the influence of the environment. No unique minimum entrainment velocity can exist therefore for low viscosity turbulent coherent jets although this has been suggested by others.

II.3 Impact of high velocity jets.

When the velocity of the jet increases, the air entrainment gradually changes in nature. The entrainment which is discontinuous at low velocities becomes more regular. Because of the gradual development of the entrainment pattern there is a transition region between low and high velocity impact. Pictures of the entrainment with these conditions all look like fig. II.5. Entrainment is more or less discontinuous but there are short periods of continuous entrainment. The picture shows a clear transition. With increasing velocity the discontinuities occur less often until at a critical velocity a countinuous supply of air will entrain. Now we are in the high velocity region. Fig. II.6 is a representative picture of the entrainment process. The amount of entrained air is so great that clear pictures can only be taken with obliquely impacting jets, under other conditions the rising bubbles completely envelop the entrainment region and nothing can be seen. Fig. II.7 shows the form of the impacting jet. As can be seen from this picture air friction forces have become important and affect the surface of the jet. Some air is captured within the roughness of the jet surface. A boundary layer of air is also carried along with the jet. The jet hits the pool liquid and through the vigourous impact both the captured and boundary layer air is carried under the water surface. A ring of air is introduced which can travel a long distance in the pool before it breaks up into seperate bubbles.
With a further increase of the velocity the jet is completely destroyed by the air friction forces. Atomisation of the jet occurs and seperate liquid particles hit the water surface each causing air filled cavities. However this situation will not be dealt within this thesis. Moreover this entrainment is described in the papers of *De Frate and Rush* (1969) and *McCarthy and co-workers* (1969).

These descriptions of the entrainment make it now obvious why

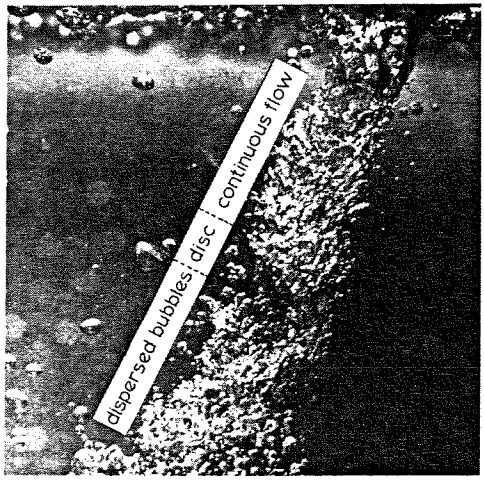

Fig. II.5 Air entrainment in the transition region

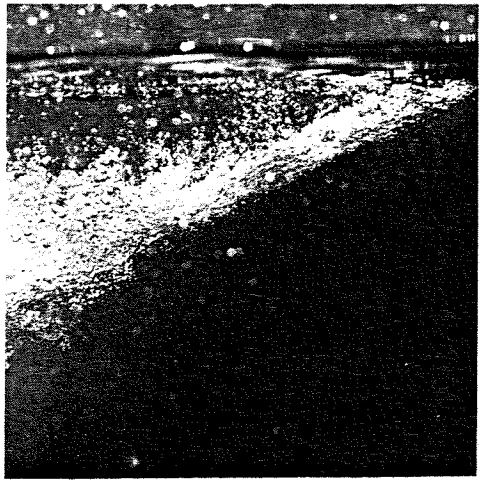

Fig. II.6 Air entrainment with a high velocity jet

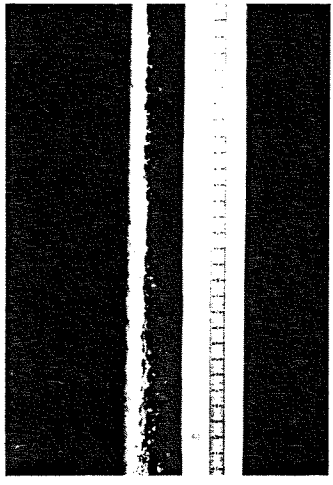

Fig.II.7 Form of a high velocity jet

the different authors disagree. It was not realized that different mechanisms for the eintrainment of coherent jets become important with increasing jet velocity. The papers of McCarthy et al only consider jet velocities greater than about 8 m/s. So most of their entrainment occurs in the transition and high velocity regions. According to their publications the entrained air only consists of air present in the surface irregularities in the jet.They do not consider the boundary layer air carried along by the jet, although this contributes significantly to the entrainment rate as will be pointed out in chapter V.
Most of the authors have tried to find one single correlation for their data. However their measurements cover all entrainment regions for coherent jets so the failure to obtain a single correlation is understandable, because of the changing dependency of the parameters in the various regions.

II.4 Phenomena that contribute to the total process

With the aid of the descriptions of the entrainment that are presented above, the influence of the various parameters can be predicted qualitatively. Increase of velocity, diameter and length of the jet is combined with an increase of entrainment rate. The velocity dependency is already explained. Increase of diameter creates more contact area between jet and receiving liquid in the low velocity region. In the high velocity region a diameter change effects the airfriction and with that the form of the jet and the amount of dragged air. The influence of jet length is also different for both regions. At low velocities deformations on the jet are mainly controlled by surface tension forces. In the other region surface tension and air friction forces together deform the jet surface. In both regions deformations grow as we move away from the nozzle. This particular aspect will be dealt with in chapter III.
For the low velocity region the angle of impact will greatly influence the entrainment rate. Contact area increases with an inclined impacting jet and moreover horizontal velocity components in the receiving fluid facilitate the movement of the liquid particles. However in the high velocity region the movement of fluid particles inside the pool has only a small effect on the entrainment and therefore it will be less dependent on the angle of impact. The characteristics of the liquid are of course relevant. The influence of viscosity has already been discussed. Another fluid property that is important is surface tension. In the low velocity region disturbances on the jet will amplify under the action of the surface tension forces. The amplification decreases with de-

creasing surface tension (chapter III). The jet will become smoother and so entrains less air. However at higher velocities air friction forces can more easily deform the jet surface. The consequence is, that in direct contrast to the low velocity region, not only will more air entrain, but also the critical velocity that defines the beginning of the high velocity range will be lower.
Nozzle design, supply of liquid to the nozzle, vibrations in the system, the influence of the environment and so on all influence the origin of the disturbances, so each of these factors can affect the entrainment.

As is clear from all these considerations the entrainment is a highly complicated process and no theoretical approximations are known at the moment.
In order to make the problem more manageable we will consider first the two most important aspects of the whole process:

1. The disintegration of turbulent jets including considerations of the influence of air friction forces upon the shape of the jet;
2. the dynamics of the impact and recovery processes that result from the interaction of the jet or jet fragments with the pool surface.

The essential difference between low and high velocity impact is covered by point 2. High velocity entrainment is almost unaffected by the physical conditions in the bath. The two phenomena will be dealt with in the next two chapters.

Chapter III

BEHAVIOUR OF LIQUID JETS

This chapter will describe the phenomena when a liquid stream issues from a nozzle with a diameter large enough to have turbulent flow at low velocities. The instability will be dealt with in the first paragraph and a review will be given of the theoretical work on this subject that has been published since *Lord Rayleigh* made the first original approach in 1878.
Although numerous investigators have studied the disintegration of a jet, a lot of problems have remained unsolved, for instance the influence of turbulence, nozzle design and the effects of ambient medium. This chapter will relate the persistence of turbulence in the nozzle to the corresponding breaking of the jet into droplets. The turbulence itself is characteristically determined by the Reynolds number and the nozzle design. Experiments are carried out which illuminate a few gaps in the knowledge of turbulent jet behaviour. Most of the present work has been done with low velocity turbulent jets in order to isolate turbulence from such other destabilising phenomena as air drag.
Paragraph 7 considers the influence of air friction. This is important at high jet velocities above a critical Weber number. The last part of this chapter relates the results to the subsequent entrainment when jets impact a water surface.

III.1 Disintegration of liquid jets

A liquid stream issuing from a round nozzle never remains perfectly cylindrical. Infinitessimal small disturbances occurring in any real environment disturb the jet surface. Some of these disturbances will grow along the jet and finally there is a transition from jet to drop flow. This familiar phenomenon, which can be seen at home and in many industrial operations, can easily be explained in terms of the continuity equation and the equations of motion.
Fig. III.1 shows a photograph of a jet. A wave is growing until separate drops are formed. This phenomenon is called capillary instability or 'varicose'. A detail of the picture is sketched in fig. III.2.

Suppose the deviation δ is very small compared to the jet radius and the velocity profile inside the jet is flat. Hence $\partial v_r/\partial r$ is zero. We consider only rotation symmetrical disturbances sothat the continuity equation reduces to (cylindrical coordinates):

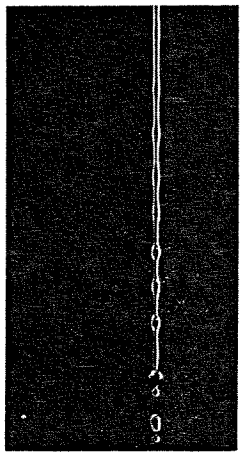

Fig. III.1 A disintegrating jet

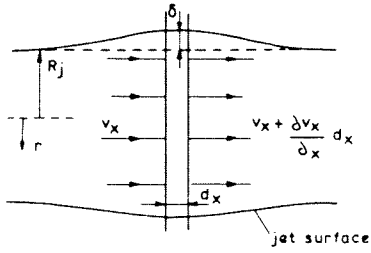

Fig. III.2 Sketch of detail of jet surface

$$\frac{v_r}{r} + \frac{\partial v_x}{\partial x} = 0 \qquad \text{(III.1)}$$

Integration over the cross section and substitution of $v_r/_{r = R_j} = \partial\delta/\partial t$ gives:

$$\frac{\partial v_x}{\partial x} = - \frac{2}{R_j} \frac{\partial \delta}{\partial t} \qquad \text{(III.2)}$$

By assuming an inviscid jet flow (valid for water) the equation of motion simplifies considerably:

$$\rho_w \frac{\partial v_x}{\partial t} = - \frac{\partial p}{\partial x} \qquad \text{(III.3)}$$

Differentiating eq (III.2) with respect to t, eq (III.3) to x leads after substraction to:

$$\frac{2\rho_w}{R_j} \frac{\partial^2 \delta}{\partial t^2} = \frac{\partial^2 p}{\partial x^2} \qquad \text{(III.4)}$$

The only possible solutions for δ and p, apart from the zero solution, are solutions which contain harmonic and exponential functions. These functions can be separated for the two variables t and x. In accordance with fig. III.1 a logical solution of eq (III.4) might be:

$$\delta = \delta_o e^{\mu t} \cos \frac{2\pi x}{\lambda} = \delta_o e^{\mu t} \cos Kx \qquad \text{(III.5)}$$

Substitution and applying the condition that $p/_{x=t=0}$ = constant (negligible disturbance in the x-direction) and $\partial p/\partial x|_{x = 0} = 0$ gives the pressure development along the jet:

$$p = \frac{- 2\rho_w \mu^2 \delta_o}{R_j K^2} e^{\mu t} \cos Kx + \text{constant} \qquad \text{(III.6)}$$

If μ has a positive value this pressure increases along the jet and it strengthens the movement of the disturbances because of the negative sign in eq (III.6). Negative or imaginary values of μ give respectively a decreasing or an oscillating value of the deformation. It is immediately evident that the value of μ must be considered in some detail because the disintegration of liquid jets is strongly

dependent on it. It is commonly known as the growth factor..

The instability of jets is usually studied by considering the break-up curve. This curve relates the break-up length (distance from nozzle exit to the point where separate drops appear) to the jet velocity. The general shape is given in fig. III.3. At very low velocities the liquid drips out of the nozzle. When a real jet is formed the relation between break-up length and jet velocity is linear. Further increase of velocity causes a deviation from the straight line and at some particular value of the velocity a maximum appears. Beyond this maximum no reliable prediction of the break-up length is given in the literature. The existence of the maximum has been shown by several authors though much disagreement exists about the physical explanation. Most authors (*Grant (1966), Weber (1931), Richardson (1954), Haenlein (1931) and Miesse(1955)*) observed a change in break mechanism near the maximum. The capillary or 'varicose' instability is accompanied by transverse wavelike deformations which effect the break-up mechanism. However *Ivanov* (1966) noticed these additional deformations persist far beyond the maximum.

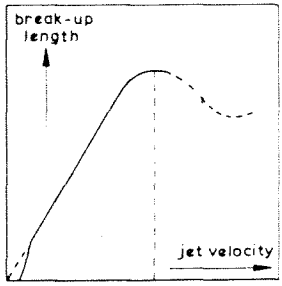

Fig. III.3 Typical break-up curve of a liquid jet

Fenn and Middleman's (1969) data made them decide that both aerodynamic and viscous forces could be responsible for the maximum.
Jets having a Weber number (= $\rho_A v_j^2 D_j/\sigma$) over 5.3 experience significant aerodynamic forces. A maximum in the break-up curve which lies below this criterion is explained by viscous forces. In that case capillary instability occurs before the critical Weber number has been reached.
On the other hand *Borisenko's* (1953) conclusions indicate that the maximum is fixed by a critical Reynolds number (= $\rho_w v_j D_j/\eta_w$).He reports a value for this of 4,500 for water jets and concluded that the jet has become turbulent. Also *Phinney* (1972) explained the existence of the maximum by turbulence mechanisms; however his critical Reynols number is much lower.

The confusion about the maximum remains and therefore some experiments will be described later in this chapter which have been designed to throw light on this. Although a lot of scientists have studied jet instability, only the first part

of the break-up curve has been theoretically analysed. A brief review of the most important theories are summarized in the next paragraph.

III.2 Existing theories about jet instability

Lord Rayleigh (1945) in 1878 provided the original theoretical approach. He assumed that there was a 'white spectrum' of disturbances at the nozzle exit and he used a flat velocity profile in his analysis. The effect of these disturbances was treated by applying the physical laws of conservation.
He separated the deformations as a Fourier series in terms similar to eq (III.5). The successive terms in the expansion are completely independent of each other as long as the deformations are small. He was able to show that the liquid jet was stable for all disturbances except for rotational symmetric ones whose wavelength exceeds the circumference of the undisturbed jet. His linearized analysis leads to the following equation for the growthfactor μ for an inviscid liquid:

$$\mu^2 = \frac{\sigma}{\rho_w R_j^3} \frac{i K R_j J_o^1(iKR_j)}{J_o(iKR_j)} (1-K^2R_j^2) = F(KR) \quad (III.7)$$

J_o is a Besselfunction of the first kind and zero order, J_o^1 is its derivative with respect to the argument and i is the imaginary unit. The function F(KR) is considered and it appears to have one definite maximum although the curve near this maximum is rather flat. The disturbances corresponding to this maximum have a wavelength of 4.51 x $2R_j$ and they will grow faster then any other disturbance finally causing break-up of the jet. He claimed that the complete analysis would be valid up to jet diameters of 10 mm.

During the last ten years some improvements on *Rayleigh's* original theory have been made by *Chandrasekhar* (1961), *Yuen* (1968), *Weber* (1968) and *Hayfeh* (1970), who extend the theory to the second and third order terms. Experimental verification of these theories has been satisfactory (*Crane (1964, 1965), Donnelly (1966), Goedde (1970) and Rutland (1970)*). None of these theories includes the influence of environment (air friction) or of turbulence. Their significance is therefore restricted to small diameters and low jet velocities.

Weber's calculation (1931) considers both capillary and

wavelike break-up. The first part of his work described the influence of surface tension and also takes the effect of viscosity into account. His analysis leads to the following equation for the growthfactor of the disturbances:

$$\mu^2 + \mu \frac{3\eta_w}{\rho_w R_j^2} KR_j = \frac{\sigma}{2\rho_w R_j^3}(1 - K^2R_j^2)K^2R_j^2 \qquad \text{(III.8)}$$

Eq (III.8) and (III.7) are similar if we consider inviscid flow and approximate the numerical value of the Besselfunction in eq (III.7). Evaluation of eq (III.8) gives a value of 4.44 x $2R_j$ for the most unstable wavelength of an inviscid jet, this differs slightly from *Rayleigh's* result. Increase of viscosity gives a higher value of the critical wavelength and a lower value of the growthfactor. This last mentioned result explains the greater smoothness of viscous jets.

If the amplitude of the most unstable wavelength is equal to the radius of the jet, *Weber's* analysis gives the following equation for the break-up length:

$$L_B = \frac{v_j}{\mu_{opt}} \ln \frac{R_j}{\delta_o} \qquad \text{(III.9)}$$

in which μ_{opt} stands for the growthfactor of the most unstable wavelength and δ_o the amplitude of the initial disturbance generated near or in the nozzle. Comparison with the results of *Haenlein* (1931) made him decide that the initial amplitude satisfies the equation:

$$\ln \frac{R_j}{\delta_o} = 12 \qquad \text{(III.10)}$$

and this can be considered as an universal constant. Equations (III.9) and (III.10) describe the linear portion of the break-up curve.

In the second part of his analysis *Weber* showed that if transverse disturbances are present on the jet, aerodynamic forces enhance the deformation. However the origin of these deformations was not treated. Wavelike deformations destabilize the jet and the analysis predicts a maximum in the break-up curve. Eq (III.8) is supplied with a term which is a function of the jet velocity. However the place of the maximum in the theoretical break curve does not correspond with experimental data. This fact made the analysis doubtful,

but even so *Weber's* analysis is still the only one in current literature that predicts a maximum.

These theories of *Rayleigh* and *Weber* analyse the essential jet behaviour. Because of the simplifications they have to assume in order to complete their complex analyses, it is no surprise that the experimental results deviate greatly from the theory. Additional data are needed to supply understanding of the physical processes that control jet disintegration.

III.3 Experimental equipment

The jet was produced from a nozzle set in the base of a round pressure vessel. This was preferred to a pumpsystem because the latter might produce undesired disturbances which influence the disintegration of the jet (*Donnelly (1966)*). The equipment is sketched in fig. III.4. Water was supplied to a certain level. Pressure was adjusted to the desired value and a certain time was allowed to permit the liquid to come to complete rest. Vertical baffles in the tank helped this. The nozzle was then opened and the jet discharged into

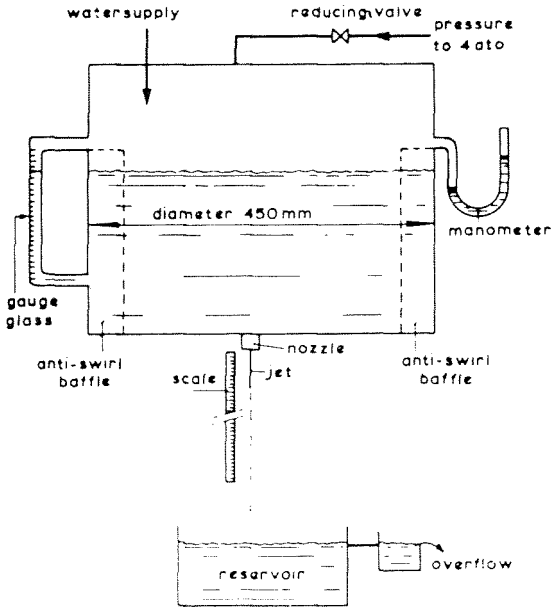

Fig. III.4 Sketch of experimental equipment

a reservoir which emptied through an overflow. Photographs were taken of the jet (with an Asaki Pentax Spotmatic Camera using a Rollei computer flash) and break-up lengths were evaluated from these. All the break-up data given later represent measurements made directly from negatives. The velocity of the jet was based on a measured volumetric flow and the cross-sectional area of the tube forming the discharge orifice.

During the measurements many interchangeable nozzles were used. The construction in the bottom of the pressure vessel is shown in more detail in fig. III.5. The nozzle itself is attached to a plate which forms a part of the vessel bottom. The nozzle construction is designed to eliminate disturbances which might influence the streamlines near the entrance region. The whole nozzle plate is fixed to the bottom of the tank and can easily be replaced by a different one. Because the flow inside the nozzle is expected to have great influence on the jet disintegration special precautions were taken with its manufacture. Several nozzles were used and hence it is better to deal with the dimensions and entry shapes of the nozzles in those paragraphs which also consider the measurements and results. This will facilitate the reading of this chapter.

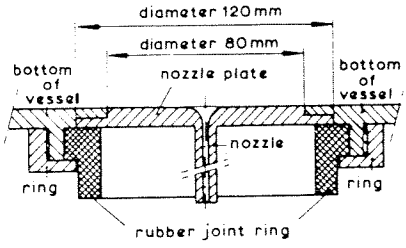

Fig. III.5 Construction of nozzle

The next section reports some preliminary investigations. The jet issues from a long brass nozzle (length to diameter ratio exceeding 50, in order to assure virtually fully developed pipe flow) with sharp-edged inlet and outlet orifices.

III.4 A preliminary study of jet disintegration

Most published data of jet disintegration have been produced by jets from nozzles with orifice diameters less then 1 mm The geometry of the nozzle has often been given only minor consideration, so direct comparison of data is hampered. Our sharp-edged nozzles had diameters of 2.85 and 5.0 mm; with the issuing velocity over 2 m/s the Reynolds number (based on that velocity and nozzle diameter) implies a fully developed turbulent flow ($Re > 5,700$). If one compares turbulent and laminar jet flows, differences in jet disintegration might be expected. The analysis of *Rayleigh* (1945) assumed a flat

velocity profile and did not require an assumption of turbulence to predict instability. It should therefore be equally applicable to laminar or turbulent conditions although that might not appear to be a very plausible result. Some authors report that turbulence has no destabilizing influence (*Grant and Middleman (1966)*).

In fig. III.6 the break-up curve is plotted. The variation in break-up length under given conditions is about 10% and each value plotted is the arithmetic mean of at least five photographs. In the same graph the data of *Richardson* (1954) are also shown which refer to comparable diameters. The agreement between his and our data is satisfactory although we have no indication what kind of nozzles he used. We presume his discharge condition was also fully developed turbulent flow.

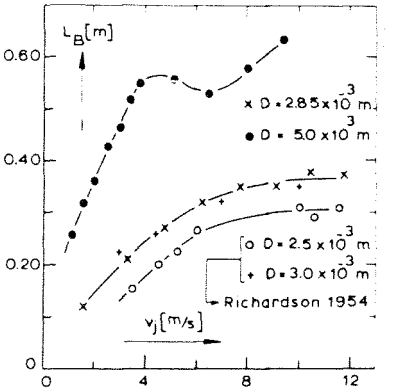

Fig. III.6 Break-up curve of turbulent jet

All the data plotted in the graph refer to vertical jets. There must be an influence of gravity. Gravity accelerates the jet and in consequence there is a decrease of diameter. There are also diameterchanges due to velocity profile relexation and surface tension forces. In most actual cases diameter and velocity differences will work against each other. When velocity increases the break-up length becomes longer (in the first part of the break-up curve) but the consequent diameter decrease shortens that same length. No theoretical predictions are made or can be made because of the complexity of the analysis. In general it is supposed that gravity does not influence the break-up curve considerably and experimental evidence with small diameter supports this assumption. In our case we use larger diameters so the break-up lengths are such that occasionally there is time for gravity to have an influence. However the velocities at which this occurs are limited to the lowest values.

Turbulent break-up data usually consider small jets (D_j < 1 mm) with high velocities. Here air friction forces become important and a distinction between friction and turbulence phenomena can hardly be made. *Richardson's* (1954) data were some of the very few that we could find in the literature

which describe break-up curves of turbulent jets at low velocities. His curve shows a linear part approaching a maximum and is therefore not in disagreement with the theory. However his break-up lengths were much shorter than would be predicted. For that reason we did some preliminary investigations with jets of comparable diameters. Since our results show the same trend as his, we conclude closer examination of turbulent jet instability is necessary.

The results of measurements of the most unstable wavelength ($4.6 \times D_j$) were in close agreement with *Rayleigh's* theoretically predicted value ($4.51 \times D_j$). The measured wavelength is the arithmatic mean taken from about 100 photographs. *Goedde and Yuen* (1970) determined the value of the growthfactor of the disturbance with a given wavenumber for jets with a diameter of 2 mm. They construct the nozzle in such a way that the issuing velocity profile was laminar even for high Reynolds numbers. In that case the agreement between theory and experiment was good. Because in the complete analysis of either *Rayleigh* or *Weber* the growthfactor and wavelength are directly related to each other, our measured value of the most unstable wavelength suggests strongly that the growing disturbance in a low velocity turbulent jet can be analysed by the existing theories.
This last conclusion enables us to study the turbulent jet disintegration in more detail and attempts will be made to explain why the break-up length is much shorter than the theory would predict.

Substitution of eq (III.10) into eq (III.9) gives for the value of the break-up length:

$$L_B = 12 \frac{v_j}{\mu_{opt}} \qquad \text{(III.11)}$$

μ_{opt} is determined by the expression:

$$\mu_{opt} = (\sigma / 8\rho_w R_j^3)^{\frac{1}{2}} \qquad \text{(III.12)}$$

Hence with eq (III.11):

$$L_B = 12\, v_j\, (8\rho_w R_j^3/\sigma)^{\frac{1}{2}} \qquad \text{(III.13)}$$

Evaluation of this expression gives a theoretical value which is two or three times that determined experimentally. The discrepancy must be explained by a different origin of the disturbances because, as has already been pointed out, the

growth of any deformation is ruled by the same laws.
The level of the initial disturbances can be calculated back from the measured break-up length using the formula:

$$\ln \frac{R_j}{\delta_o} = \frac{L_B}{v_j} (\sigma/8\rho_w R_j^3)^{\frac{1}{2}} \qquad \text{(III.14)}$$

Comparison between previous investigations and the present one shows a considerable deviation of the initial disturbance level. Weber found a value of $\ln R_j/\delta_o$ of 12 (eq III.10) whereas our data give values which lie between 4 and 5. The difference is of the order of three magnitudes and can only be explained by turbulent influences.
In general the curves (which are of the form of figure III.3) show a maximum. In our results this sort of behaviour is plainly shown by the 5 mm jet (figure III.6). This is clearly contrary to equation (III.13) which predicts monotonic increase of L_B with v_j. Since the onset of turbulence has already been passed, there must be some interaction with the surface tension forces that could arise from viscous forces or air friction *(Penn and Middleman (1969))*. It seems likely that the laminar to turbulent transition in the jet would lead to a maximum in the break-up curve because of the larger initial disturbance level. Under certain conditions this can be reached before the air friction maximum is attained. This would lead to a situation where the two maxima could be confused and might account for the variety of opinions *(Phinney (1973))*. It should be remembered that most work on jet stability has been carried out with very fine jets where the air resistance will always be controlling, and that only larger jets like those studied here will show this effect.

The most important conclusions drawn from this preliminary investigation are:

1. The disintegration of low velocity turbulent jets can be analysed by the existing theories of laminar jet flow;
2. because the level of the initial disturbance becomes several orders of magnitude greater when the jet becomes turbulent, the break-up curve may contain more than one maximum;
3. the relationship between turbulence and the origin of the initial disturbance is unknown. Some theoretical models must be assumed in order to describe the deformations of a jet.

III.5 Theoretical considerations

If turbulence plays a role in the disintegration process it must first be shown that this is theoretically possible. The eddy size distribution originating inside the nozzle pipe will alter after leaving the nozzle and this changing pattern must influence the jet behaviour. Fig. III.7 shows a picture of the surface roughness that turbulence produce. The eddies that are present migrate to the jet surface and their effect is visible. The high frequency disturbances will be damped out by surface tension forces while the deformations with longer wavelengths will remain so assumptions about the influence of turbulence are justified if the frequencies needed to break down the jet are in the same order of magnitude as the frequencies occuring in turbulence energy spectra of low viscosity liquids such as water. And this happens to be so.

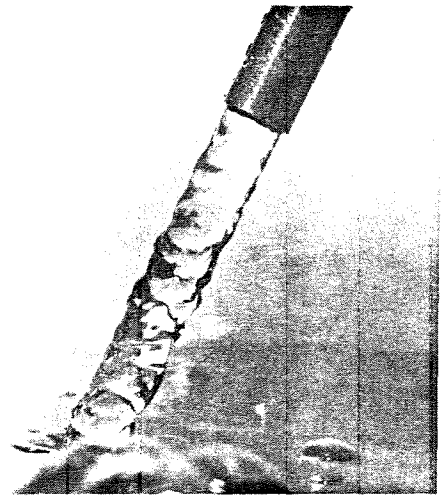

Fig. III.7 Surface roughness development

III.5.1 Turbulent pipeflow

The study of turbulent pipeflow is mainly restricted to theoretical and experimental considerations of fully developed turbulence at moderate and high Reynolds number (*Hinze (1959), Schlichting (1968)*). Many attempts have been made to relate the measured velocity profile to various descriptions of the turbulent flow (*Prandl (1910), Nikuradse (1932), Lindgren (1969), Kleinstein (1971) and others*). The approaches come to a reasonable degree of agreement, even though the nature of turbulence is still not completely understood.
In fully developed turbulent pipeflow three regions can be considered. Complete eddy motion occurs in the core of the pipe, where the viscous contribution to the shear stress is negligible. In the neighbourhood of the wall itself viscous forces dominate and the velocity gradient can be assumed to be constant. This region is called the laminar sub-layer. The region between is the buffer layer. The rate of energy transfer by eddy motion is influenced by viscous dissipation.

A universal velocity profile has been proposed which describes the time-mean average velocity profile over the whole cross section. The following dimensionless variables are used:

$$u^+ = u/u^*, \quad y^+ = \rho y u^*/\eta, \quad u^* = \sqrt{\tau_{wall}/\rho} \qquad \text{(III.15)}$$

in which u is the local time-mean axial velocity, y is the radial distance from the pipewall and u^* is the 'shear stress velocity'. By considering the three different regions relationships between the variables were established. The dimensions of the layers are described by the equation:

$$\begin{aligned} 0 < y^+ &< 5 : \text{laminar sub-layer} \\ 5 < y^+ &< 30: \text{buffer layer} \\ y^+ &> 30: \text{turbulent region} \end{aligned} \qquad \text{(III.16)}$$

Less attention is given to 'turbulent' Reynold numbers below 10,000. With decreasing velocity the influence of viscous forces is expected to be greater. The turbulent eddy motion is affected and the buffer layer might become thicker. *Pennell et al* (1972) investigated the effect of varying the Reynolds number from 3,200 to 24,000.
Time-mean velocity and turbulent intensity distributions relative to the 'shear stress velocity' were measured. The turbulent structure near the wall deduced from the relative intensity data appears to be similar for all measured Reynolds numbers. Comparison was also made with the data of *Laufer* (1954) whose results extend to a Reynolds number of 500,000. This comparison made them decide that in the wall region there is a similar controlling law for all Reynolds numbers which is valid up to a value of y^+ of 25. Data of the time-mean velocity distribution indicate that flows with a Reynolds number over 10,000 obey the *Von Kármán* (1939) universal velocity profile. Deviations in the buffer layer only occur for Reynolds numbers less than 5,000. Therefore it may be concluded that the structure of turbulence near a wall is largely determined by the presence of this wall and is independent of the Reynolds number as long as it exceeds 5,000.

III.5.2 The entrance region of turbulent pipe flow

The entrance region of a pipe largely controls the transition from laminar to turbulent flow. Induced instabilities in the inlet section can develop into turbulent motion when the Reynolds number is over 2,000. However the persistence of turbulence in pipe flow cannot be predicted in advance. A

reasonable choice of the shape of inlet section together with careful polishing can prevent the onset of turbulence. Situations are reported in which laminar flow exists up to a Reynolds number of 18,000 (*Rotta (1956)*).

There is no clear agreement on a definition of an entry length for the establishment of fully developed turbulent flow at a pipe entry. *Schlichting* (1965) shows that this entry length is stated to be between 25 and 100 pipe diameters according to a few cited authors. Theoretical approximations of *Fillippov* (1958) do not agree with those given by *Bowlus and Brighton* (1968). These last cited authors also give data of other workers which deviate. The result of their own calculations can be presented by the following equation:

$$\frac{L_e}{D} = 14.25 \log_{10} Re - 46 \qquad \text{(III.17)}$$

in which L_e is the entry length. The range of Reynolds numbers for which this relation is valid is not given. This is probably only true for high Reynolds numbers (of order 10^6 or greater). The theoretical approximations concerning the entry length assume expressions which describe the velocity profile in the inlet section. Most common are power law profiles and logaritmic velocity distributions but these relations were seldom experimentally verified. The only authors known who measured turbulent characteristics and velocity profiles in the inlet section are *Barbin and Jones* (1963).
They measured velocity profiles, pressure drop, Reynolds stress and turbulence intensities from the inlet point to 40.5 diameters downstream for a fixed Reynoldsnumber of 388,000. Turbulence was artificially initiated at the beginning of the pipe and their main conclusions are cited below:
"1. For the used Reynolds number fully developed smooth pipe flow is not attained in an inlet of 40.5 diameters. Velocities, turbulence intensities and Reynolds stresses are still changing;
2. the wall shear stress and static pressure gradient are influenced only by the flow adjacent to the wall and attain their fully developed values in the first 15 pipe diameters;
3. most of the turbulence produced near the wall is apparently dissipated there, the region of high production near the wall does not play the role of supplier to the rest of the flowfield;
4. contrary to the assumption of some previous treatments,

velocity profiles in the inlet region are not similar." This last conclusion made the theoretical treatment of the inlet length very complicated and only measured data can be useful. However as mentioned before no definite and reliable measurements are known in the literature.

The literature cited above indicates that very little information is available concerning the phenomena in the inlet region of a pipe. However nozzles which produce jets still operate within the inlet region or a part of it. Flow geometry and turbulence inside the nozzle are hard to determine and therefore relationships between turbulence and the corresponding turbulent break-up of the jet are difficult to analyse. Special precautions in the manufacturer and the design of the nozzle might greatly influence the jet behaviour. Experiments were carried out and described in the next sections which will relate disintegration of jets to the geometry of the nozzles used.

III.6 Experimental results for low velocity jets with diameters over 2 mm

III.6.1 Effect of nozzle inlet geometry upon jet disintegration

If the flow that issues from the nozzle is fully developed turbulent, no influence of the inlet shape can be expected. The initiation of eddy formation at the inlet section can only be shown with the use of short nozzles. If there is a direct influence of the generated eddies this must clearly be seen by a shortening of the break-up length.
The transition from laminar to turbulent pipeflow in relation to the inlet geometry has apparently been investigated only by *Kurzweg* (1933). He used a sharp-edged and a rounded inlet section. The sharp opening gives a flow contraction (vena contracta) and a 'dead water area' at the wall. Shear stresses between these regions create instabilities and turbulence can develop (see fig. III.8a). The rounded opening (fig. III.8b) streamlines the flow and transition to turbulence occurs at higher Reynolds numbers. The transition number for the sharp edged opening was found to be approximately 3,500. In the other case the number was about 7,000. However the geometry of the rounded opening was not published and the only remark he made on it was that is was 'rounded'. The conclusion that can be drawn from his study is that turbulence in a sharp-edged inletsection of a pipe is directly created in contrast to the case with streamlined entry sections.

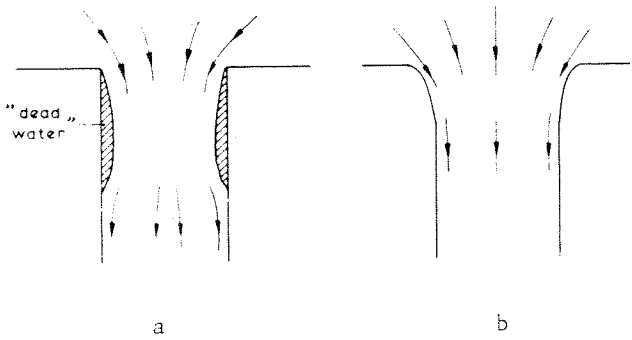

Fig.III.8 Inlet geometry used by *Kurzweg* (1933)

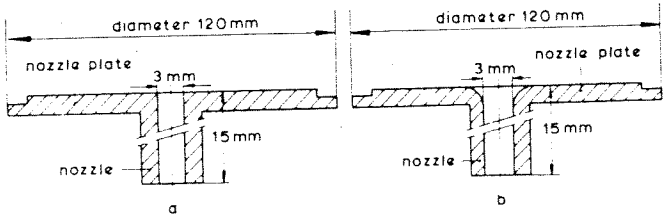

Fig. III.9 Nozzle geometries

Fig. III.9 shows the nozzles used. The plate in which the nozzle is attached is part of the reservoir bottom as was shown in fig. III.5. The geometry of the rounded nozzle is arbitrarily chosen.
Break-up lengths were measured (from single photographs) and are plotted in fig. III.10. As is obvious, a maximum appears for both curves which is not due to air friction forces (here We<< 1). The only explanation for the decrease of the break-up length is the increase of the initial disturbance level which is caused by eddy formation i.e. turbulence. Also the Reynolds number for which the decrease of break-up length starts is consistent with the findings of *Kurzweg* (1933) for turbulent pipeflow. The critical Reynoldsnumber for the sharp edged nozzle is hard to determine. Severe fluctuations of the break-up length occur due to the irregularity of the eddy formation.
From the results of *Kurzweg* it is clear that the entry condition affects the onset of turbulence and we have shown that this entry disturbance and its subsequent turbulent development clearly controls the break-up length. The exact relationship is difficult to obtain since instabilities in the inletsection can be initiated by miniscule disturbances and hence the transition points can differ for two nozzles with the same macro inlet geometry.

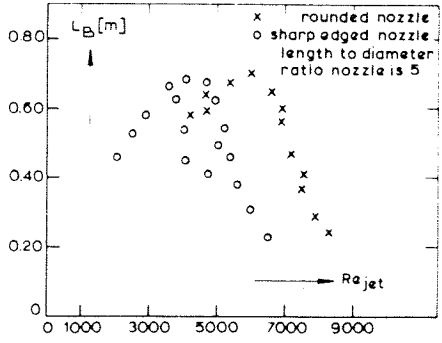

Fig. III.10 Break-up curve of jets from short nozzles

III.6.2 Effect of outletshape of the nozzle

Deliberate disturbance sources were produced at the two nozzle outlets. Burred edges were made with a file. In one

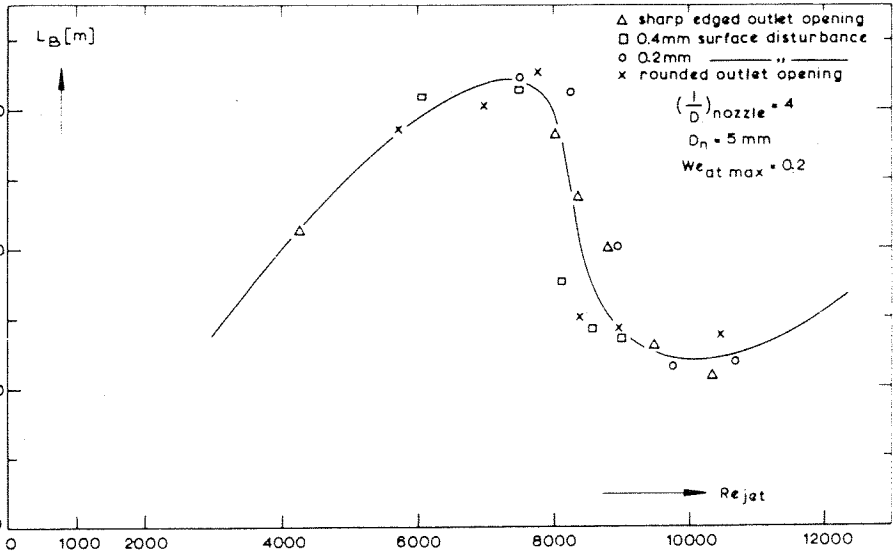

Fig. III.11 The influence of nozzle outlet geometry

case the roughness height was approximately 0.4 mm and in the other case 0.2 mm. Both are orders of magnitudes greater than the level of the initial disturbance calculated from eq (III.14).A third nozzle had a sharp-edged outlet opening and a last one was rounded. Fig. III.11 gives the corresponding break-up curves. Again the maximum due to the influence of turbulence is obvious. The various curves for all nozzles are however the same within the accuracy of the measurements so the conclusion is that the outletshape of the nozzle is only of minor importance.
This is easy to explain with the line of thought that has been followed. Turbulence inside the nozzle determines the level of disturbance, whereas deformations at the outlet opening only influence the jet flow outside. The turbulence inside the nozzle can create rotation symmetric disturbances whereas any turbulence that is produced at the exit is eventially local and is less likely to destroy the jet.

III.6.3 Influence of nozzle length

The outlet shape is of minor importance. In order to exploit this, we started with a long nozzle and examined the jet break-up length after successive pipe sections had been cut

from the discharge end. In this way confusion that might have arisen from different entry condition and other factors was avoided.
A sketch of the inlet geometry is given in fig. III.12. This inlet shape was chosen for manufacturing reasons. The

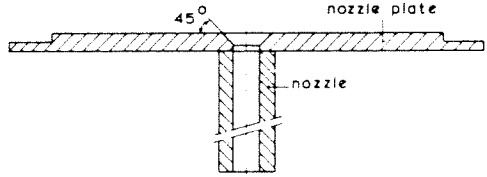

Fig. III.12 Inlet geometry of nozzle used for entry length study

nozzles were made of brass.
Fig. III.13 gives a representative example of the graphs. They all show the same trend and it looks like a 'family' of curves. The common curve for all lengths at lower Reynolds numbers was well established in experiments with other nozzles. For a given nozzle length the break-up length suddenly decreases with increasing Reynolds number. At some

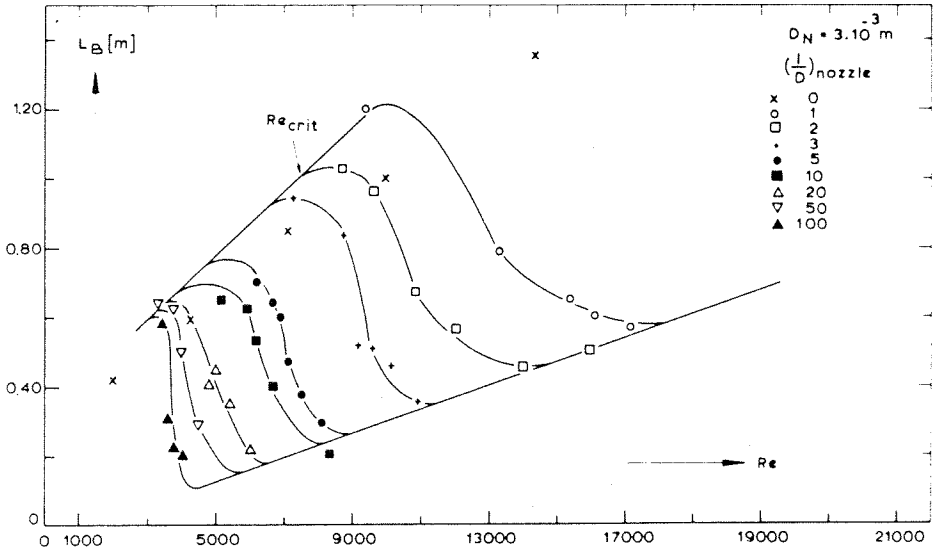

Fig. III.13 The influence of decreasing nozzle length upon jet break-up

critical Reynolds number eddies begin to form which can destroy the jet. This Reynolds number however does not necessarily determine the transition from laminar to turbulent flow.
Points obtained for a simple orifice (zero nozzle length) are also plotted in fig. III.13. The points are somewhat shifted with respect to the other lines. There are two factors which may be relevant. Firstly, this nozzle was specially manufactured which could influence the inlet flow as has already been mentioned. Secondly, the nozzle discharge shows a 'vena contracta' so that the jet diameter is smaller than with nozzle pipes. This 'vena contracta' changes the relevant Reynolds number to a higher value.
No maximum was observed for this zero nozzle length right up to a Reynolds number of 14,000, implying that turbulence does not occur. This fact is in complete agreement with the probable origin of turbulence as suggested earlier.

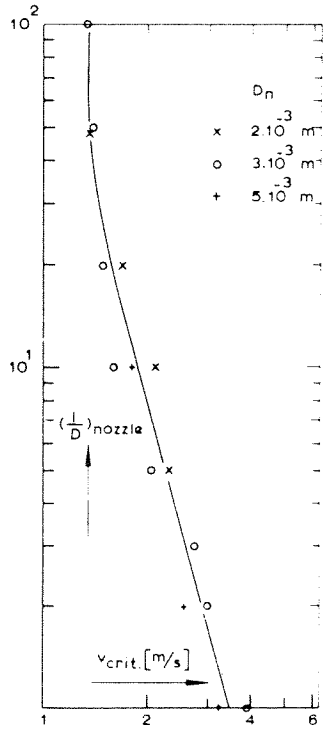

Fig. III.14 The relation between the nozzle length and the critical velocity at which turbulent eddies originate.

In fig. III.14 the velocities corresponding to the critical Reynolds number are plotted. Those velocities are now a function of the length to diameter ratio of the nozzle. As was pointed out before, small irregularities in the inlet region strongly influence this velocity. The method of manufacturing the nozzles did not assure geometrical uniformity on a micro scale. The disturbances eventually present are approximately of the same order of magnitude but, relative to the pipe diameter, the inlet region of larger pipes is smoother. A plot of the critical Reynolds number is therefore less useful and it is better to consider the average velocity in the nozzle. This velocity can be considered proportional to a Reynolds number based on surface roughness.
It is the disturbances in the inlet region that create turbulence and hence the relation between the transition to turbulence and the nozzle length is not determined by a Reynoldsnumber based only or even mainly on the length of the

nozzle. A detailed explanation of the course of the curve demands further knowledge and investigation of the characteristics of the origin of turbulence in pipeflow and is a question that lies far beyond the scope of this thesis. The only conclusion to be drawn from the graph is that for nozzles with a pipe length over 50 diameters the issuing jet stream does not significantly change anymore with respect to the turbulence structure.

III.6.4 Break-up lengths of low velocity turbulent jets from long nozzles ($(l/D)_{nozzle} = 50$)

The turbulent flow inside the nozzle has time to develope fully. The corresponding break-up lengths are plotted in fig. III.15. Five different diameters are used and because all data points represent turbulent break-up a maximum does not occur. These lines are curved because of the increasing influence of gravity with decreasing velocity. Unfortunately these data can be compared only with those of *Richardson* for 2.5 and 3 mm diameter jets (see fig. III.6).

Influence of air friction is not detected for such low speeds; this will be discussed in another section.

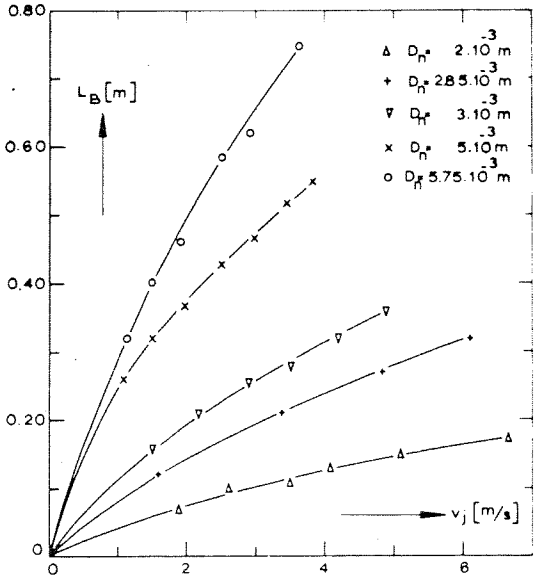

Fig. III.15 Break-up curves of low velocity turbulent jets

Values of the size of the initial disturbance deduced from the break-up lengths of fig. III.15 calculated using eq (III.14) lie between $1.5.10^{-5}$ and $6.5.10^{-5}$ m. There is no systematic trend for the influence of diameter upon this value. If the ratio of disturbance level to diameter is evaluated, as is usually done, again no diameter dependence emerges. However for a fixed diameter, the disturbance level certainly increases with

increasing velocity. Even if we remember that gravity does play a role at very low speeds (which will give a calculated value of the initial disturbance which is too low) this argument cannot be used for higher velocities. A physical explanation might be as follows.
The fluid that constituted the laminar sub-layer is brought into turbulent movement after it is discharged into the free jet. As the velocity is the pipe increases, the thickness of the sub-layer and hence the quantity of this fluid, is reduced. It is therefore easier for the macroscopic eddies to penetrate to the jet surface. As well as this the energy of the turbulent eddies is greater at higher velocities. The level of the initial disturbance must be of the same order of magnitude as the thickness of the laminar sub-layer and with increasing velocity be somewhat greater than this thickness.
For the nozzles and velocities used the thickness of the sub-layer varies between 2 and 3.10^{-5} m. Considering the value of the disturbance level ($1.5.10^{-5}<\delta_o<6.5.10^{-5}$ m) the trend of the line of thought is not contradicted but it must be admitted that this cannot be regarded as proof.

III.7 Behaviour of high velocity turbulent jets

The effect of eddies in producing distortions of the jet surface is mainly controlled by surface tension forces. With fast jets the influence of air friction forces must also be taken into account. These two factors make the shape of the surface too ill-defined to expect a simple mathematical expression to hold. Fig. II.7 showed a 5 mm jet with a velocity of 20 m/s which illustrates the phenomenon . The disruption is so violent that the persistence of long wavelength disturbances is not observed. Break-up lengths can only be determined with difficulty and the utility of such measurements is in any event doubtful.

The velocity at which the air forces distort the jet surface has been investigated by *Richardson* (1954) who used comparable jet diameters. According to him, that velocity is determined by a critical Weber number defined as the ratio of air friction forces to surface tension forces. Photographic observation led him to decide that the value of this Weber number is about 10. One must not confuse this Weber number with that of 5.3 previously reported by *Penn and Middleman* (1969). The latter determines the place of the observed maximum in the break-up curve where aerodynamic forces can no longer be neglected. The value given by *Richardson* is higher because it is that at which aerodynamic forces

visibly distort the jet. The factors affecting the shape of the jet influence each other; nearly all of them are dependent upon the same variables, viz. the properties of the fluid, the length and velocity of the jet and the diameter of the nozzle orifice. Photographs with a long exposure time were taken (fig. III.16) and from measurements of the width of the jet as functions of these variables we have been able to develop an empirical relationship for the spreading of a turbulent water jet.

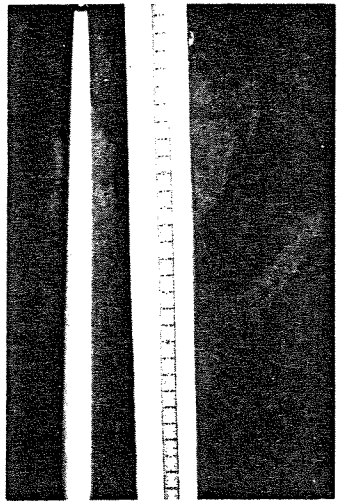

Fig.III.16 Long exposure photograph of the same jet as shown in fig. II.7

In order to find the important dimensionless groups we have considered the physical phenomena occuring in the system. The development of the velocity profile inside the nozzle and the persistence of turbulence are determined by the nozzle length to diameter ratio and the Reynolds number.
The influence of air friction is determined by two groups viz. Weber number and a Reynolds number based on the length along the jet. The physical meaning of the Weber number has already been discussed above. Re_L defines the development of the accompanying air boundary layer. The boundary layer is presumed to be laminar because the value of Re_L is always less than 5.10^5.
Turbulent pipeflow at higher Reynolds numbers (based on nozzle diameter) is slightly dependent upon that same Reynolds number (*Pannell (1972)*) but it is felt that a small change in the structure of turbulence does not significantly alter the issuing jetflow. Also for nozzle length to diameter ratios over 50 the shape of the jet is always the same. All the measurements were therefore done with long nozzles and the velocity was so high that the corresponding Reynolds number was over 50,000.
From fig. III.17 we derived the following equation for the local with of a high velocity water jet:

$$\frac{D^*}{D_n} = 0.125\ (We.Re_L)^{1/6} \qquad \text{(III.18)}$$

which is valid for $We.Re_L > 7.10^5$. D^* stands for the local width of the jet.

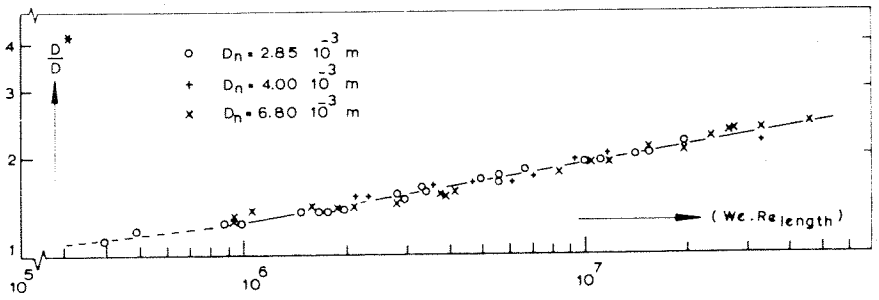

Fig. III.17 Average width of turbulent jet as a function of $We.Re_L$

III.8 Jet behaviour in relation to the air entrainment

In the low velocity region disturbances of the jet are responsible for the creation of cavities in the receiving liquid. All factors which influence the shape of the jet directly effect the amount of entrained air. The large difference in disturbance level of laminar and turbulent jets explains the remarkable increase of entrainment rate (*Lin and Donnelly (1966)*).
This chapter has dealt with the influence of turbulence upon the disintegration of the jet. An important fact is that the shape of a low velocity turbulent jet can be analysed with the same description given for laminar jets. The only modification arises because of the changed disturbance level. When the energy transfer to the target liquid and the reaction of that same liquid is known, all factors needed to calculate the amount of air are in principle present. For low velocity jets the response of the target liquid will affect the efficiency of capture of this entrained and conveyed air, as will be explained in the next chapter. However, jets usually have no regular shape and it is not only the fastest growing disturbance that controls the deformation of the jet. For that reason an approximation of the air entrainment cannot be simple.
The correlation obtained for the spreading of the high velocity jet will enable us to give an approximation of the amount of air carried within the jet. A closer view of the entrainment mechanism showed (chapter II section 3) that air carried along with the jet surface (as distinct from that within the jet envelope) is brought under the water surface. Estimation of this induced air flow can also probably now be made.

Chapter IV

ENERGY TRANSFER AND CAVITY FORMATION IN COLLISIONS WITH LIQUID SURFACES

This chapter deals with the phenomena that occur when a liquid surface is distorted by the impact of objects. After a general introduction collisions of drops or a 'train' of drops upon the surface are considered. The experimental equipment, which is described in detail, allows a close examination of the events after impact. After considering the shape of the cavity that is formed, a theoretical model is derived which gives the time dependency of cavity depth. Experimental verification with distilled water shows a good agreement between theory and experiment. Also data of other workers are compared.

In the light of the theoretical predictions of the single droplet impact, the effect of subsequent droplets is studied. The photographic technique is the same excepting for the drop supply equipment. Cavity shapes are considered and theoretical prediction match the experimental evidence. The last paragraph of this chapter evaluates the relation between jet and drop impact.

IV.1 Introduction

The behaviour of a liquid surface after the impact of an arbitrary object is only slightly understood. Experiments during the last 40 years have not solved the impact problem and theoretical approximations are limited to particular cases. *May* (1970) gives a review of water entry theories and data which is particularly relevant to the impact of missiles. This review draws attention to the gaps existing in current literature. Buoyancy forces, cavity shapes and friction drag are only determined experimentally and his conclusion is that in spite of all the data much work is required before the water-entry regime can be treated on a scientific and precise basis.
In 1971 *Abelson* used *Birkhoff's* method (1951) to calculate cavity shapes caused by impacts of bluff-nosed projectiles. His calculation is however only applicable to impacts of solid missiles and not for the impact of liquid elements, because he used the knowledge already existing of the cavity running drag coefficient which is less relevant for liquid-liquid collisions.

The literature concerning impact of liquid elements is

limited to the collisions of drops with liquid surfaces. Since *Worthington* in 1882 reported his first qualitative results of the impact phenomena a lot of experimental data has appeared. The complete work of *Worthington* is covered by the book 'A study of splashes' (1908) which described qualitatively the cavity formation and explained the existence of the so-called 'Rayleigh jet' originating from the bottom of the cavity.
In 1962, 1966 and 1967 *Engel* published three papers in which she derived expressions for the cavity depth as a function of time and impact energy. Her calculations were based upon the energy conservation law. However the starting point of her analysis has no physical meaning. She arbitrarily assumed that only half of the total impact energy is transferred to the target liquid. Likewise the proposed velocity potential in the target liquid does not, even approximately, satisfy the Laplace equation.
The work of *Hobbs*(1967) and *Macklin* (1969) concerned measurements of the number of spray droplets produced from the crown resulting after impact and their charge to mass ratio. Also they investigated the relevance of the depth of the target liquid to impact phenomena. It was found that with depths of 25 mm or greater the impact and consequent cavity formation is the same as for splashing on a deep liquid. The impinging drops have a diameter of about 3 mm.
Jenkins (1967) studied the high speed impact of liquid drops using equipment in which the liquid surface is moved with a speed of 47.7 m/s against a stationary drop of 1.75 mm diameter. However the results he obtained did not agree with earlier work, possibly because his complex and artificial measuring equipment.

Although a lot of experimental work has been done and a few theoretical approximations tried no reliable theory is available in literature at the moment which predicts the cavity growth as a function of time and impact energy. Therefore the impact phenomena of an impinging single drop will be critically analysed in order to develop a theoretical model which will be dealt with in the next paragraph. Also the events associated with the impact of subsequent falling drops will be considered.

IV.2 The impact of single droplets

IV.2.1 Experimental equipment

The most important components are a high speed camera, a time delaying electronic circuit, a spark light source and a

watertank. The watertank is a round reservoir of 30 cm diameter and 45 cm high. The water surface is maintained 30 cm above the bottom. On a level with the watersurface there are four windows which allow a close view of the impact. The dimensions of the tank were sufficient to assure no wall or bottom effects. Wall effects only occur when the diameter is less than five cavity diameters (*May (1951)*).
The kinetic energy of the drop is varied by using different heights of free fall. To ensure that the drop lands in the middle of the tank it falls along the axis of a protecting pipe.
The high speed camera (type 61112, Strobodrum, Impuls Physic GmbH) has a fixed open shutter and is hence used in a dark environment. Camera and spark light source are placed at opposite sides of the tank, with the latter at the focus of a positive lens. A parallel light beam with a diameter of 5 cm illuminated the area of drop impact. The spark frequency could be chosen to suit the drum speed of the camera.
The procedure for filming was as follows. The camera was brought up to speed and the dripper activated to produce a drop. The falling drop passes a photocell. The pulse from the cell is delayed by the circuit whose block-scheme is given in fig. IV.1. The delay time is hence chosen so that the spark discharge generator is started by the delayed pulse when the drop is just above the water level.

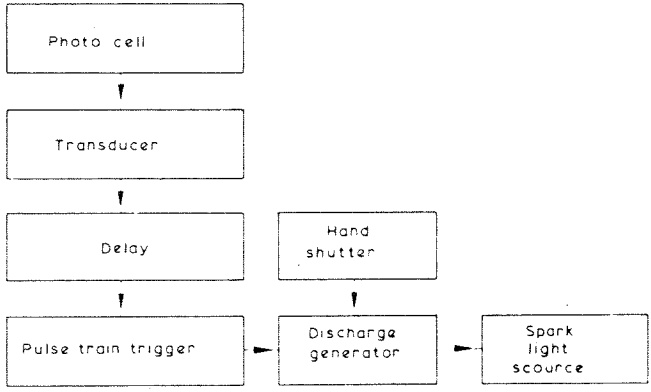

Fig. IV.1 Block scheme of electronic delay circuit

In order to measure distances under and above the water level, several calibration films were made. The total accuracy of the measurements is within 0.1 mm.

IV.2.2 Qualitative description of impact phenomena

The events following the drop impact are shown in fig. IV.2. The impinging drop produces a hemispherical cavity and a cylindrical wave in the target liquid. Above some critical impact velocity (our measurements give a value of 5 m/s independent of the mass of the drop) a thin film rises out of the edge of the wave due to surface tension forces. This film can sometimes close above the cavity and form a bubble dome (fig. IV.3).

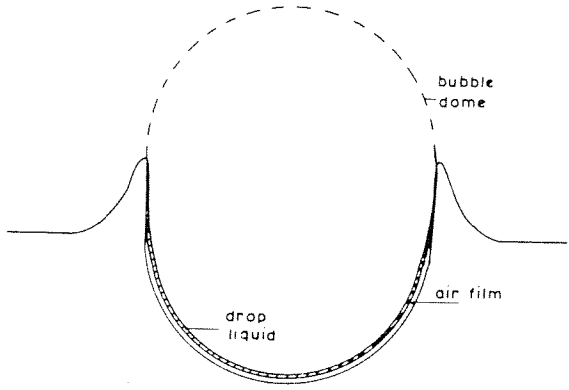

Fig. IV.3 Sketch of cavity shape. The dotted line represents a bubble dome which is formed when impact velocities exceed 5 m/s

Immediately after impact the target liquid starts moving. At the same time the drop spreads out over the bottom of the cavity. This process occurs within a few tenths of a millisecond. Photographic observation shows that a thin layer persists (possibly an air film) which separates the liquid of the impinging drop from that of the target liquid (fig. IV 2). This thin layer has not been previously reported. The layer can remain for a relatively long time (of the order of 25 ms). The presence of this layer is not well understood. In this context fig.IV.2b is particularly important. The original drop fluid is clearly seen to have a horizontal upper surface at this short time after impact (+ 1 ms) despite the fact that it is being observed through a highly curved air/water interface. The subsequent development of curvature of this uppersurface can easily be followed on the original photographs and it proves that this double layer is not simply an optical illusion.

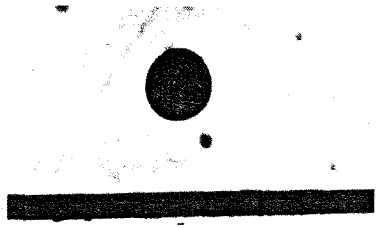

a. - 3 ms

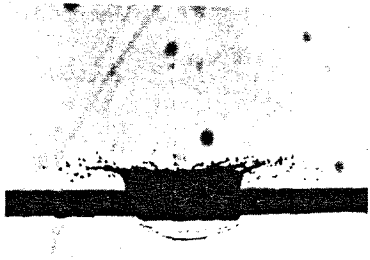

b. 1 ms

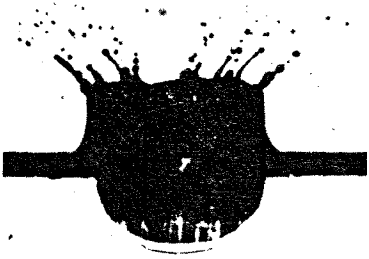

c. 7 ms

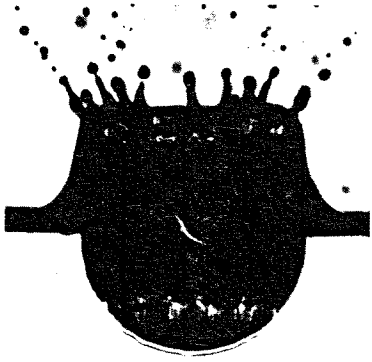

d. 13 ms

e. 17 ms

Fig. IV.2 Impact of water drop against a water surface. Cavity growth as a function of time (Impact energy 31.10^{-5} Nm)

Two possible explanations for the existence of the thin layer are:

1. The air film that must exist between the drop and target liquid immediately after impact cannot escape quickly enough because the drop itself is also spreading out. One must remember that the entire duration of cavity formation is only a matter of milliseconds;
2. the high pressure between the drop and the target fluid causes the movement of the target liquid. This movement itself hinders a direct mingling of the molecules of the drop with the molecules of the target liquid. The surface molecules of the drop and those of the target liquid will still be ordered; they are subject to surface tension forces and are being further stretched rapidly. This could also lead to the existence of two separate surfaces, each possessing surface energy.

Another phenomena strengthens the hypothesis of the persistence of this layer. After the cavity has reached the maximum depth the flow reverses and a Rayleigh jet rises from the bottom of the cavity. Experiments with coloured drops (*Worthington (1908) and Engel (1966)*) show that this jet consists largely of the original drop liquid.

All the elements needed to analyse the problem are now given. The theoretical model of *Engel* (1967) did not consider the existence of the thin layer. Visible observation also shows that the transfer of impact energy to the target liquid is not restricted only to the moment of impact itself. Both surfaces are deformed and the transfer of energy continues. This is essentially different from her assumptions. Her analysis was based on the hypothesis of instantaneous transfer, at the moment of impact, of just half of the total import energy to the target liquid while the other half remains in the drop. This rather illogical assumption will be shown to be unnecessary.

IV.2.1 Theoretical analysis

Fig. IV.4 shows the coordinate system used. Below the original water surface spherical coordinates are chosen in which r is the distance from the central point of impact and θ the angle between the normal at the surface and the radius r. Above the water surface we use cylindrical coordinates in which r is again the radius and h is the height above the water surface. R_c is the radius of the cavity wall.

By considering the shape of the cavity crater, the cylindri-

cal wave and the bubble dome, *Engel* (1967) was able to derive expressions for the energy content of each of these three regions. We use the same procedure; however the values we have calculated are different and we have added the contribution of the spreading drop.

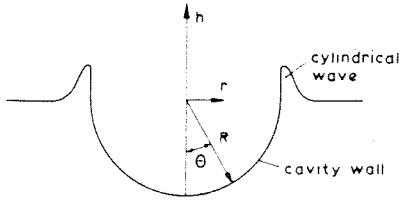

Fig. IV.4 Coordinate system for analysis

As far as the gravitational potential energy is concerned, the most important contributions came from the liquid originally present in the hemispherical cavity and that in the circular cylindrical wave. The gravitational energy is the work needed to bring a particle from one place to another under the influence of gravity. So in general this energy is given by (cylindrical coordinates)

$$U = \pi \rho_w g \int_{r_1}^{r_2} h^2 r \, dr \qquad \text{(IV.1)}$$

First we consider the cavity crater. After the first few milliseconds it has a hemispherical shape and therefore the relation between h and r is:

$$h^2 = R_c^2 - r^2 \qquad \text{(IV.2)}$$

Substitution of eq (IV.2) into eq (IV.1) gives:

$$U = \pi \rho_w g \int_0^R (R_c^2 - r^2) \, r dr = 0.25 \, \pi \rho_w g \, R_c^4 \qquad \text{(IV.3)}$$

In the case of the cylindrical wave, the difficulty is to find an analytical expression for h, the vertical coordinate of the free liquid surface. Since that the volume of the wave must be equal to the volume of the crater, *Engel* (1966) proposed the relationship

$$h = R_c^4 / 3r^3 \qquad \text{(IV.4)}$$

However, experimental observation by both *Engel* and ourselves shows that at $r = R_c$ (i.e. the lip of the cavity) the height of the wave is $0.8 \, R_c$ so eq(IV.4) is not a realistic approxi-

mation. Therefore, we have tried to find another expression which also satisfies this condition. The two conditions to be satisfied are:

$$2\pi \int_{R_c}^{\infty} h.r.dr = \frac{2\pi R_c^3}{3} \qquad \text{(IV.5)}$$

and, at $r = R$, $h = 0.8\ R_c$ (IV.6)

Substitution of a function of the form

$$h = \frac{c_1}{r^3} + \frac{c_2}{r^4} \qquad \text{(IV.7)}$$

in equation (IV.5) and (IV.6) gives the result:

$$h = \frac{-2R_c^4}{15r^3} + \frac{14R_c^5}{15r^4} \qquad \text{(IV.8)}$$

It must be admitted that eq (IV.8) does not exactly describe the shape of the wave, because in reality it is not as smooth as eq (IV.8) predicts, but we believe it to be a reasonable approximation.

The substitution of eq (IV.8) into eq (IV.1) leads to:

$$U = 0.11\ \pi \rho_w g R_c^4 \qquad \text{(IV.9)}$$

The total gravitational potential energy is the summation of the terms given in eq (IV.3) (the contribution of the cavity crater) and eq (IV.9) (the contribution of the wave). We have neglected other terms because they are at least an order of magnitude smaller

$$U_{pot} = 0.36\ \pi \rho_w g R_c^4 \qquad \text{(IV.10)}$$

The energy of newly generated surface of the wave can be calculated with the following expression (cylindrical coordinates)

$$U = 2\pi\sigma \int_{R_c}^{\infty} r\{1+(\frac{dh}{dr})^2\}^{\frac{1}{2}} - 2\pi\sigma \int_{R_c}^{\infty} rdr \qquad \text{(IV.11)}$$

Substitution of eq (IV.8) in (IV.11) gives, after numerical

integration:

$$U = 0.8 \pi R_c^2 \sigma \qquad \text{(IV.12)}$$

Also, the surface of the vertical wall of the wave with height o.8 R_c must be taken into account:

$$U = 1.6 \pi R_c^2 \sigma \qquad \text{(IV.13)}$$

Then the total surface energy of the wave is the sum of eq (IV.12) and (IV.13)

$$U = 2.4 \pi R_c^2 \sigma \qquad \text{(IV.14)}$$

The surface energy of the cavity crater is:

$$U = 2\pi R_c^2 \sigma - \pi R_c^2 \sigma = \pi R_c^2 \sigma \qquad \text{(IV.15)}$$

The spreading drop also contains surface energy and this is equal to:

$$U = 2(2+1.6)\ \pi R_c^2 \sigma = 7.2\pi R_c^2 \sigma \qquad \text{(IV.16)}$$

The factor 2 before the brackets represents the contribution of upper and lower surfaces. The term 2 within the brackets comes from that which covers the whole hemispherical cavity and the term 1.6 from the fluid lining the cylindrical wall above the original water surface. When the impact velocity is higher than 5 m/s an additional term is needed which expresses the surface energy of the bubble dome. The mass of the thin film is negligible, but the surface energy can be approximated by assuming the dome has a hemispherical shape and rests on the cylindrical wall. Therefore the additional term is equal to:

$$U = 4\pi R_c^2 \sigma \qquad \text{(IV.17)}$$

remembering that the film has two sides.

In total the energy of newly generated surface is now equal to the sum of all contributions of the various parts:

$$U_{surf} = B\pi R_c^2 \sigma \qquad \text{(IV.18)}$$

with B = 10.6, when $v < 5$ m/s and B = 14.6, for $v > 5$ m/s.

Kinetic energy must also be considered. The velocity of the target fluid must be known as a function of time and co-ordinates. One can define a velocity potential which meets the boundary conditions of the actual flow. The first trivial condition is that all velocities are zero when r and t are infinite. In addition all velocities must be zero as soon as the cavity has reached the maximum depth as then all kinetic energy has been converted into potential energy. Further, the velocity potential must satisfy the Laplace equation $\nabla^2\phi = 0$.

Engel's proposal was a potential of the form:

$$\Psi = \frac{AR_c}{r} \cos \theta \qquad \text{(IV.19)}$$

However, this solution is open to the following objections: Firstly, eq (IV.19) does not satisfy the Laplace equation even approximately. Secondly, the r-component derived from eq (IV.19) is proportional to cos θ. This means that $\theta = \pi/2$ (at the original surface) no velocity in the r-direction exists, which is inconsistent with a spherical growth of the cavity. For this latter reason particularly we assume a velocity potential of the following form:

$$\Psi = A\, r^{-n} \cos {}^{\theta}/_{2} \qquad \text{(IV.20)}$$

which has a finite velocity component at $\theta=\pi/2$, and does satisfy Laplace's equation. Substitution of eq (IV.20) in the Laplace equation gives the following expression for the value of n:

$$n = 0.5 + 0.5\, (4-\cos^{-2} \theta/2)^{\frac{1}{2}} \qquad \text{(IV.21)}$$

θ varies from 0 to $\pi/2$, hence $1.21 < n < 1.36$. Because substitution of eq (IV.21) into eq (IV.20) gives a cumbersome expression, an approximation is made, i.e. it is assumed that $n = 1.3$. This has the consequence that Laplace equation is not exactly satisfied, but a calculation of the total kinetic energy term shows that in the final result of the equation, which describes the growth of the cavity the differences that arise as a result of the chosen values of n from 1.21 to 1.36 are less than 3%. A solution involving the exponent of r being a function of θ is obviously not worthwhile when the variation lies within such narrow limits, so the average value of 1.3 was taken for n in all subsequent stages of the analysis.

With the aid of the proposed velocity potential the kinetic energy of the target liquid can be estimated. The kinetic

energy is:

$$U = -\rho_w/2 \iint \Psi \left(\frac{d\Psi}{dr}\right) dS$$

Substitution of the velocity potential gives:

$$U = \rho_w/2\ 2.6\ \pi\ R_c^{-1.6}\ A^2 \int_0^{\pi/2} \cos^2 \theta/2 \sin \theta\ d(\theta/2)$$

$$= 0.975\ \pi \rho_w R_c^{-1.6} A^2 \qquad \text{(IV.22)}$$

The value of A can be found by considering the velocity of the cavity at $\theta = 0$, because that is the point where we measure

$$v_r = -\frac{\partial \Psi}{\partial r}\ ;\ v_r \Big|_{\theta=0} = 1.3\ Ar^{-2.3} \qquad \text{(IV.23)}$$

Hence for the fluid close to the interface at this point

$$\frac{dR_c}{dt} = 1.3\ Ar^{-2.3} \qquad \text{(IV.24)}$$

so:

$$A = 0.77\ R_c^{2.3}\ \frac{dR_c}{dt} \qquad \text{(IV.25)}$$

Substitution of eq (IV.25) into (IV.22) is not directly allowed. The value of A is dependent on the value of θ. However in the measurements we consider only the depth of the cavity, and because the velocity potential is only approximation, substitution of this value of A gives an estimate. Hence:

$$U = 0.58\ \pi \rho_w R_c^3 \left(\frac{dR_c}{dt}\right)^2 \qquad \text{(IV.26)}$$

Another term which we have to include is the kinetic energy of the spreading drop after impact. If we neglect the tangential spreading and the internal flow of the drop and only take the radial velocity into account, we get:

$$U = \tfrac{1}{2}\ m \left(\frac{dR_c}{dt}\right)^2 \qquad \text{(IV.27)}$$

in which m is the mass of the impinging drop.

Neglecting all other kinetic energies the total amount of energy is equal to the sum of eq (IV.26) and (IV.27)

$$U_{kin} = (\frac{m}{2} + 0.58\ \pi\rho_w\ R_c^3)\ (\frac{dR_c}{dt})^2 \qquad \text{(IV.28)}$$

IV.2.4 Equation for cavity depth

The energies which are not taken into account are smaller by at least one order of magnitude. These energies are associated with sonic and electrostatic forces and with viscous dissipation. The last of these is probably the most significant.
Application of the energy conservation law gives:
Energy before impact = sum of energies after impact
Hence:

$$E = U_{pot} + U_{surf} + U_{kin} \qquad \text{(IV.29)}$$

E is in the kinetic energy of the impinging drop. Substitution of eq (IV.10), (IV.18) and (IV.28) and rearranging:

$$\frac{dR_c}{dt} = \{\frac{E/\pi - 0.36\ \rho g R_c^4 - B R_c^2 \sigma}{0.58\rho R_c^2 + m/2\pi}\}^{\frac{1}{2}} \qquad \text{(IV.30)}$$

With B = 10.6 (v < 5 m/s) and B = 14.6 (v > 5 m/s).

The differential equation cannot be integrated analytically in a simple form. The integral may be easily evaluated, however, by any of the standard computer methods. However the equation can be interpreted by considering the form in which it stands.
At the moment of impact (t=R=0) eq (IV.30) reduces to:

$$\frac{dR_c}{dt} = (\frac{E/\pi}{m/2\pi})^{\frac{1}{2}} = v \qquad \text{(IV.31)}$$

This result is physically understandable. The velocity of the bottom of the cavity is equal to the impact velocity. The maximum cavity depth is reached when the numerator is eq (IV.30) is zero. Hence this maximum depth is directly related to the kinetic energy of the impinging drop.

One final remark about the equation for cavity depty and the approximation we have permitted ourselves. In a more detailed

analysis, not presented here, the dissipation energy was taken into account because we thought it was an energy that we could not neglect. However numerical integration of the much more complicated equation that corresponds to eq(IV.30) shows a result for water, which , as a result of the low viscosity, differs by only 1%.

IV.2.5 Results and concluding remarks

The first frames of each sequence of the photographic record would show the drop just above the water surface. From these pictures the mass, velocity and the kinetic energy are determined. Fig. IV.5 and IV.6 compare theory and experiment. The

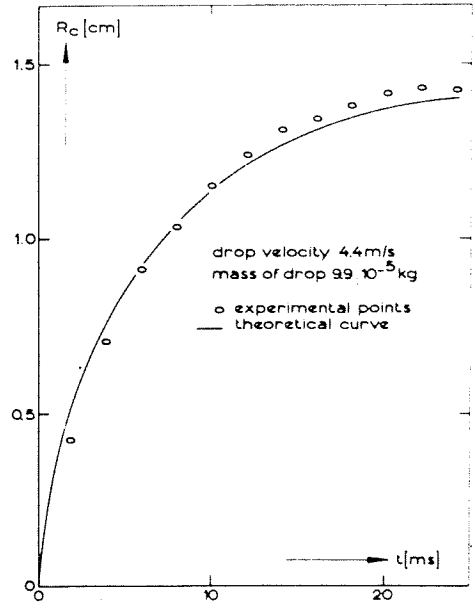

Fig. IV.5 Normal cavity growth with time

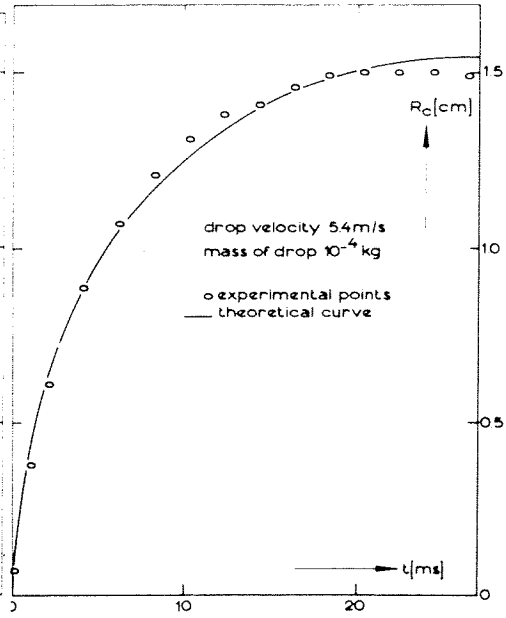

Fig. IV.6 Growth of cavity with bubble dome with time

value of B in eq (IV.30) is 10.6 for fig. IV.5 and 14.6 for fig. IV.6. Agreement between experiment and theory is satisfactory. The graphs given above are typical of all the measurements.
Table IV.1 gives a review of the data. The agreement gives support to the sometimes crude approximations of the various energies. The persistence of the air layer between drop and target liquid is a necessary feature of this agreement, and when this is considered in association with the photographic

evidence, we believe its existence to be proved.

mass	kin. energy	max.cavity depth		dev.	time to reach maximum depth	
(10^{-3} kg)	(10^{-7} Nm)	(10^{-2} m		%	ms	
		meas.	calc.		meas.	calc.
0.09964	10714	1.38	1.47	6	25	26
0.03122	3109	1.02	0.96	5.5	22	20
0.101	14858 *	1.51	1.55	2.5	23	26
0.0638	9689 *	1.30	1.34	3	24	23
0.0838	11553 *	1.37	1.424	4	20	24
0.0371	6566 *	1.14	1.16	1.5	21	19
0.096	9958	1.37	1.44	5	26	25
0.098	9422	1.44	1.41	2	24	24
0.098	13013 *	1.51	1.48	2	25	24
0.100	4540	1.12	1.09	2.5	24	20

Table IV.1: Comparison of theory and experiment (*with bubble dome)

Comparison is also made between *Engel's* experiments and our theoretical model. However *Engel* also used much higher impact velocities nearly always producing a bubble dome. Moreover the height of this dome, with these high impact energies is reported by her to be $2R_c$, this implies an increase in the surface energy which can be accommodated in our equations by replacing the $4\pi R^2\sigma$ used in eq (IV.17) by $8\pi R^2\sigma$. Substitution in eq (IV.18) has to be with a value of B of 18.6. Therefore this value of B is chosen for impact energies greater than 18.10^{-4} Nm. Table IV.2 shows the result and again the agreement is good. In spite of these much higher impact energies the model including the air layer still leads to the correct result.

Concluding remarks

A model is developed to predict the craterdepths in target liquids after the impact of single liquid drops. This model is based upon the energy conservation law and experimental verification fits very well. The analysis is similar to that

mass	kin. energy	max. cavity depth		dev.	time to reach maximum depth	
(10^{-3} kg)	(10^{-7} Nm)	(10^{-2} m)		%	ms	
		meas.	calc.		meas.	calc.
0.0509	25247 *	1.77	1.78	0.5	26	26
0.0416	20345 *	1.56	1.65	5.5	26	24
0.0515	14639 *	1.48	1.54	4	26	24
0.055	20529 *	1.52	1.65	8.5	25	24
0.0484	18483 *	1.51	1.59	5	27	24
0.00133	1698 *	0.73	0.75	1.5	16	13

Table IV.2: Comparison of theory and Engel's data (* with bubble dome)

used by *Engel* (1967). However, a few fundamental assumptions are different:

a. At least during the initial stages of the impact, when most of the energy transfer takes place, a thin layer which separates the liquid of the drop from that of the target liquid persists;
b. the transfer of energy from the drop to the target liquid is essentially different, not being completed instantaneously;
c. the mathematical expression used to describe the form of the outer surface of the cylindrical wave is based on a higher order approximation; this gives a more realistic fit to the known height of the crest.

IV.3 Impact of subsequent drops

Usually studies of drop impact consider smooth surfaces of the target liquid. However in reality such surfaces seldom occur. The impingement of the subsequent drops or a cloud of droplets is much more common both in industry and nature. Almost no work has been done concerning cavity shapes and the consequences of multiple impact.
The only known publication is from *Sisco and Levin* (1971) who studied subsequent drop impact in order to examine some transport rates and atmospheric - electrification processes. Their investigation was primarily concerned with impact

phenomena in the presence of surface waves. The impinging drop interacts with the reflected wave produced by proceeding drops which had a time between impacts varying from 50 to 150 ms. Two extremes occur.
When a drop falls on a wave maximum, it amplifies the surface wave and it produces only a small Rayleigh jet. Conversely when it lands in a wave trough, the surface wave does not change significantly but in the first instance the extra energy is used to produce a much higher Rayleigh jet. When they considered the behaviour of actual rain drops falling into an ocean or a lake they concluded that because the two modes and the intermediate states are intermixed there is an increase in the diffusion (or dispersal), both horizontal and vertical, of substances - such as nutrients or pollutants - in the resevoir water.

IV.3.1 Experimental procedures

The equipment to measure cavity sizes was the same as that used for the single droplets except that the dripper was changed. We wished to vary the time between subsequent impacts from 1 to about 25 ms. (to allow the development of the maximum cavity size from the first drop) No dripper can produce droplets at such high frequencies. The only possible solution which is obvious in connection with this thesis, is a jet which is broken up. However we know that natural break-up is rather irregular. Therefore attempts were made to produce a train of drops with a regular separation and size.

The linear theory of *Rayleigh* (1945) predicts that at the break-up length a jet will disintegrate into equal drops. However his theory is only valid for regions in which the perturbations on the jet are small. The non-linear theories (*Chandrasekhar (1961), Yuen (1968), Wang (1968), Nayfeh (1970)*) can consider the shape of the jet near the break-point. *Rutland* and *Jameson* (1970) measured drop sizes and compared these sizes with those predicted by *Yuen* (1968) using his non-linear theory. This theory says that alternate main and satellite drops are formed which usually have different diameters. However when there is a disturbance on the jet which has a wave number ($= \pi D/\lambda$) between 0.35 and 0.50 the main and satellite drops are of approximately the same size. The maximum instability occurs for wave numbers of 0.7 so imposing a harmonic oscillation will produce a regular drop train.

The arrangement used to introduce these disturbances is

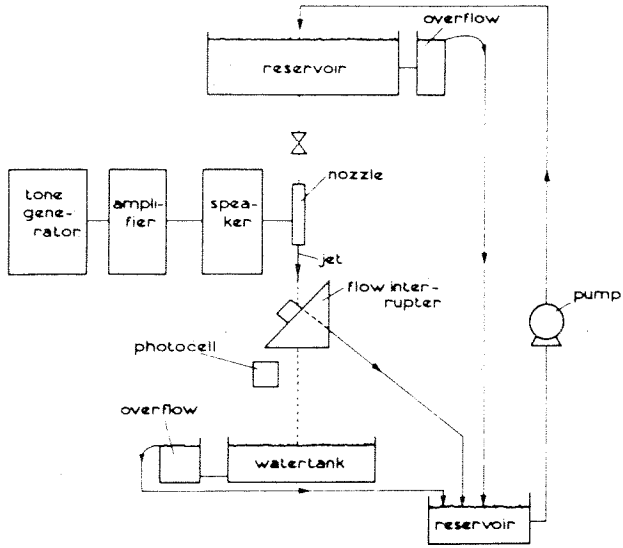

Fig. IV.7 Arrangement of drop train apparatus

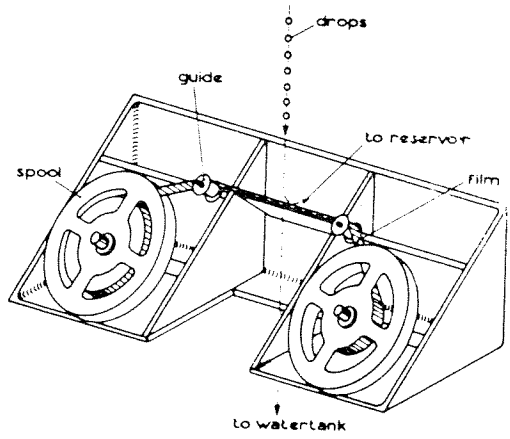

Fig. IV.8 The flow interrupter

shown in fig. IV.7. A loudspeaker connected to a tone generator and an amplifier is attached to the nozzle. The jet of distilled water issues from the nozzle and by making use of stroboscopic light the frequency of the generator is adjusted until uniform drops appear. In the meantime the water is flowing via a 'flow interrupter' into a reservoir and pumped again to the topreservoir. When the stream of drops is uniform the interrupter is opened and the drops pass the photocell from which the pulse is delayed by the same circuit as described in section 4.2.1.

This interrupter is of special design. The minimum interimtime of successive drops is about 8 ms. Therefore the opening time of this interrupter must be less than 3 ms in order to have a change of making good high speed pictures. This difficulty was solved by winding up an old cine film, 20 m long on one spool and releasing the film to another which is driven on by an electromotor (fig. IV.8). A 20 meter film is needed in order to allow the electromotor to develop full speed. The film now moves with a velocity of about 10 m/s. In terms of distance over which the drop can be influenced (say 4 mm) this means an opening time of 0.4 ms.

With this equipment about 30 runs were made. Because the variation of parameters (mass, velocity of droplets and interimtime) was bounded by the possiblities of the equipment and also by the natural difficulties of high speed work, the number of good films was limited to about 10 that were suitable for measurement. The variations of the parameters was therefore also limited. The velocity was varied between 3.7 to 5.1 m/s, the mass between 1.15 to 2.9 10^{-5} kg and the interimtime between 7 and 24 ms.

IV.3.2 Description of cavity shapes

The first impinging drop creates the hemispherical crater. When the second drop impacts it strikes the bottom of the crater, which may still be developing. An example of impact at the moment of maximum development is shown in fig. IV.9. The depth of the primary cavity immediately decreases and it becomes flatter. This phenomenon always happens irrespective of whether the cavity crater is still growing or has reached the maximum size. The secondary cavity produces radial streamlines and these lines interact with the streamlines associated with by the primary impact.
The second drop hits the cavity bottom and since the energy transfer cannot be instantaneous the spreading drop will push against the secondary cavity wall for a certain time.

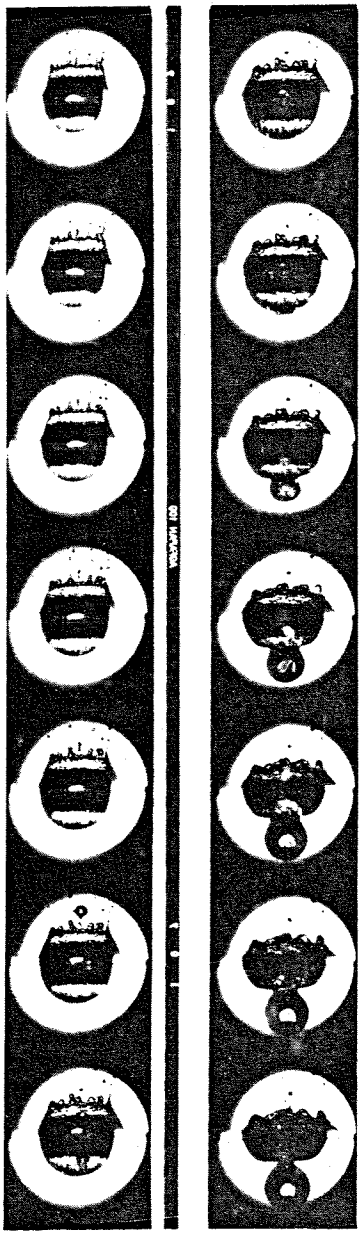

Fig.IV.9 Subsequent drop impact at moment of maximum primary cavity development

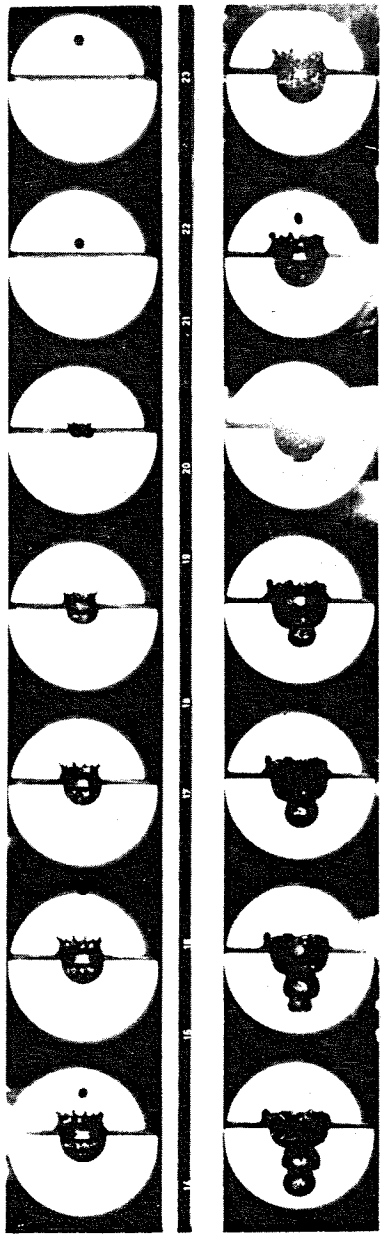

Fig. IV.10 Impact of drops with short interimtime

The existence of the primary cavity and the interaction between the flow fields of both cavities hinders a growth of the secondary cavity near the bottom of the first. The secundary cavity can more easily grow below the first one and the result is a more spherical shape. The normal recovery of the primary cavity may lead to the necking off and separation of the second one, when a spherical bubble is left under the waterlevel.

In fig. IV.10 the interimtime τ is less so that the first cavity is still growing at the moment of second impact. The base of the first cavity flattens immediately. The secondary cavity grows but in the situation shown a third drop appears which strikes the bottom of this. The secondary cavity does not grow significantly further radially and an elongated cavity hole remains which ultimately loses its form and is closed by the impact of the following drops.

As is shown by the last two figures, these multiple impact phenomena are highly complicated and a calculation similar to that succesfully applied to the impact of single drops appears impossible. The interaction between the various streamlines cannot be expressed in mathematical terms and the total energy transfer depents upon the interimtime τ. However with the knowledge acquired from single droplet impact some aspects of secondary cavity growth can be predicted reasonably.

IV.3.3 The size of the secondary cavity

According to eq (IV.30) the maximum cavity size of the primary crater is directly related to the impact energy. Therefore it seems obvious to see if the secondary cavity is also dependent on this energy, even if this assumption cannot be made in advance since the interaction between the primary and secondary cavities is not known.
At the moment of secondary impact the primary hemisphere stops growing immediately, which implies that all the energy that remains from the impact energy of the first drop now is used in developing the secondary cavity. This means that when the interimtime between subsequent impacts is short the secondary cavity will be larger than for longer interimtimes. Therefore if we want to investigate the direct influence of the kinetic impact energy alone we must choose situation in which the interimtime is the same for both measurements. First we compare two situations in which the interimtime and impact energy are approximately the same, but the mass and velocity are different. The resulting secondary cavity growth

will be the same if its development is controlled by energy and not by momentum balances. The data are plotted in fig. IV.11. The kinetic energy is approximately the same in the two cases. If we compare the data and consider that the mass and velocity are different for both situations the first impression is that the kinetic energy is an important parameter. However a closer view of the data shows that the larger cavity was produced with less energy. This seems to contradict previous findings. The reason almost certainly lies in the fact that the interimtime τ is not exactly the same. Because this interimtime is very short (7 and 8 ms) the primary craters were still growing at the moment of impact. The residual energy not at that moment used in forming the primary cavity can be calculated with the aid of the equation derived for the single drop impact.
This available energy is equal to:

$$E_{av} = E - U_{pot} - U_{surf} \qquad (IV.32)$$

in which all the energies are evaluated at the moment of secondary impact. Substitution of the various terms expressed in the equations (IV.10) and (IV.18) gives:

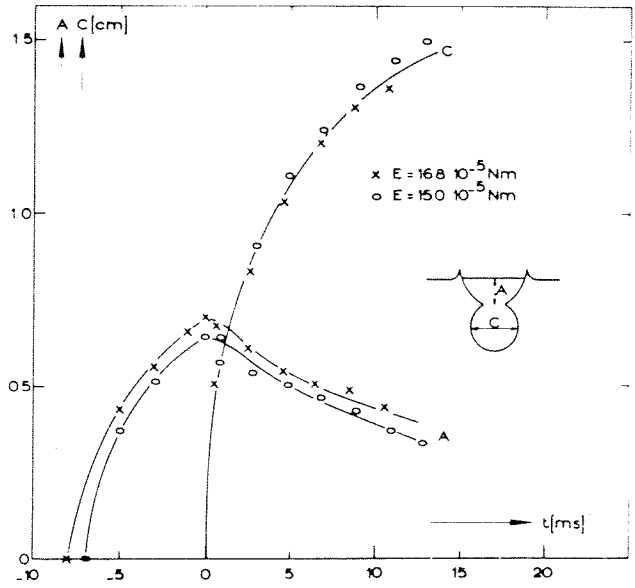

Fig. IV.11 Primary and secondary cavity growth. Drops of different mass but similar energy.

$$E_{av} = E - 0.36\ \pi\rho g R_c^4 - B\pi R_c^2 \sigma \qquad \text{(IV.33)}$$

When this amount is added to the impact energy of the second drop the total energy used for the secondary cavity growth is approximately known. Evaluation of R_c at the moment of impact with eq (IV.30) and substitution of the numerical values in eq (IV.33) gives than for the total energy of the two situations values of $19.8.10^{-5}$ Nm and 19.10^{-5} Nm respectively. The former corresponds with the upper points in the graph so the apparent paradox is resolved.

Fig. IV.12 shows the influence of increasing impact energy. The interimtime is the same and one can see that the greater secondary cavity is produced by the drop with the higher value of impact energy, which corresponds with the theoretical expectation.

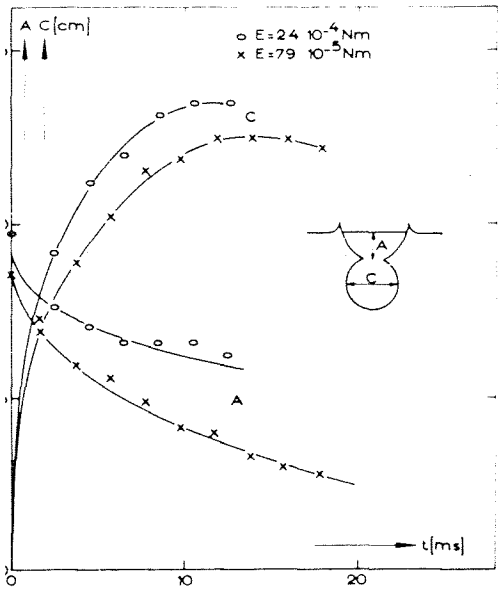

Fig. IV.12 Secondary cavity growth. Drops of different energy content

The influence of variation of the interimtime is clearly shown in figs.IV.13 and 14. Fig. IV.13 compares the situation of a still growing hemispherical cavity with one which has reached the maximum size. The impact energy is in both cases approximately the same. However when one compares again the total available energies the deviation between both curves is quite understandable.
In fig. IV.14 one of the curves belongs to a situation from which the depth of the primary cavity decreases (maximum depth has been passed) and the streamlines are reversed, so it has a negative contribution to the impact energy. This can easily be seen by comparing the two curves because although the impact energy of the described situation is 1.5 times the impact energy of the other case the cavity dimension is approximately the same.
It is difficult to draw firm quantitative conclusions about the

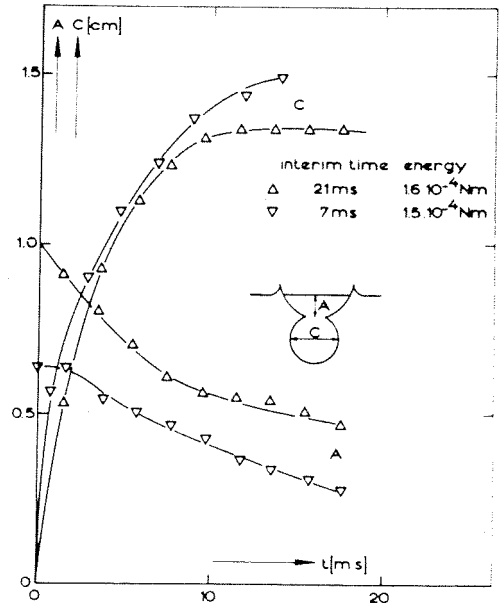

Fig. IV.13 Growth of secondary cavity. Influence of available energy

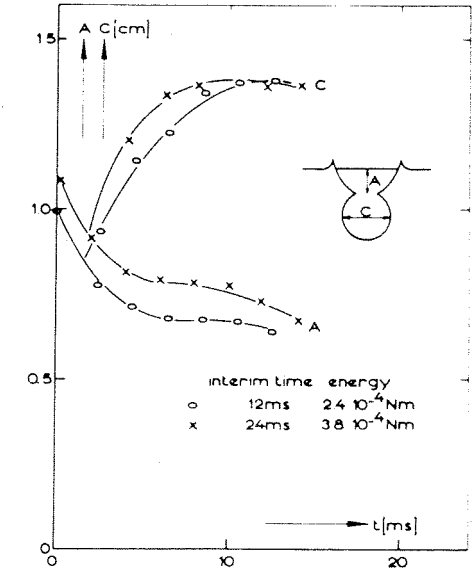

Fig. IV.14 Growth of secondary cavity - primary growing or recovering

secondary cavitation process. However it is clear that energy considerations are controlling and that the important influence of the time-interval between successive impacts can logically be considered in these terms also.

IV.4 Relation between jet and drop impact

The disturbances on a jet deform the surface of the receiving liquid. Particularly when these deformations are large the liquid surface is highly deformed. High-speed films of the impact of such distorted jets look very similar to the photographs of multiple drop impacts (Fig. IV.9 and 10). Primary cavities develop and in the bottom of such cavities secondary cavities are created which also have globular shapes. Even tertiary and quarternary cavities can be observed. However in the jet case the cavity formation is even more complicated because of the irregular character of the jet disturbances.
With small disturbances on the jet, the deformation energy is much less and the air entrainment will therefore decrease. The study of drop impact shows that the process of cavity formation is mainly ruled by this deformation energy. Theoretical predictions of the amount of entrained air as function of the various parameters should in principle be possible therefore.

Chapter V

THEORETICAL CONSIDERATIONS CONCERNING THE AMOUNT OF ENTRAINED AIR

This chapter describes the theoretical difficulties which are encountered if the results of chapters III and IV are to be combined. For short jet lengths no predictions are given, since theoretical description of the jet shape is impossible because of the complexity of the interacting phenomena. As soon as definite rotational symmetric deformations appear on the jet surface, some attempt can be made to generate reasonable forecasts.
The second paragraph is devoted to a model which can be used to estimate the amount of entrained air in the high velocity region.

V.1 Entrainment with low velocity jets

With the results of the previous two chapters a qualitative insight is gained about the factors which control the amount of entrained air. Both chapters indicate that a quantitative approach of the problem is hampered by the complexity of the phenomena. A mathematical description of the shape of the jet can only be approximated by a Fourier series of which not all the components are known.
The recovery processes occurring in the pool due to the interaction between the jet- and the liquid surface are regulated by the kinetic energy of the mass associated with the jet surface deformations. No exact expression which relates cavity sizes and volumes to energy is known. The predictions presented in this section are therefore limited to simplified approximations of the parameters which describe the air entrainment.

First we consider the volume present in the irregularities of the jet surface. The shape of the jet can be described by:

$$r = R_j + \sum_{i=1}^{N} \exp(a_i x/v_j) \cos K_i x \qquad (V.1)$$

with a sufficient number of terms (i.e. values of i), all possible (rotationally symmetric) disturbances of the jet can be described. However for shorter lengths of the jet eq (V.1) is not applicable since in this region the deformations are not symmetrical. Growth factors cannot be analysed and are therefore unknown.

The irregular distortions are dominated by rotation symmetric deformations only for jet lengths that are near the break-up point. These deformations are described by the theories of *Rayleigh* and *Weber*. Because the analyses pointed out that these distortions are ruled by rapidly growing exponential functions, the shape of the jet can only be approximated near the break point. With the mathematical expressions derived for the jet shape, and the modification of the value of the initial disturbance level, the kinetic energy of the mass inside the disturbances on the jet surface can be estimated. However such a calculation would lead to very complicated expressions.A more simple approach is therefore proposed. Near the break point these rotation symmetric deformations hit the receiving liquid surface. Because most of the jet liquid is concentrated inside the 'swell' of the disturbances and only a minor part in the 'necks', it is reasonable to suppose that the kinetic energy which creates cavities is alsmost the same as the total kinetic energy of the jet stream. The jet is considered as an 'train of drops'. For impacting drops the formation is an energy controlled process, so the amount of entrained air can be expected to be a direct function of the kinetic energy of the jet, i.e.:

$$\phi_A = \text{Function } (\tfrac{1}{2}\rho_w \frac{\pi}{4} D_j^2 v_j^3) \qquad (V.2)$$

This function is independent of the jet length although only values near or beyond the break-up length are allowed. The most simple form of the function in eq (V.2) would be a linear relation-ship but at this stage of the investigations this is only conjecture.

As is pointed out the entrainment for shorter lengths cannot be analysed theoretically. Even quasi-theoretical prediction is difficult. It seems reasonable to adopt a simple approach and assume that again the kinetic energy is the controlling parameter. This energy also determines the eddy distribution and migration. However the influence of surface tension is unknown. Both the decay of turbulence and the damping out of the distortions has a jet length dependency. With these facts in mind the simplest group which might be a parameter for the entrainment is proportional to:

$$D_j^2 v_j^3 L^a$$

in which a can be determined experimentally.
It should not be forgotten that the impact angle is also an important parameter. With decreasing angle the entrainment

increases. In the first place the contact area between jet and pool liquid is inversely proportional to sine α (where α is the angle between jet and the pool surface). The horizontal velocity component also has this dependency and both factors will influence the entrainment. Again the simplest approach is suggested and a relation-ship of the form

$$\dot{\nu}_A \sim (\text{sine } \alpha)^{-b} \qquad (V.3)$$

will be sought in which b lies between 1 and 2. Combination of the supposed parameter dependencies gives the equation:

$$\dot{\nu}_A = \text{function } \left(\frac{D_j^2 v_j^3 L^a}{(\text{sine } \alpha)^b}\right) \qquad (V.4)$$

Because these simple approaches consider only parts of the jet length it cannot be known beforehand to what extent the latter parametergroup and the previous one (eq V.2) are valid. This can only be determined from experimental data. The parameters which occur in the equations must, in accordance with the assumptions, be determined at the point of impact. The influence of gravity cannot be neglected especially at very low velocities. The effect will be to change the diameter, velocity and angle of impact from those values that obtain near the nozzle.

As is clear the complexity of the entrainment process forces an approach which is so rough that an experimental verification is the only way to defend the arguments. We have studied the separate phenomena (chapters III and IV), but the results have made it evident that the total process is even more complicated than had been supposed.

V.2 Entrainment in the high velocity region

The behaviour of high velocity water jets is described in section III.7. A correlation (eq(III.18)) is derived experimentally which gives the jet envelope a function of the various parameters. The velocity used here is the average velocity of the jet at the point of discharge from the nozzle. However, the jet velocity decreases as a result of the action of air friction and an estimate of the decrease is difficult . On the other hand gravity will accelerate a vertical jet. The first assumption for a model is that these forces will balance each other and the velocity of the jet is essentially constant.
Comparing figs.III.16 and II.7 it seems reasonable to postulate that inside and at the rough surface of the jet a core

of air is captured and carried with the water. This air will travel with more or less the same velocity as the jet. The total amount of this air will be to a first approximation (neglecting the contraction of the jet at discharge):

$$\phi_{AI} = \frac{\pi v_j}{4} (D^{*2} - D_n^2) \qquad (V.5)$$

and together with eq (III.18)

$$\phi_{AI} = \frac{\pi v_j D_n^2}{4} (1.56.10^{-2} \, We^{1/3} \, Re_L^{1/3} - 1) \qquad (V.6)$$

Burgess et al (1972) assumed that only the air inside the jet is entrained. However we may also consider that at the periphery of the time-averaged jet an air boundary layer will be developed. Then the question arises as to whether this boundary layer in total is brought by the jet under the watersurface.
The jet itself introduces a flow in the receiving liquid whose streamlines at the plunging point, are directed parallel to the jet (*Häusler 1961*). A hole appears round the jet, not caused by the pressure of the air boundary layer, but by the flow of the liquid itself. This creates an underpressure which will help the entrainment of the captured air and the boundary layer. Therefore it is reasonable to assume that the total amount of entrained air is equal to the amount given in eq (V.6) added to the contribution of the boundary layer.

The calculation of the volume flow of a boundary layer is restricted to the case where it remains laminar, since no reliable solutions for a turbulent boundary layer are well established.
We assume that the velocity of the captive air inside the long time-averaged jet envelope is equal to the jet velocity. Thus one boundary concition is:

$$r = D^*/2; \; v_A = v_j \qquad (V.7)$$

According to eq (III.18) the rate of increase of the jet width is very small so we can reasonably take the boundary layer solution of a moving continuous cylinder with radius $D^*/2$ when there is no slip at the wall.
Sakiades (1961) developed an approximate solution. His analysis shall briefly be repeated. The increase of the total momentum flux in a cross section of the boundary layer must

be equal to the momentum flux from the jet wall:

$$\frac{d}{dx} \int_{r=D^*/2}^{\infty} v_A^2 \, 2\pi r dr = \frac{\pi D^* \tau_j}{\rho_A} \qquad (V.8)$$

Further be supposed that very close to the surface of the cylinder no momentum is lost by accelerating the fluid. So:

$$r = D^*/2; \; \frac{\partial}{\partial r}\left(r \frac{\partial v_A}{\partial r}\right) = 0 \qquad (V.9)$$

Only a logarithmic velocity profile will satisfy eq (V.9). *Sakiadis* chose:

$$\begin{cases} \dfrac{v_A}{v_j} = 1 - \dfrac{1}{\beta} \ln\left(\dfrac{2r}{D^*}\right) \text{ for } r < \dfrac{D^*}{2} + \gamma \\ v_A = 0 \text{ for } r > \dfrac{D^*}{2} + \gamma \end{cases} \qquad (V.10)$$

The coefficient β is related to the boundary layer thickness:

$$\beta = \ln\left(\frac{D^* + 2\gamma}{D^*}\right) \qquad (V.11)$$

Unfortunately this velocity profile does not satisfy the boundary conditions:

$$\frac{\partial v_A}{\partial r} = \frac{\partial^2 v_A}{\partial r^2} = 0 \text{ for } r = D^*/2 + \gamma \qquad (V.12)$$

Rotte (1969) therefore suggested a velocity profile that also satisfies eq (V.12)

$$\frac{v_A}{v_j} = 1 - \frac{2}{\beta^*} \ln\left(\frac{2r}{D^*}\right) + \frac{2}{\beta^{*3}} \ln^3\left(\frac{2r}{D^*}\right) - \frac{1}{\beta^{*4}} \ln^4\left(\frac{2r}{D^*}\right) \qquad (V.13)$$

Substitution of the velocity profile in eq (V.8) and applying Pohlhansen's procedure, a differential equation can be described to calculte β^*:

$$\{ e^{2\beta^*}(45\beta^{*-5} - \frac{585}{2}\beta^{*-6} + \frac{2835}{4}\beta^{*-7} - 630\beta^{*-8}) +$$

$$(\beta^{*-1} + 2\beta^{*-2} - \frac{9}{2}\beta^{*-3} - 30\beta^{*-4} - \frac{75}{2}\beta^{*-5} + 135\beta^{*-6} + \frac{2205}{4}\beta^{*-7} +$$

$$630^{*-8}) \} \frac{d\beta^*}{dx} = \frac{8\eta_A}{\rho_A v_j D^{*2}} \qquad (V.14)$$

A numerical solution of eq (V.14) has been obtained and after substitution of β^* into eq (V.13) the volume rate of dragged air can be calculated by:

$$\phi_{AII} = \int_{r=D^*/2}^{\infty} v_A \, 2\pi r dr \qquad (V.15)$$

For the evaluation of this integral, see section VI.6, fig. VI.13.
The total amount of air carried by the jet is:

$$\phi_A = \phi_{AI} + \phi_{AII} \qquad (V.16)$$

Eq (V.16) predicts the entrainment for a laminar boundary layer.

The transition to turbulence for a boundary layer on a moving continuous cylinder is not known. *Tsou et al* (1967) found experimentally a transition to turbulence for a moving continuous flat plate at:

$$Re_L = 1.5.10^5$$

Therefore we expect the transition to turbulence for the cylinder to occur at a length based Reynolds number between 10^5 and 10^6.
In the case of a turbulent boundary layer, the air friction upon the jet increases. This results in a greater spreading and the prediction of the simple model will certainly underestimate the entrainment.

The boundary conditions in which the model can be used are therefore

$$We > 10; \; Re_L < 10^5 \text{ à } 10^6 \qquad (V.17)$$

Chapter VI

THE AMOUNT OF ENTRAINED AIR AS A FUNCTION OF THE VARIOUS PARAMETERS

After a general introduction which summarises the experimental correlation formulae and the equipment used by other workers our own measuring equipment is described. By considering the entrainment over the complete velocity range the different regimes which were predicted from the findings in previous chapters can be recognised. The following paragraphs therefore deal with the low- and high velocity regions.
Low velocity data are correlated in the way that was 'theoretically' expected. The entrainment in the high velocity region is also described by the proposed theoretical model.
Comparison is made with data from the literature.
This chapter ends with a summarising review of the formulae which describe air entrainment. These formulae relate specifically to turbulent jets.

6.1 Introduction

Data of the volume flow of air entrained by impacting water jets are limited to a few authors. All the correlations that have been obtained are based on experimental data.
Ohyama et al (1953) found the relationship:

$$\frac{\phi_A}{\phi_j} = 0.75\left(\frac{v_j^2}{gL}\right)^{-0.447}\left(\frac{D_j v_j \rho_w}{\eta_w}\right)^{2.18}\left(\frac{L}{D_j}\right)^{0.281} \qquad \text{(VI.1)}$$

The dimensionless groups (Froude and Reynolds numbers) which suggest a physical insight in the entrainment mechanism are of doubtful applicability. These authors used vertical jets and the only parameters varied were L, D_j and v_j. Their measurements probably cover both the low and high velocity regions and that could explain the spread of their data (which is sometimes 100%). The nozzles used were all short converging ones.
De Frate and *Kuo* (1969) present a much simplier equation:

$$\frac{\phi_A}{\phi_j} = 10^{-6}\left(\frac{\rho_A v_j^2 L}{\sigma}\right) \qquad \text{(VI.2)}$$

However their data deviate sometimes by a factor 20 from their correlating equation. No details were given of the

nozzle geometry.
The work of *Henderson et al* (1970) mainly considers high velocity jets. The measurements were done with nozzles which had a length to diameter ratio of zero, one and ten. The derived experimental correlation was:

$$\frac{\phi_A}{\phi_j} = \left(\frac{D^*}{D_j}\right)^2 - 1 \qquad \text{(VI.3)}$$

with D^* the diameter of the jet envelope as discussed previously. This equation states that only the air inside the surface roughness of the jet is brought below the water surface. Also this equation was of limited value because no method of predicting D^* was presented.
Ciborowski and Bin (1972) constructed the most complicated correlation:

$$\frac{\phi_A}{\phi_j} = 5.10^{-11} D_j^4 \left\{\left(\frac{v_j}{gL}\right)\left(1 - \frac{400}{We}\right) + 2 - A\right\}^{0.0479 D_j - 1.603} \left(\frac{L}{D_j}\right)^{1.8} \qquad \text{(VI.4)}$$

with the Weber number based on liquid density and A a 'constant' which depends on the jet parameters. The value of A varies between zero and one.

As is evident from this review of experimental data, the four correlations cannot be combined into one single expression. The reason for failure could be that various authors have used different nozzle geometries. Further, the distinction between high- and low velocity entrainment was not recognised and mixed data were correlated. For this reason all the correlating figures within the individual papers show a considerable spread of data.

Common to all investigations is a bubble trap device. Because most authors used vertical jets special precautions had to be taken in order to prevent air escaping from the trap. Fig. VI.1 shows the several experimental designs.
Rogers (1953) and *Ciborowski* (1972)(fig. VI a and d) used the same trap construction. Because in both cases the hole in which the jet plunges is rather large some entrained bubbles can rise to this hole and escape into the free air. Besides the air trap of *Ciborowski* is very small (depth is only 140 mm) which might be insufficient with higher jet velocities.

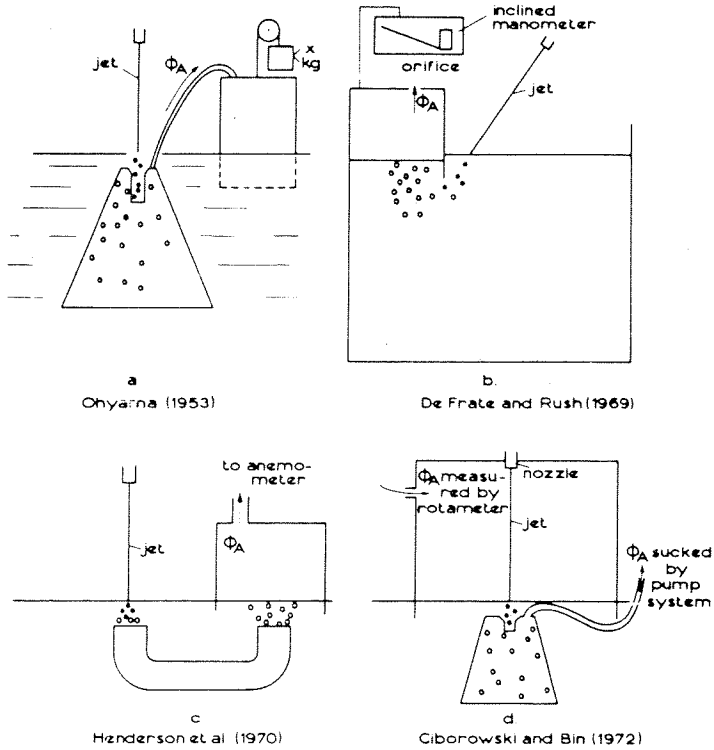

Fig. VI.1 Experimental arrangements used by various authors to measure the volumetric capture

In the low velocity region the sideways motion of the water is hampered by the solid walls of the inlet opening. In *Ohyama's* equipment the method of measuring the volume flow rate is less accurate. We can conclude that both apparatusses influence the entrainment itself and probably the measured flow rate of entrained air is too low.

De Frate and Rush (fig. VI.1b) measured only inclined jets. Because of the pressure difference between atmosphere and the bubble trap the water level in the latter is a few centimeters below the rest of the bath. This implies that the entrained air has to be carried laterally through the water before it enters the trap. From our own experiments it was shown that this way of measuring also gives too low a value of the volume flow rate.

Fig. VI.1c shows the apparatus of *Henderson et al* (1970). The air flow was pushed into a pipe and then conveyed to the metering station. A disadvantage of this measuring equipment is that it is only possible to use high velocities. The presence of the pipe in the bath must affect the circulation within the bath and hence it may influence the entrainment..

In all these arrangements the method of measuring can disturb the entrainment under certain circumstances and therefore a method was sought in which this disturbance was minimised.

VI.2 Experimental apparatus

Obliquely impacting jets produce air bubbles which rise at some distance from the plunging point. When the entrained bubbles have to be collected, the choice between using vertical or inclined jets favours the latter. The reason for this is that only at one side of the plunging point the flow pattern can be disturbed. If this disturbing influence can also be minimised, the best way of measuring is obtained. No method of measuring volume flow rates without changing the natural situation is possible.

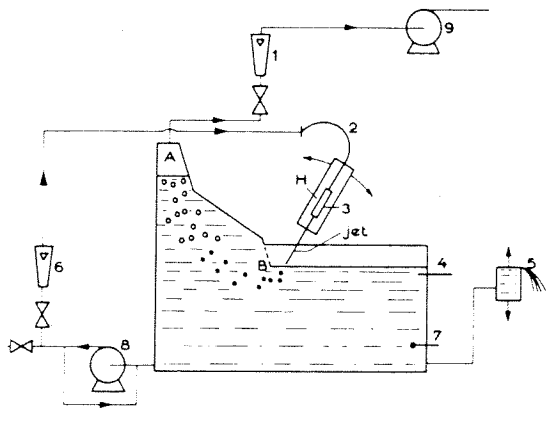

rotameter
ih pressure tube
zzle
4 supply of water
5 overflow
6 water rotameter
7 thermometer
8 waterpump
9 vacuum pump

Fig.VI.2 Experimental apparatus

A sketch of the apparatus used is shown in fig.VI.2. The water level, adjusted by means of an overflow, just reached point B; there are scarcely any solid surfaces close to the jet. All bubbles which rise come into compartment A, which was kept at a constant underpressure. This way of measuring eliminates the need for air bubbles to be brought to a pressure above atmospheric (below a water seal) before they reach the metering station. The air collected in compartment A was removed by an adjustable air pump via a rotameter. With a constant pressure in A, the rotameter measured the volume flow rate of the entrained air directly.

Water was circulated by a centrifugal pump through calibrated rotameters to the jet pipe. The last part of the pipe between the rotameters and the nozzle could be moved to allow variations of jet length and angle of impact. The various nozzles (length to diameter ratio exceeding 50) were attached to a movable arm H. The flexible pipe coupling also served to prevent the transmission of pump vibration.

The temperature of the water could be varied by a continuous supply of cold- and continuous removal of 'used' water. For

each run the temperature was constant within 1^{o} C.
The jet stream produces a circulating flow in the bath which might influence the entrainment. Experiments showed that the bath used (1 * 0.2 * 0.6 m) was big enough for this circulation not to be significant.

VI. 3 Some experimental results

The experimental set-up which makes use of inclined jets will emphasize the existence of the various entrainment regions. As is shown in chapter II the influence of the angle of impact is much greater in the low velocity region than it is for high velocities.
Fig. VI.3 gives some data of air entrainment for different diameters. The angle of impact is 30^{o}. As is obvious from the graph two distinct areas are present as predicted from the study of the entrainment mechanism.

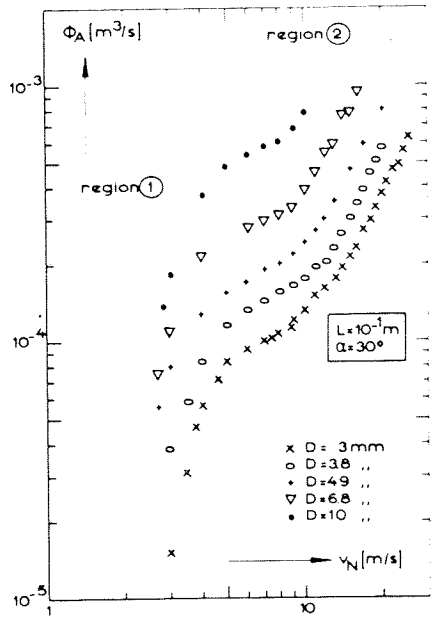

Fig. VI.3 Air volume entrained as a function of jet diameter and velocity

The low velocity region is below about 5 m/s. There is no definite diameter dependence of this velocity. A physical explanation cannot be given and a criterion for the value of that critical velocity has not been established. In chapter IV it is reported that for single drop impact the formation of a bubble dome occurs at a velocity of about 5 m/s independent of the dropdiameter. This may be merely a remarkable coincidence.

The high velocity region has no clearly defined lower value of the velocity. The previous chapters indicate that in this region the jet is subjected to violent air friction. As was pointed out this was controlled by a Weber number and the value of this number should be at least 10.
Table VI.6 gives a list of the Weber numbers corresponding to the starting points for the data shown in fig. VI.3. The con-

D_n	We
3 mm	9.7
3.8 mm	9.0
4.9 mm	9.0
6.8 mm	9.1
10.0 mm	10.5

Table VI.1

sistency of the Weber numbers at this transition is reasonable confirmation of the underlying assumption of the significance of air resistance as so characterised. Because the two regions are physically not directly connected there is a transition regime. However this region, cannot be analysed theoretically and prediction of the amount of entrained air is difficult. However since the limits of the transition are set by the low velocity curve up to a velocity of 5 m/s and the high velocity curve at a Weber number of approximately 10, it will be found that direct interpolation between values calculated for these limits gives a reasonable prediction of the entrainment.

VI.4 Entrainment with low velocity jets

In chapter V all the findings about the strong interaction between the deformations of the jet and the growth and closure of the cavities that are produced were collected. It was shown however that the impact phenomena are too complex for theoretical treatment. For that reason the following parameter dependency was proposed:

$$\beta_A = \text{function}\left(\frac{D_j^2 v_j^3 L^a}{(\sin\alpha)^b}\right) \qquad (V.4)$$

For jets near or beyond the break-up length is felt that the results reported in chapter IV show that the kinetic energy of the jet alone is the important variable for vertical jets, i.e.:

$$\beta_v = \text{function}\left(\tfrac{1}{2}\rho_w \tfrac{\pi}{4} D_j^2 v_j^3\right) \qquad (V.2)$$

The velocity (and associated change in diameter) must be determined at the value appropriate to the moment of impact. For vertical jets the parameter groups in equations (V.2) and (V.4) are modified to accommodate this as follows:

$$\beta_A = \text{function}\left\{D_n^2 v_n L^a (v_n^2 + 2gL)^{\frac{3}{2}}\right\}$$

$$\beta_A = \text{function}\left\{D_n^2 v_n (v_n^2 + 2gL)\right\} \qquad (VI.5)$$

In the case of inclined jets a calculation is not so simple (see Appendix I).

The regions in which the parameters are varied are as follows; D_n between 2.85 and 10 mm, α between 20^o and 60^o and L between 5 and 40 cm.
Because there is an influence of nozzle geometry, the measurements were always made with nozzles whose length to diameter ratio was 50. It could then be assumed that turbulence inside the nozzle pipe is almost fully developed and similar flow conditions exist for every experiment. A disadvantage is however that no other data known in literature can be compared directly because none of the authors worked with this nozzle geometry.

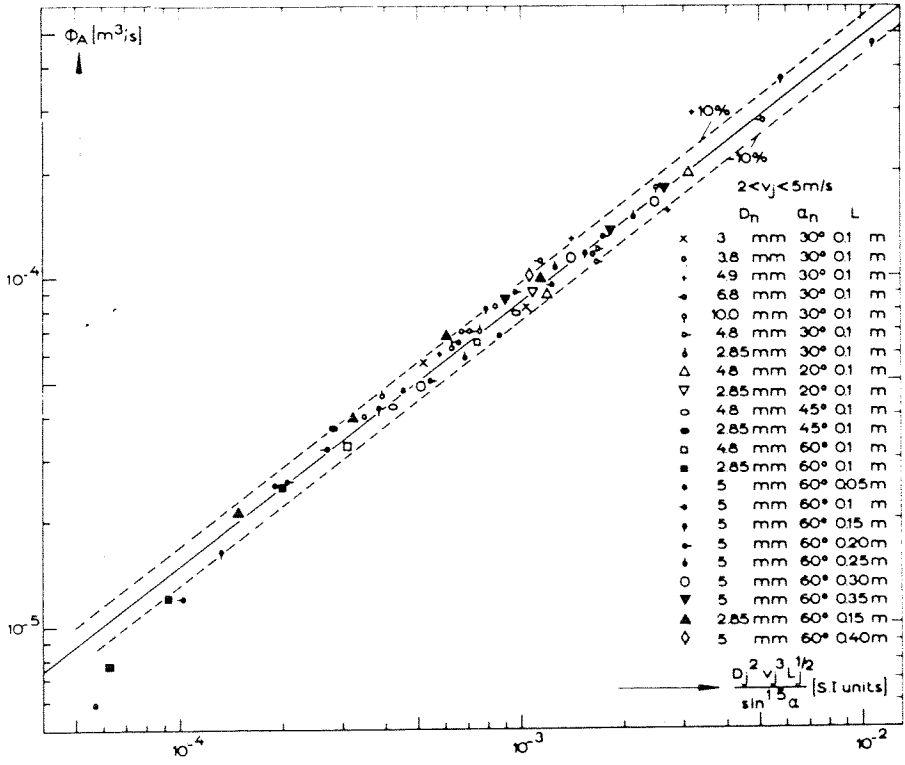

Fig. VI.4 Correlation of data of low velocity water jets

A curve-fitting procedure is applied and the constants a and b in equation (V.4) are 0.5 and 1.5 respectively. All the

measurements are shown in fig. VI.4 which proves that the parameter group proposed essentially controls the entrainment. Because definite rotation symmetric deformations only occur near the break point of the jet it is no surprise that the same parameter group is valid for lengths up to 80% of the break-up length. From the graph the following correlation is derived:

$$\phi_A = 0.015 \left(\frac{D_j^2 v_j^3 L^{\frac{1}{2}}}{\sin^{1.5}\alpha}\right)^{\frac{3}{4}} \quad \text{for } \phi_A > 1.5.10^{-5}\ \frac{m^3}{3} \qquad \text{(VI.6)}$$

which is accurate within 10%.
Because no correction is made for the contraction factor of the stream leaving the nozzle, this in now expressed in the numerical factor of eq (VI.6). Deviation from the correlation only occur for values of the flowrate below $1.5.10^{-5}$ m^3/s. In these cases the entrainment rate is so small that accurate determination with the air rotameters was not possible. Moreover such jets can hardly create cavities and are therefore near the critical situation at which no entrainment occurs. Comparison with the results of other workers was hampered by the differences in the nozzle geometry. Furthermore *Ciborowski* and *Bin* (1972) are the only other workers who have measured with low velocity jets. Their nozzle had

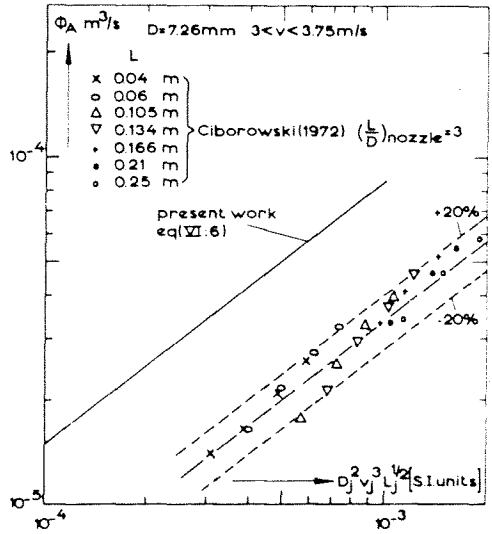

Fig. VI.5 Comparison with the data of *Ciborowski and Bin* (1972)

a length to diameter ratio of three and the diameter was 7.26 mm. Because they used only vertical jets the sine α is always unity.
Correlation of their date is shown in fig. VI.5. The solid line represents the results of our own measurements. From this figure it appears that the same parameter group describes their low velocity entrainment withing 20% accuracy. However the numerical factor from eq (VI.6) had to be modified. Although their measuring arrangement is expected to give too low a value of the entrainment rate this cannot explain the consistent deviation.
They used jet velocities between 3 and 3.75 m/s with a nozzle of 3 diameters long. Considering figures III.13 and 14 it will be realised that their jets have no definite turbulent structure. All their measurements concern jets which belong to the descending part of fig. III.13. This implies that although some turbulence is created the initial disturbance level lies below our values. It is therefore not unexpected that entrainment data deviate from ours, but because some turbulence is present the same parameter group can be applied. If we consider now all our data together with those of *Ciborowski* and *Bin* we conclude that low velocity jets which are neither broken nor alsmost broken-up entrainment is proprotional to a single parameter group i.e. $D_j^2 v_j^3 L^{\frac{1}{2}}$. The proportionality constant is dependent upon the nozzle geometry which directly determines the turbulence structure of the issuing jet stream.

Data obtained with jets which are near or beyond the break-up length are given in fig. VI.6. For this situation it is supposed that cavities are formed by an approximation to a train of impacting drops so that the kinetic energy of the jet is the controlling parameter. All data presented in the figure concern jets with an impact angle of 60°. Only for very low values of the entrainment rate is there a slight deviation from a straight line through the data. It is not surprising that there is some critical energy necessary to produce any entrainment. These data points only consider measurements at jet lengths that were at least 90% of the break-up length. Data for shorter jets show clear deviation from this line.
There is no reason to expect a different angle dependency than obtained before. From fig. VI.6 we have derived the following approximate equation for vertical impacting jets:

$$\phi_A = 0.85.10^{-5} + 21.10^{-5}(\tfrac{1}{2}\rho_w \tfrac{\pi}{4} D_j^2 v_j^3) \qquad \text{(VI.7)}$$

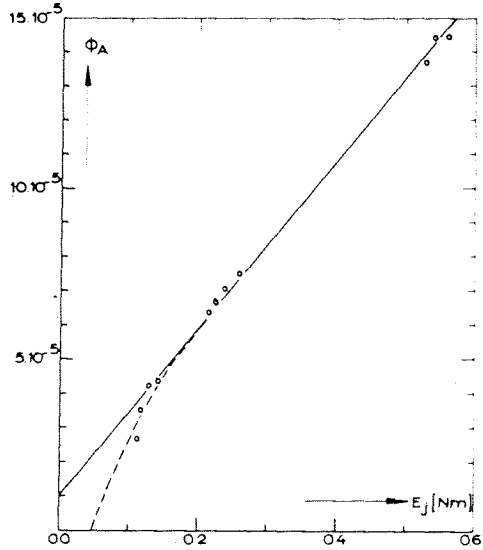

Fig. VII.6 Amount of entrained air near the break point of the jet

VI.5 Entrainment at high velocities

A direct comparison of experimental data and theory is hampered somewhat by the limitations of the measuring apparatus. The bubbles from obliquely impacting jets are collected under the 'bubble trap' and direct measurements of vertical jets at very small incident angles cannot be made satisfactorily. An obliquely impacting jet introduces a horizontal velocity component in the bath and the hole created by the jet in the liquid gets larger. The underpressure increases and more air will entrain. Experimental results confirm this hypothesis. Therefore the angle dependency has been investigated in order to extrapolate to 90°. Increasing the angle from 30° to 60° the entrained air decreases. Measurements done at impact angles from 60, 70 and 75° show no further significant angle dependency and have been taken as also representative for vertical jets. Use of the angle dependency derived for low velocity jets is not allowed because the physical conditions have changed and another relation can be expected. In spite of a slight dependence of L, v_j, D^* and probably the characteristics of the fluid, a sufficient accurate relation for the angle dependency is:

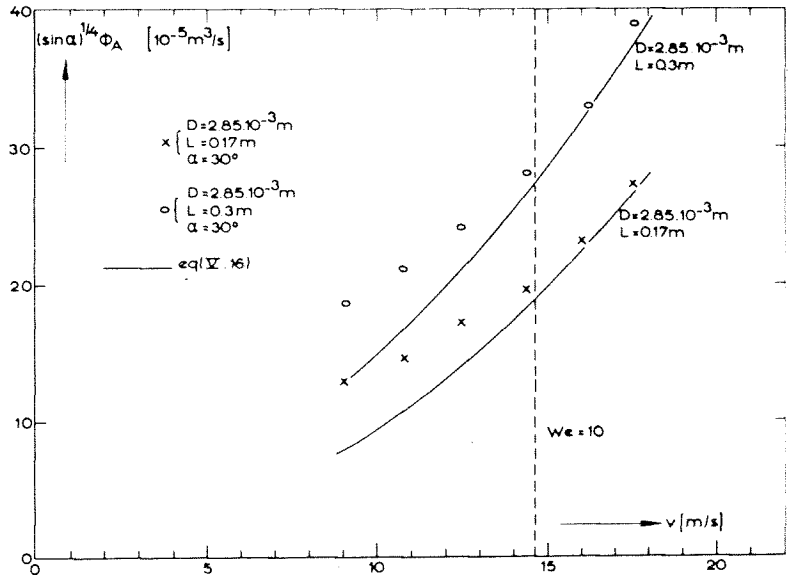

Fig. VI.7 Divergence of measured air flow predicted for Weber numbers less than 10

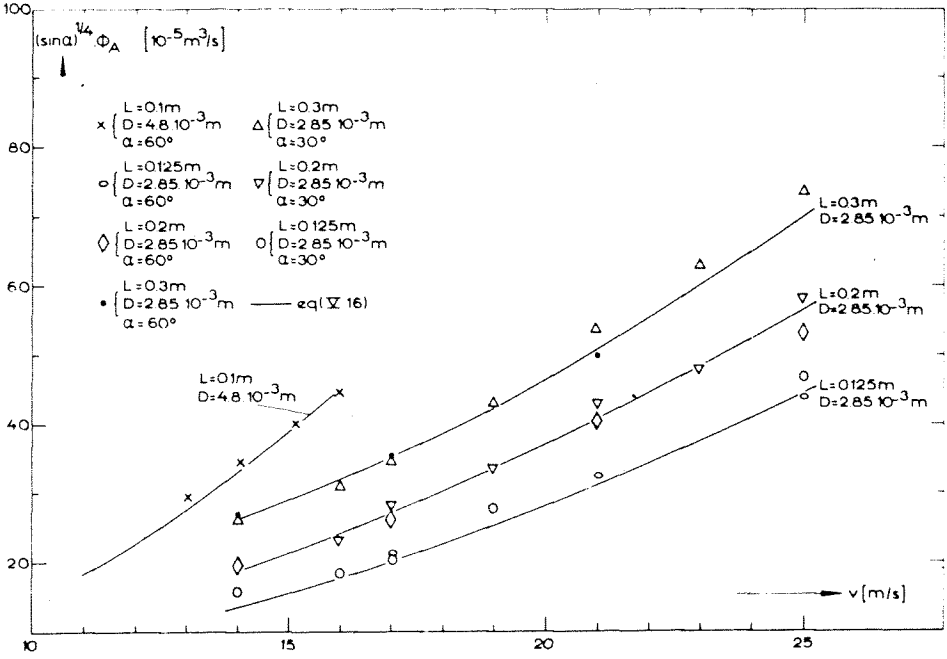

Fig. VI.8 Measured and predicted air entrainment rates for the range We>10; Re<5.10^5

$$\phi_A \ (\text{sine } \alpha)^{\frac{1}{4}} = \text{constant} \qquad \text{(VI.8)}$$

which is valid within 10 percent for any given situation. A correction for the influence of gravity is not made in the calculations. The velocities are almost always above 10 m/s. Since $(\text{sine } 60^o)^{\frac{1}{4}} = 0.965$ the small sensitivity to impact angles at values nearer the vertical than this is consistent.

Fig. VI.7 shows data near the critical velocity of 15 m/s corresponding (for this diameter) to Weber number = 10. It can be seen that the extrapolation to lower velocities becomes increasingly inaccurate. Providing this criteria is satisfied, agreement between theory and experiment is good as may be seen in fig. VI.8. Deviations only occur for situations in which $Re_L > 5.10^5$, when it is reasonable to assume that transition to a turbulent air boundary layer has taken place (fig. VI.9). As might be expected, the amount of entrained air increases in comparison with that from a laminar boundary layer because of the greater spreading of the jet due to turbulent air friction.
The dependency on jet diameter is shown in fig. VI.10. The data points which deviate most from the predicted equation are those for high gas flows (when some of the captured gas probably escaped the bubble trap) and those for the thinnest jets (which are of course most sensitive to accurate determination of the nozzle diameters).

Comparison with other workers is again difficult. Table VI.2 gives a few results of *Henderson et al* (1970) and *Ciborowski* (1972). The measurements of the latter lie in the low velocity- and transition, except for the one listed in Table 2. Comparison shows that there is a deviation of 16% relative to the measured value. The probable reason for this becomes obvious if we consider the group Re_L We. The formula derived from the jet spreading is only valid when the value of this group is above 7.10^5. Fig. III.18 shows this, together with an upward deviation from linearity in the value of D^* at the lower end, which might explain their larger value of air entrainment since for them $We.Re_L = 6.6.10^5$. *Henderson's* data lies also beyond the range of the predictive theory. The Weber number corresponding with the diameter and velocity used is nine,so the data are not really in the high velocity region. As is shown in fig. VI.7 for these conditions the theory predicts too low a value. In conclusion we can say that the order of magnitude is comparable and that influence of air friction is the major scource of jet spreading because the nozzles used were rather short.

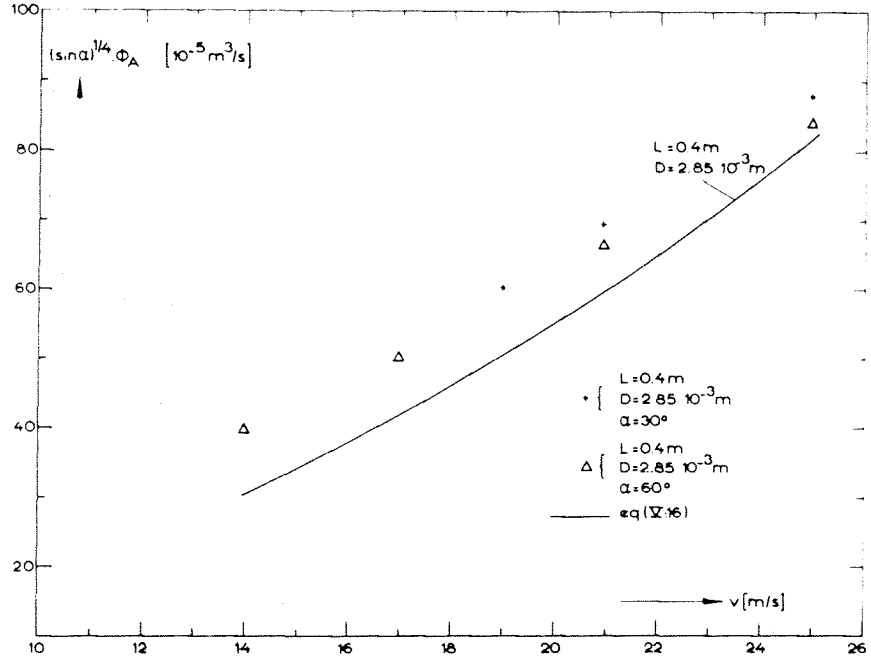

Fig. VI.9 Divergence between predicted and measured air entrainment for $Re_L > 5.10^5$

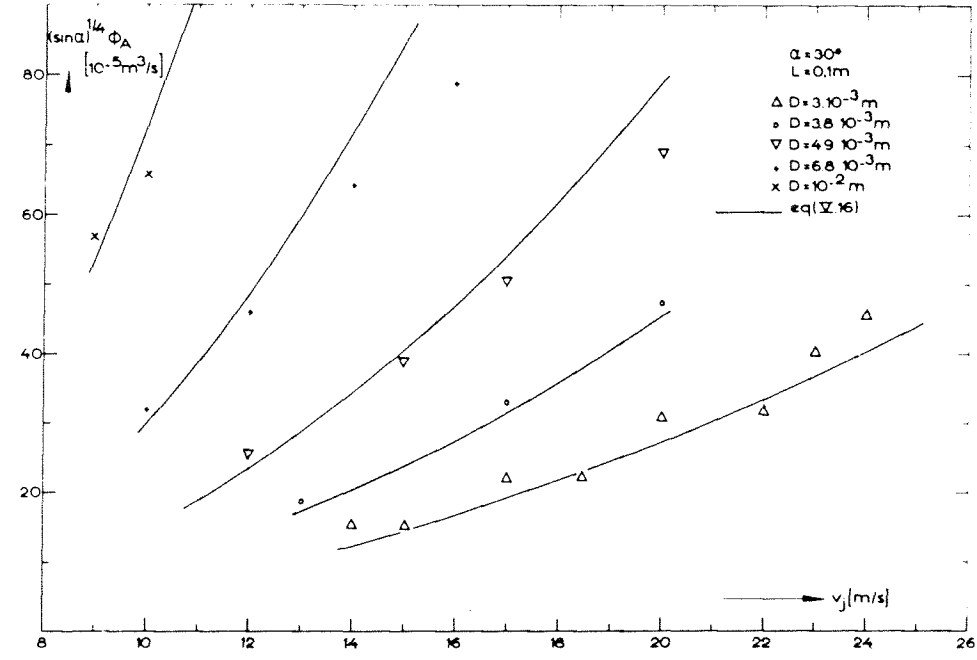

Fig.VI.10 Jet diameter and velocity dependence of air entrainment

$(1/D)_{nozzle}$	v_j	L	D_j	ϕ_A(measured)	ϕ_A(theory)	
8	20m/s	0.041m	1.64mm	$5.10^{-5}m^3/s$	$4.2.10^{-5}m^3/s$	1
10	10.7	0.158	6.3	$6.5.10^{-4}$	$4.2.10^{-4}$	2
10	10.7	0.27	6.3	$8.8.10^{-4}$	$6.1.10^{-4}$	2
10	10.7	0.38	6.3	$1.1.10^{-3}$	$7.7.10^{-4}$	2
10	10.7	0.46	6.3	$1.2.10^{-3}$	$8.6.10^{-4}$	2
10	10.7	0.55	6.3	$1.28.10^{-3}$	$9.6.10^{-4}$	2

Table VI.2

1. Ciborowski
2. Henderson

Comparison of volume flow rate other workers with theoretical model

VI.6 Discussion and conclusions

It has been possible to use only a small amount of data from other workers in the previous paragraphs, since all the other measurements concern situations from which we cannot compare the result with our own findings. However the trend of the various curves can be qualitatively predicted by the knowledge and understanding of the entrainment process.
With relatively short nozzles turbulence is scarcely created (fig. III.13). In most cases the upstream flow is laminar so the surface structure of the isuing jet stream is rather smooth. Surface tension forces cause jet break-up but visible deformation of the jet occurs only in the last few centimeters before the break point. Therefore length dependency is not expected to be significant for the low velocity- and transition regions. Experimental results with short nozzles of *Henderson et al*, *Ciborowski and Bin* confirm this hypothesis.
Ciborowski extended his measurements plotted in fig. VI.5, which have some length dependence because of the presence turbulence, to lower values of the velocity. In that case his jets, having Reynolds numbers below 20,000, behave like real laminar streams (fig. III.13). No length dependency was found for these.
Henderson et al used three nozzle geometries. A length to diameter ratio of zero, one and ten. In the low velocity and transition regions the two shortest nozzles give equal values of the entrainment and, in contrast to results with the longer nozzle, jet length is not important. As soon as air friction deforms the surface of the jet the situation changes. Nozzle geometry is not the most important factor

anymore because the jet will always spread under the influence of drag forces (see previous paragraph). To what extent the spreading will take place is however determined by the turbulence in the liquid stream. For this reason the entrainment of the two shortest nozzles used by *Henderson et al* is no longer equal. From their results it can be shown that as soon as the Weber number is greater than ten, a significant jet length dependency is observed for all the nozzles used.

The data obtained from our own measurements can be plotted in a different way. Fig. VI.11 and 12 show some data for the volume ratio between the entrained air and the water jet as

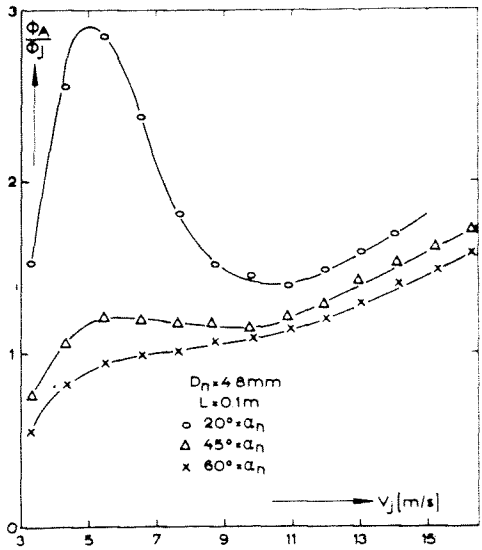

Fig.VI.11 Influence of impact angle upon entrainment ratio

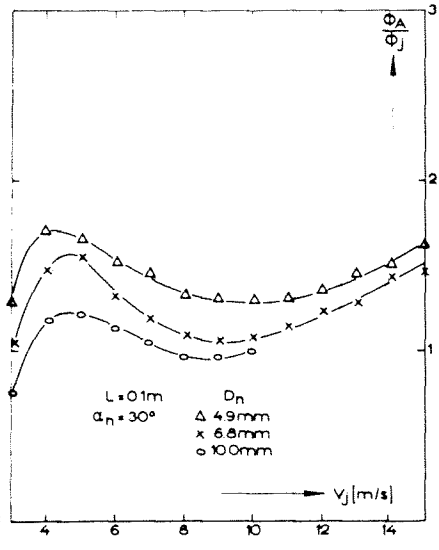

Fig.VI.12 Influence of diameter upon entrainment ratio

a function of the velocity. Only a few representative curves are given buth they are fully characteristic of the large number of results that have been obtained. The great influence of the angle of impact on the relative air entrainment is striking (fig. VI.11). Another point of interest is the increase of the relative amount of entrained air with decreasing diameter (fig. VI.12). Both graphs emphasize the existence of various regions. In particular the first transition is marked at low impact angles by a maximum in the curve. The second transition occurs near a minimum. As is evident from the graphs, simple relationships between entrainment and dimensionless groups cannot be obtained and this is the reason why published correlations for the entrainment do not agree. The only way to analyse the data

is to separate consideration of the different regimes and to consider the physical phenomena happening during the entrainment process.

The two approximations proposed for the low- and high velocity regions have proved satisfactory. Deviations from the predictive equations and correlations can be explained on physical grounds. The best way of closing this chapter is to summarize the relations and to show how the amount of entrained air can be calculated when the issuing jet is presumed to be turbulent.

THE LOW VELOCITY REGION (v_j < 5 m/s; vertical jets)

$$\flat_A = 0.015\ (D_j^2 v_j^3 L^{\frac{1}{2}})^{\frac{3}{4}} \qquad \text{(VI.9)}$$

when the jet length is less than 80% of the break-up length.

$$\flat_A = 0.85.10^{-5} + 21.10^{-5}(\tfrac{1}{2}\rho_w \tfrac{\pi}{4} D_j^2 v_j^3) \qquad \text{(VI.7)}$$

if the length of the jet is beyond 90% of the break-up length.
The variables must be estimated at the impact point (Appendix I). The break-up length can be estimated using the results obtained in chapter III.
For example from figure III.15.

The influence of impact angle is governed by:

$$\flat_A(\text{sine } \alpha)^{1.1} = \text{constant} \qquad \text{(VI.10)}$$

THE HIGH VELOCITY REGION ($\frac{\rho_A v_j^2 D_j}{\sigma}$ > 10; vertical jets)

$$\flat_{AI} = \frac{\pi\, v_j D_j^2}{4}\ (1.56.10^{-2} We^{1/3} Re_L^{1/3} - 1) \qquad \text{(V.6)}$$

Together with the boundary layer solution this gives the total amount of entrained air. Because of the complexity of the formulae a quick calculation of the boundary layer cannot be made. Therefore fig. VI.13 is given to facilitate such an estimation. The parameter D^* on the axes is determined by the equation:

$$\frac{D^*}{D} = 0.125\ (We.Re_L)^{1/6} \qquad \left\{ \begin{array}{l} We.Re_L > 7.10^5 \\ We>10;\ Re<5.10^5 \end{array} \right\} \qquad \text{(III.17)}$$

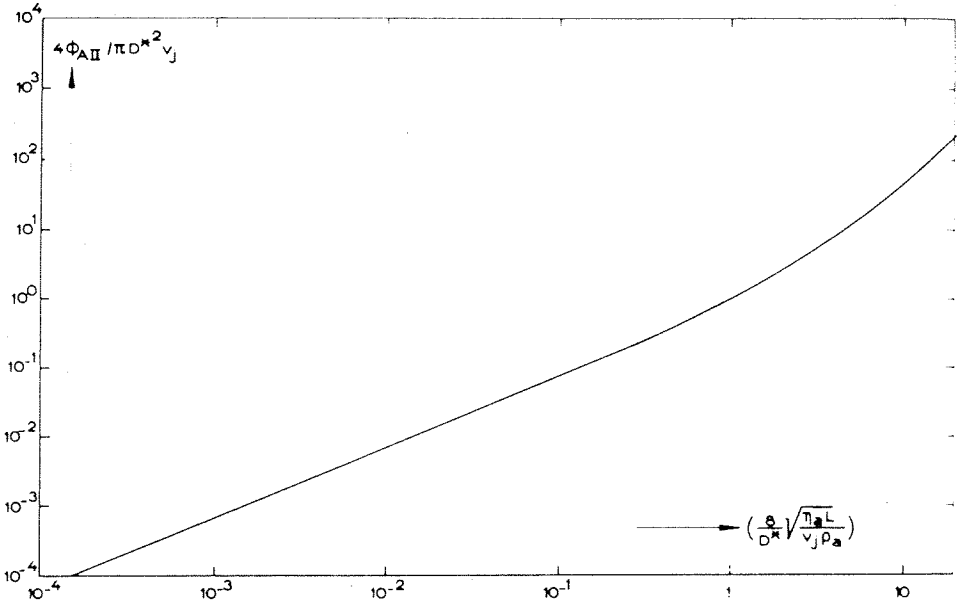

Fig. VI.13 Theoretical relationship for the volume of air carried in the boundary layer around the jet

The influence of impact angle is governed by:

$$\phi_A \ (\text{sine } \alpha)^{\frac{1}{4}} = \text{constant} \qquad \text{(VI.8)}$$

THE TRANSITION REGION

Estimations of the entrainment in the transition region can be made by considering that no discontinuities exist when the velocity gradually increases. The low velocity correlation can be used to estimate the entrainment at 5 m/s, and the high velocity prediction for the critical velocity given by $v_j = (10\sigma/\rho_A\ D)^{\frac{1}{2}}$. Interpolation between these values for any intermediate velocity fits as well as the raw data for the limiting regions ($\pm$ 15%).

Chapter VII

MASS TRANSFER FROM PLUNGING LIQUID JETS

This chapter is devoted to some aspects of the oxygen transfer from the entrained bubbles to the target liquid. A review of the existing literature is given. There is a description of the liquid mixing in the pool and the results of measurements of bubble sizes are also presented. The penetration depth of bubbles is considered and the relation to the mass transfer characteristics established. The chapter ends with a comparison with some other gas-liquid contacting devices.

VII.1 Introduction

Mass transfer from the bubbles below the liquid surface has not been extensively investigated. Most authors describing the entrainment consider only the volume flow rate of gas. However the subsequent mass transfer must be the ultimate objective of the application of such a process.
Swiggett (1969) studied carbondioxide absorbtion in water pools using the impinging jet system. The parameters he varied were nozzle diameter (1/8, 1/4 and 5/16 inch), Reynolds number of jet (7,000-11,000), jet length (1-5 inch) and the liquid depth (3-8 inches). After considering the entrainment results of *De Frate and Rush* (1969) he arrived at the following relation for the CO_2-concentration in the pool as a function of time:

$$c_{CO_2} = \{ M(We)^F \rho_{CO_2} + \frac{1.7.10^{-6}}{\phi_j} \}\{1-\exp(\frac{-\phi_j}{V_l} t)\} \qquad (VII.1)$$

V_l is the pool liquid volume. M and F are determined experimentally. Both symbols are functions of the Reynolds number of the jet. The Weber number was based on the liquid density and diameter of the nozzle. Eq(VII.1) can be simplified considerably.
The level in the pool was maintained at a constant value by means of an overflow. Therefore a CO_2 -balance was made over the pool in the form:

$$V_l \frac{d\, c_{CO_2}}{dt} = K_l A(c^*_{CO_2} - c_{CO_2}) + \phi_{m/surf} - \phi_j c_{CO_2} \qquad (VII.2)$$

with $K_l A$ the product of mass transfer coefficient and total

bubble area, c^*_{CO2} the saturation concentration and $\phi_{m/surf}$ the diffusive contribution through the pool surface. In his parameter range this contribution seems to be constant and reported to be equal to $1.7.10^{-6}$ kg/s. At t = 0 the concentration of CO_2 is zero. In his derivation he stated that

$$c^*_{CO_2} - c_{CO_2} \approx c^*_{CO_2}$$

because only a fraction of the saturation concentration was achieved. The complete solution is then:

$$c_{CO_2} = \left(\frac{K_1 A\, c^*_{CO_2} + 1.7.10^{-6}}{\phi_j}\right)\left(1-\exp\left(\frac{-\phi_j\, t}{V_l}\right)\right) \qquad \text{(VII.3)}$$

Comparison with eq (VII.1) gives:

$$K_1 A = M(We)^F \rho_{CO_2}\, \phi_j / c^*_{CO_2} \qquad \text{(VII.4)}$$

This result is physically unlikely because both the mass transfer coefficient and the contact area would not be expected to be functions of the saturation concentration.

Ciborowski and Bin (1972)studied bubble sizes. Their photographic results indicated that mean bubble diameters in an air-water system vary between 1.3 and 3.6 mm, depending upon the jet parameters. They reported that the bubble sizes usually followed a normal distribution.
Burgess et al (1972) studied the impact of 2 N Na OH jets with pure CO_2 as surrounding medium. All bubbles dissolved completely. The results of the measured specific interfacial area S_b are correlated by the equation:

$$S_b \sim \left(\frac{\phi_A}{\phi_j} + 1\right)^{\frac{1}{3}} v_j \qquad \text{(VII.5)}$$

Ahmed and Glover (1972) found that within the range of the variables that they studied the aeration rate in an air-water system was directly proportional to the power of the jet. Expressed in K_1A terms the relation is:

$$k_1 A = 3.1.10^{-4} + 4.85.10^{-2} D_j^{\,2} v_j^{\,3} \qquad \text{(VII.6)}$$

No influence of the angle of impact (60^o-80^o) was observed.

The authors cited above treated the subject purely experimentally. Theoretical arguments were not considered and no insight was presented into the real situation below the water surface. In fact, flow patterns, bubble sizes and residence time distributions determine the mixing and transfer of oxygen throughout the pool liquid.

VII.2 Mass transfer from bubbles and bubble swarms

Various models are proposed to describe mass transfer at gas-liquid interfaces. In general there is a distinction between two basic concepts; bubbles with a rigid surface and bubbles whose surface is continuously refreshed.
The most succesful theory in predicting mass transfer from mobile interfaces was first formulated by *Higbie* (1935). His penetration model leads to the following expression for the mass transfer coefficient of a rising bubble:

$$K_l = 1.13 \left(\frac{D_f v_b}{d_b}\right)^{\frac{1}{2}} \qquad \text{(VII.7)}$$

in which v_b is the terminal rise velocity of the bubble. The dependence on the diameter of the bubble, which influences the rise velocity and the mass transfer was investigated experimentally by *Calderbank* (1967). He found that considering the correlation of *Allen* (1900) for the rise velocity of bubbles, the mass transfer coefficient is equal to:

$$K_l = 0.56 \left(\frac{\eta g}{\rho_l}\right)^{1/3} \left(\frac{D_f}{\nu}\right)^{\frac{1}{2}} \quad (d_b > 2 \text{ mm}) \qquad \text{(VII.8)}$$

provided that the bubbles have an internal circulation.
For bubbles in the range $0.5 < d_b < 2$ mm the mass transfer coefficient should be proportional to the bubble diameter. With even smaller diameters, when the interfacial surface is supposed to be rigid, the mass transfer coefficient is given by the well-known *Frössling* equation (1938) with the numerical factor determined by *Gröber* (1960):

$$K_l = \frac{2D_f}{d_b} + 0.58 \frac{D_f^{2/3}}{\nu^{1/6}} \left(\frac{v_b}{d_b}\right)^{\frac{1}{2}} \qquad \text{(VII.9)}$$

For creeping potential flow the relation approaches the theoretical value:

$$\frac{K_l d_b}{D_f} = Sh = 2 \qquad \text{(VII.10)}$$

The mobility of bubble surfaces is affected by the presence of impurities in the system. This is shown by *Benedek and Heideger* (1971) who compare the results of a few authors. Surfactants restrict the transition to a mobile interface to larger bubble diameters. The relations given above determine the mass transfer for bubbles in free rise. The question remains as to whether an added flow pattern in the liquid phase changes the mass transfer coefficient.
Prasher and Wills(1973) described the results of workers who measured transfer coefficients in agitated vessels. There is a variety of opinions. For instance, *Calderbank* (1967), *Hyman* (1962) and *Reith* (1968) reported no influence of flow conditions. *Davies et al* (1964) and *Yoshida* (1963) found a definite effect of agitation intensity. The confusion about this subject can best be illustrated by comparing the results of *Koetsier* (1973) and *V. Dierendonck* (1970). The former reports an increase of the mass transfer coefficient and the latter a decrease with increasing impeller speed. In the light of such results the influence of flow pattern remains an open question. The differences in results can be explained by the fact that mass transfer coefficients in most cases are determined from results of K_1A values (which are also doubtful, see below)which were compared with the value of A. The estimated value of A is particularly dependent upon the measuring procedure.

Benedek and Heideger (1971) gave a review of seventeen authors who measured the product K_1A as function of the variables in a vessel. The large variation of results is explained by differences in measuring techniques, the impurities of the system and the effect of scale of operation. The confusing literature cited above shows that transport processes in bubble swarms needs even more attention. Standarised quantitative results are required. In relation to the bubble swarm created by impinging jets the present knowledge is insufficient and scarcely applicable.

VII.3 Pool liquid mixing

In general the bubble swarm does not fill the entire volume of the pool. Oxygen has to be transferred from the locality where the bubbles are present to regions where the liquid is less mixed and which have a lower oxygen content. The transfer can take place by two mechanisms; diffusion and convection. In most cases diffusion can be ignored and convection determines the overall mixing. Hence the general flow patterns induced by the impinging stream must be considered.

VII.3.1 Flowpattern

Studying a fixed vertical jet system for which the jet velocity gradually increases, three successive flow patterns are observed. With very low velocities no air bubbles entrain and the flowpattern is similar to the pattern caused by a submerged jet. Approximately the same flowstructure occurs when only a few bubbles are induced. The mixing performance below the plunging point might then be expected to be slightly better than with a submerged jet because of the shear stresses that buoyancy forces produce at the bubble surfaces. On the other hand buoyancy forces reduce the range of the circulation. In fig. VII.1a the general streamlines are sketched. This flow situation is valid for very low jet

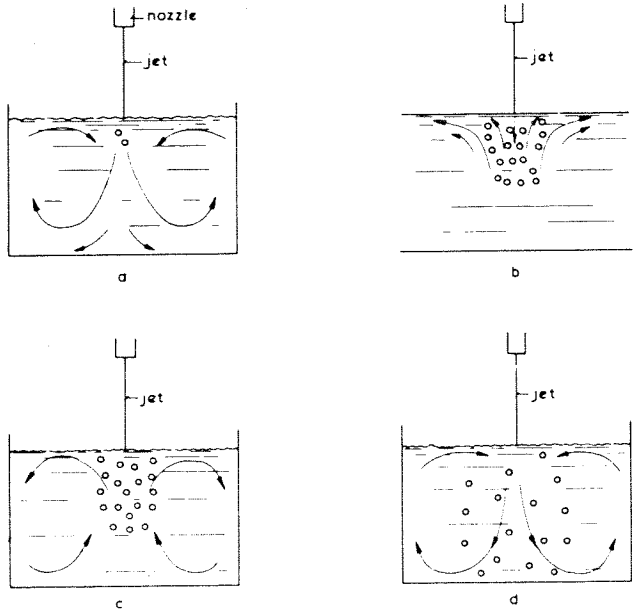

Fig. VII.1 Simplified flow patterns

velocities. Not surprisingly, with increasing velocity the penetration depth of the bubbles increases. Further, the quantity of freshly entrained air increases and the buoyancy forces then present eventually overrule momentum of the impacting jet. The main flow will reverse.
The transition between these two patterns takes place at rather low jet velocities. This can be illustrated by the

following rough estimation. The impact force of the jet is equal to:

$$K_j = \frac{\pi}{4} D_j^2 v_j^2 \rho_w \qquad \text{(VII.11)}$$

The buoyancy forces of the bubbles can be roughly estimated by assuming that all bubbles have the same diameter:

$$K_b \simeq \frac{\pi}{6} d_b^3 \rho_w n g \qquad \text{(VII.12)}$$

with n the total number of bubbles present in the pool. This amount is equal to:

$$n = \frac{\tau_r \phi_A 6}{\pi d_b^3} \qquad \text{(VII.13)}$$

where τ_r is the average residence time of the bubbles in the pool. Inserting eq (VII.13) into (VII.12) gives:

$$K_b \simeq \tau_r \rho_w g \phi_A \qquad \text{(VII.14)}$$

Buoyancy forces will dominate if $K_b > K_j$, i.e.

$$g \tau_r \phi_A > \frac{\pi}{4} D_j^2 v_j^2 \qquad \text{(VII.15)}$$

Suppose: $D_j = 5.10^{-3}$ m; $L_j = 0.1$ m and $v_j = 3$ m/s, then the numerical value of the right hand side of eq (VII.15) is approximately $1.8.10^{-4}$. The real value of the impact force must be even smaller because friction losses of the induced flow pattern are not taken into account. For the given situation the air entrainment is equal to 3.10^{-5} m^3/s. So with a mean residence time of less than one second the buoyancy forces, even for such low velocities, overrule the impact action of the jet.

Typical flow patterns are shown in figs. VII 1b and c. Fig. VII.1b represents a situation in which the size of the pool is infinite. The main flow is upwards and the fluid spreads radially over the surface. The considerable velocity gradients give rise to high shear stresses within the bubble swarm and this region can therefore be considered as perfectly mixed. Fig. VII.1c shows the flow situation with use of a bath of finite dimensions. Continuity considerations now require a circulation pattern. Similar mixing can be expected within the bubble swarm, and there will also be a blending of aerated fluid moving radially near the surface

with the bulk of that in the pool.
At high enough velocities the bubbles may hit the bottom of the vessel. A stagnation point appears and the bubbles are distributed over the entire pool volume if the depth to width ratio is in the order of one. This situation is sketched in fig. VII.1d and this flow pattern promises the best mixing performance of the three situations described.

VII.3.2 The process of mixing

The most relevant and actual flow pattern is that of fig. VII.1c, because in general the bubbles do not hit the pool bottom. Understanding of the mixing process is obtained if both the micro- and macro mixing are considered. Micromixing, determined by molecular diffusion and turbulence intensity, is rather effective because of the presumed existence of an ideally mixed part of the total volume (i.e. the bubble swarm), through which all the circulating fluid passes. Macromixing is determined by the overall flow pattern. The circulation occuring in the pool liquid can be schematically represented as given in fig. VII.2. V_1 is perfectly mixed and the fluid is circulated through a pipe with volume V2 which represents the rest of the bath. *Voncken* (1966) succesfully used this model for describing the mixing performance of an agitated vessel. In his calculation he neglected the volume V1 and estimated the influence of the longitudinal dispersion coefficient which is determined by the Bodenstein number. This number relates the transport by convection with the transport by dispersion. Because we want to know the influence of the ratio V1/V2 we suppose that no dispersion occurs which implies that in volume V2 plug flow exists. Combination of *Voncken's* results and these calculations must give the response of the concentration throughout the entire volume as a function of time after a pulse injection.

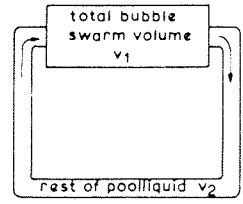

Fig.VII.2 Simplification of the flow pattern

A mass balance over volume V_1 leads to:

$$\frac{dc}{dt} = \frac{\phi}{V_1} \{c(t-t_c) - c(t)\} \qquad \text{(VII.16)}$$

with the boundary conditions:

$$t < 0;\ c = 0 \qquad \text{(VII.17)}$$

$$\left.\begin{aligned} t = 0;\ c &= c_o \\ t > 0;\ c &= c \end{aligned}\right\} \qquad \text{(VII.18)}$$

In these equations ϕ stands for the volume flow rate through V2, t_c the circulation time, c is the concentration as measured at the injection point, which is assumed to be within V1 and c_o the instantaneous concentration produced by the injection of a pulse into the completely mixed volume V1. Solution of equation VII.16 is complicated by the interacting of the decay tail of successive circulations, but it is clear that when the swarmvolume V1 is less than about 20% of the residual volume V2 that dispersion during the circulation is necessary in order that good mixing be obtained. An experiment was carried out to confirm that the concentration throughout the tank was substantially uniform.

The liquid was made alkaline with a small quantity of NaOH. Bromothymolblue was injected with the jet stream and the colouration was measured by point light transmission measurements. A representative curve is given in fig. VII.3 obtain-

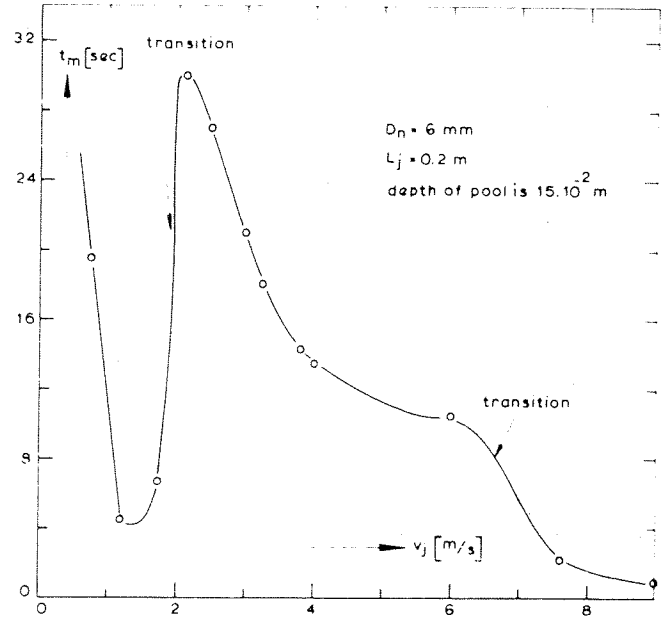

Fig. VII.3 Mixing time in the pool as a function of jet velocity

ed from data measured in a round vessel with a volume of 30 liters. Transitions in the flow patterns change the mixing performance as can be seen in the graph. The measurements indicated that mixing times (deviation less than 5% of the final concentration) were always considerably less than one minute and also less than 6% of the mean residence time in the vessel.
A substantially uniform concentration of oxygen through the entire pool liquid can therefore be assumed.

VII.4 Bubble size distribution

VII.4.1 Measuring procedure

The total contact area of the bubble swarm is determined by the entrainment of air and the size or size distribution of the bubbles. Usually the sizes in a swarm are assumed to be described by a normal distribution (*Houghton (1967), Siemes (1960) and Marucci (1967)*) but others show that different distributions can occur (*Anderson (1970)*). The influence of the size distribution upon the total mass transfer is however not clear from current literature.
Cal-or (1966) and *Hanratty* (1956) have studied this problem theoretically but could not experimentally verify their results. A change of the bubble population did not significantly effect the mass transfer. It was shown that the error is usually small when the variable bubble size is replaced by the mean. The mean bubble diameter of a swarm can only be determined if the distribution is known approximately. Several methods are available in literature, though each has disadvantages. The photographic method (*Calderbank (1967)*) only gives information in two dimensions. Also the shape of the bubbles for larger diameters is so ill-defined that a reasonable guess of the equivalent diameter is hard to obtain.
Optical methods (transmission, reflection or depolarisation) have the disadvantage that they are only applicable for bubble diameters below 1 mm.
The technique used here is based on the principle introduced by *Todtenhaupt* (1971). Bubbles are sucked away from the swarm through a capillary. They are elongated to long cylinders with sharply defined front and back edges as long as the velocity in the capillary is less than 4 m/s. The length of the cylinder is proportional to the cube of the equivalent diameter. The diameter is determined for each individual bubble by using the phenomena that the light transmission changes after the passage of a water-air interface. In fig. VII.4 the detection part of the apparatus is des-

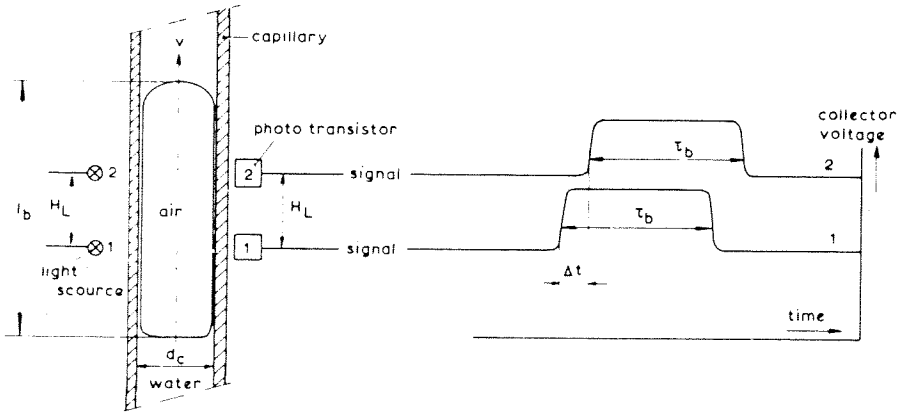

Fig. VII.4 Principle of bubble size measurement.

cribed.
If there is a constant pressure drop over the capillary, the velocity v of the bubble is constant. Hence:

$$v = \frac{H_L}{\Delta t} \qquad \text{(VII.19)}$$

The length l_b is equal to:

$$l_b = v\,\tau_b = \frac{H_L}{\Delta t}\tau_b \qquad \text{(VII.20)}$$

The equivalent diameter of the bubble d_b is therefore approximately:

$$d_b \simeq \left(\frac{3}{2} d_c^2 l_b\right)^{1/3} = \text{constant } \left(\frac{\tau_b}{\Delta t}\right)^{1/3} \qquad \text{(VII.21)}$$

By measuring the two times τ_b and Δt the bubble diameter is determined. A data processing apparatus was designed which classified the bubble sizes and calculated the total bubble size distributions directly.
The method is extremely fast in comparison with all other existing methods. Another advantage is that a measurement can be done at any place inside an apparatus or a bubble swarm. A change of the capillary diameter allowed the range of bubble diameters to be extended.

However there are sources of error which must be minimized. Therefore the following subjects are treated in Appendix II.

a. A calibration curve has to be accurately determined;
b. slugflow inside the capillary must be considered;
c. flow velocities and fluctuations occurring near or in the capillary on the outcome of the measurements must be estimated;
d. the sample withdrawn must be representative of the local distribution. Break-up or coalescence at the capillary mouth must be avoided if possible.

There should be no preference for particular bubble diameters, but for the measured bubble sizes ($1 < d_b < 6$ mm) the terminal rise velocity is reasonably constant.

Most of the measurements were done in the rising part of the bubble swarm where the bubble velocities are comparatively low. For that reason the measured size distributions are fairly accurate (Appendix II) and the derived local sauter mean bubble diameters ($d_{SM} = \Sigma n d_b^3 / \Sigma n d_b^2$) can be determined as a function of the jet parameters.

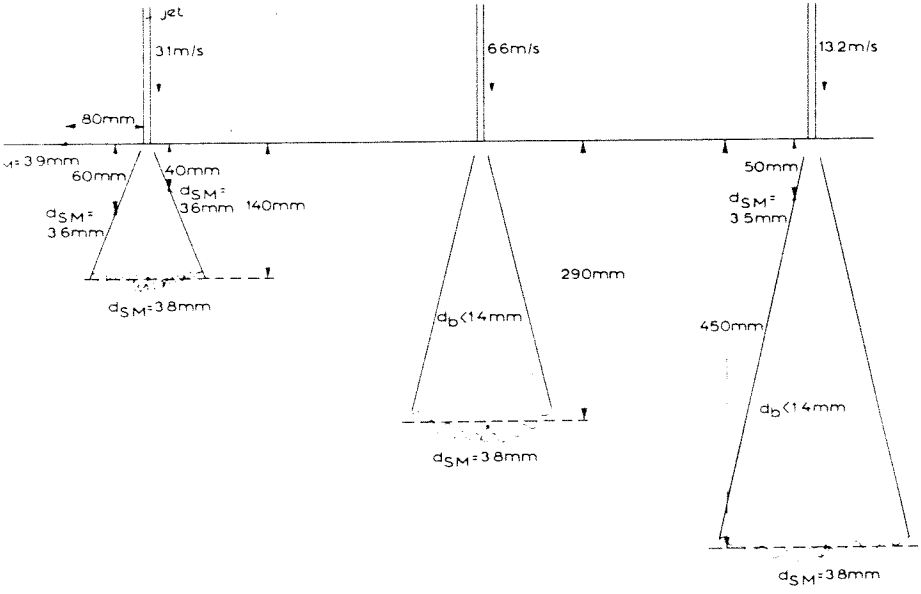

Fig. VII.5 Sizes of bubbles produced by the impact of vertical jets.

VII.4.2 Results and discussion

All the measurements were done with a nozzle of 5.8 mm diameter and a jet length of 0.2 m. The parameters were the angle of impact and the velocity of the jet. Fig. VII.5 shows the results for vertical jets. The bubbles just escaping from the cone of the swarm have a sauter mean diameter of about 3.5 mm independent of the jet velocity. A direct conclusion is that the flow structure near the cone is the same for each velocity. This is understandable because at that place the buoyancy forces of the bubbles overcome the momentum of the impacting jet. The same situation occurs at the end of the cone. Also here the bubble diameters are comparable although they have grown because of coalescence during the downwards movement.
Some measurements also were done in the centre of the cone. However the flow velocities made the data doubtful because the flow field is too strong (Appendix II). The results of these measurements only indicate that 95% of the measured bubbles have a diameter less than 1.4 mm. In spite of the unaccurate data this result could be reasonable for the following reason.
The flow structure has a high turbulence intensity which is understandable considering the high relative turbulence intensity of 30% in a submerged jet (*Van de Sande and Cordemans (1973)*). This intensity will be even further increased by the shear stresses created by the bubbles themselves. An important conclusion from this is that inside the cone the mass transfer from the bubbles to the water must be higher than the transfer from the bubbles rising outside the cone. The oxygen concentration will therefore be dependent upon location in spite of the good mixing performance of the jet system.

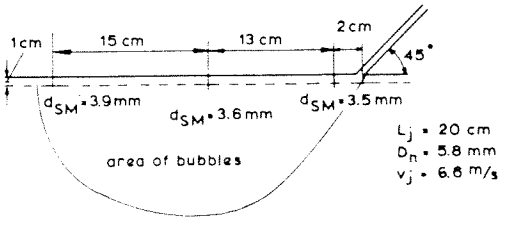

Fig.VII.6 Sizes of bubbles produced by the impact of inclined water jets

The sauter mean bubble diameters produced from the impact of an inclined jet are given in fig. VII.6. The values increase somewhat in a horizontal direction. Adjacent to the impact point a slightly lower diameter is found then for vertical jets but this is because the buoyancy force of a rising bubble makes an angle with

the impact force of the jet. Smaller bubbles can therefore more easily escape.

VII.5 Penetration depth of the bubbles produced by vertical jets

Ciborowski and Bin (1972) assumed that the penetration depth of the bubbles was only determined by the momentum of the impacting jet. A very simple experiment proves that this is not correct.

Consider a given jet and measure the depth of bubble penetration. For a jet with the same momentum (same diameter and velocity) but with a longer jet length, according to the results given in chapter VI the amount of entrained air is greater. For this reason the total resistance and buoyancy forces of the bubbles are no longer the same at the impact point. If one now considers the shape of the bubble cone and the depth of penetration, it is observed that the cone has become wider and the depth has decreased. This experiment shows that a simple momentum approach is insufficient.

The way to correlate the depth with all the various parameters is to consider what happens at the plunging point and inside the cone. As stated above, the total momentum downwards is ruled by both the momentum of the jet and the buo-

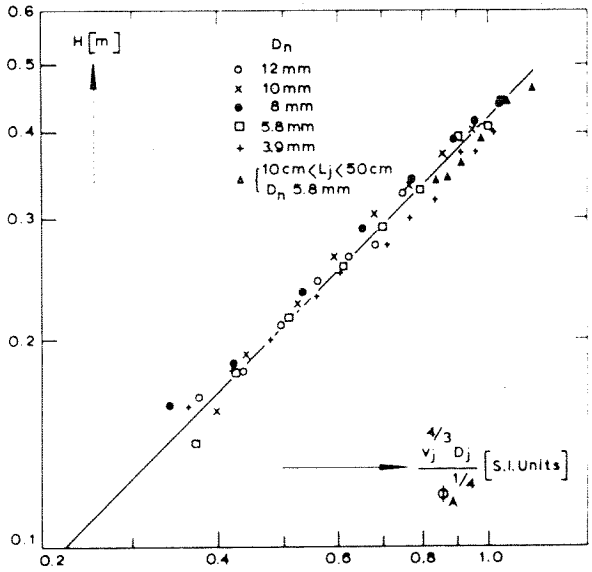

Fig. VII.7 Bubble penetration depth as a function of jet parameters

yancy momentum of the entrained air. Inside the cone the relative density will increase as we move downwards. In order to calculate the total buoyancy force one must know the following:

a. bubble size distribution in both horizontal and vertical direction in the cone;
b. the variations in relative density;
c. the amount of bubbles that escape from the cone as a function of the depth.

Points a and b are completely unknown. From c one can only say that the total amount of air which rises from the cone must be equal to ϕ_A from continuity considerations, but this does not give any information about the depth dependency.

Again we conclude that the total jet entrainment process is so complex that only the most simple approaches are worthwhile. From considerations given above the most relevant parameters which determine the penetration depth are v_j, D_j and ϕ_A and measurements were done to correlate the depth with these three parameters.

Fig. VII.7 shows the ultimate result. This graph shows that the penetration depth is given within 10% accuracy by the formula:

$$H = 0.42 \frac{v_j^{4/3} D_j}{\phi_A^{\frac{1}{4}}} \qquad \text{(VII.22)}$$

The depth shows strong fluctuations and H was defined as a usually assessed mean.

Equation (VII.22) has a very important meaning. A simple measurement of the penetration depth alone gives direct information about the amount of entrained air, though naturally a $\pm$ 10% accuracy in H implies only $\pm$ 40% for ϕ_A.

VII.6 Oxygen transfer

Mixing and aeration action are both produced by the jet impact and this might promise a rather high oxygen take-up. Also from the construction point of view the equipment can be very simple . Although theoretically the entire process is complicated, the experiments are relatively simple. With this in mind the mass transfer has been studied experimentally and correlations are based on models, which simplifies the process considerably.

VII.6.1 Experimental procedures

Fig. VII.8 shows the experimental arrangement. The vessel, which is part of the circulation loop, is made of perspex to

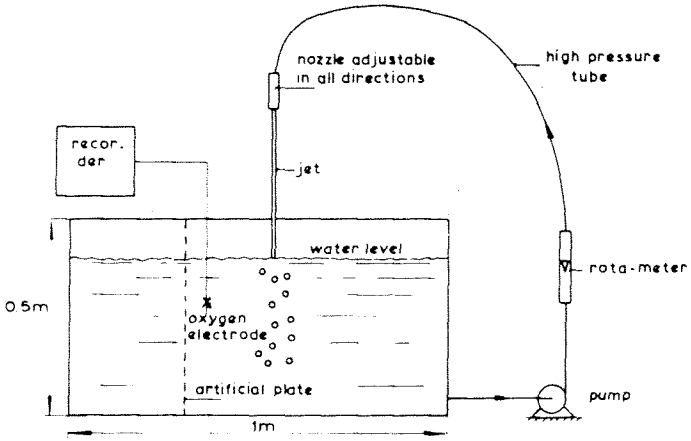

Fig. VII.8 Experimental arrangement

allow observation of the bubble swarm. The volume of the bath can be varied by regulation of the water level or by inserting an artificial side wall.
Water is circulated by a centrifugal pump through a rotameter. The jet itself is produced by interchangeable nozzles, all of which have a length to diameter ratio exceeding 50.
The water used to fill the apparatus was mains water which was partially deaerated in a vacuum vessel or by purging with nitrogen. This gives a more objective assessment of mass transfer in the oxygen-water system than the usual cobalt-catalysed sulphite oxidation. Not only does it avoid any possibility of the kinetic of the reaction confusing the mass transfer coefficient determination but it also eliminates any of the known dangers of ionic materials interfering with bubble dispersal and coalescence mechanisms.
Oxygen take-up in the pool liquid is registered on a recorder taking the output from an Y.S.I. electrode with temperature compensation. Although the experiments described in section VII.3.2 showed a good mixing performance, the mixing in the vessel was further improved by lowering the liquid level until the bubble swarm penetration depth approached the bottom of the tank. Measurements showed an uniform oxygen concentration throughout the pool liquid.

An oxygen balance over the vessel gives:

$$\frac{dc(t)}{dt} = \frac{K_l A}{V_t} (c^* - c(t)) - \left| c(t) - c(t-t_b) \right| \frac{V_b}{V_t t_b} \qquad \text{(VII.23)}$$

with V_t and V_b the volume of the liquid in the vessel and the circulation pipes respectively and t_b the residence time of water outside the vessel. Because t_b is of the same order of magnitude as the response time of electrode the second term on the right hand side of eq (VII.23) can be written as

$$- \frac{dc(t)}{dt} \quad \frac{V_b}{V_t}$$

Eq (VII.23) simplifies to:

$$\frac{dc}{dt} = \frac{K_l A}{V} (c^* - c) \qquad \text{(VII.24)}$$

in which V is the volume of the total liquid used. The last equation can be integrated and the result is the familiar:

$$\frac{c^* - c(t)}{c^* - c_o} = \exp \left(- \frac{K_l A}{V} t \right) \qquad \text{(VII.25)}$$

c_o is the oxygen concentration at $t = 0$.
By determining the rate of oxygen take-up the $K_l A$ value is easy to calculate.

A closer examination of the measuring procedure must be made because a few sources of error are present. Influences of the temperature dependence of the electrode were eliminated because during any given measurement the liquid had a constant temperature. A temperature compensation was provided to allow for different operating conditions.
Another possible error source is that the electrode consumes oxygen. This will produce too low a value of the oxygen level just alongside the membrane. A small stirrer close to the electrode prevents this error being significant.
The response time of the electrode and its influence upon a continuous changing oxygen content has to be considered. The principle of the electrode is based upon a determination of oxygen concentration by an electric current which is measured by the voltage over an fixed resistance. The voltage is now directly proportional to the oxygen concentration. In general an electrode can be considered as a first order

system. So:

$$U_v + \tau_{el} \frac{dU_v}{dt} = a\, c \qquad \text{(VII.26)}$$

in which U_V is the output voltage, τ_{el} the response time of the electrode and a a proportionality constant dependent upon the electrode. Substitution of eq (VII.25) gives:

$$U_v + \tau_{el} \frac{dU}{dt} = ac^* + a(c_o - c^*) \exp\left(\frac{-K_l A}{V} t\right) \qquad \text{(VII.27)}$$

The complete solution is:

$$U_v = a\Big|c^* + (c_o - c^*)\Big\{\frac{1}{1 - \tau_{el}\frac{K_l A}{V}} \exp\left(-\frac{K_l A}{V} t\right) +$$

$$\left(1 - \frac{1}{1 - \tau_{el}\frac{K_l A}{V}} \exp\left(\frac{-t}{\tau_{el}}\right)\right)\Big\}\Big| \qquad \text{(VII.28)}$$

Because $\tau_{el} << V/K_l A$ the last exponential product can be neglected relative to the other. Evaluation of what remains shows that even for very short times when the greatest deviation occurs the error is at most 5%. The response time of the electrode has therefore no significant influence upon the measurements.
The use of this measuring equipment enables us to measure with an accuracy of 10%.

VII.6.2 Theoretical considerations

Theoretical approximations of the total mass transfer cannot be made because both K_l and A are unknown. Even the relatively simple configuration of a bubble swarm causes difficulties as was shown in section VII.2. In the case of impinging jets the subject must therefore be treated on a purely experimental base. The relevant parameters involved are not a priory perceived. In order to solve this problem the following approach is used.
Inside the cone the following circumstances exist.

a. At the top of the cone, i.e. the plunging point, the air is in close contact with the surrounding liquid and at, or just below this point the bubbles are created. This fact should lead to rapid mass transfer;
b. in section VII.4.2 it was seen to be plausible that in-

side the entire volume of the cone relatively small bubbles exist. This also gives rise to high transfer rates when associated with the high intensity of turbulence.

These two facets together lead to the assumption that the water inside the cone is nearly saturated with oxygen. Now a similar model to that used for the mixing process inside the bath is proposed.

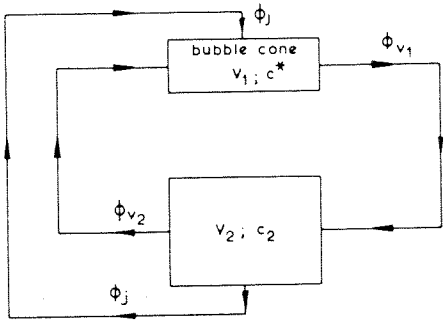

Fig.VII.9 Proposed model for the flowrates in the pool liquid

A sketch is given in fig. VII.9. V1 represents the volume of cone, V2 the rest of the pool liquid. The volume flowrates ϕ_{V1} and ϕ_{V2} are exchanging water streams. A mass balance over both V1 or V2 gives:

$$\phi_j + \phi_{V2} = \phi_{V1} \qquad \text{(VII.29)}$$

An oxygen balance for V2 leads to:

$$V_2 \frac{dc_2}{dt} = \phi_{V1} c^* - \phi_{V2} c_2 - \phi_j c_2 = \phi_{V1} (c^* - c_2) \qquad \text{(VII.30)}$$

in which c_2 is the oxygen concentration in volume 2. Because $V_1 << V_2$ (at most 3% in the experiments described) V_2 is equal to the total liquid volume. Comparison with eq (VII.24) results in the relation:

$$K_l A = \phi_{V1} \qquad \text{(VII.31)}$$

The meaning of the result is important since it implies that the mass transfer problem has been transformed into a flow rate problem which can more easily be studied.

All the processes which determine the flow rate ϕ_{V1} happen near the imaginary surface of the cone. Water is carried into this cone by momentum forces and dragged out of the cone with the escaping bubbles. Because(as shown in section VII.4.2) both bubble sizes in the surface of the cone and the structure of the flow are independent of the jet parameters, it is reasonable to assume that the exchange rate is

a function only of ϕ_A and the penetration depth H. Hence:

$$\phi_{VI} \sim H^{\alpha} \phi_A^{\beta} \qquad \text{(VII.32)}$$

in which α and β are constants to be determined experimentally. Combination of eq (VII.32), (VII.31) and (VII.22) leads to the relation in which all the relevant parameters are present for the water-air system:

$$K_l A \sim (V_j^{4/3} D_j)^{\alpha} \phi_A^{(\beta - 0.25\alpha)} \qquad \text{(VII.33)}$$

The values of the exponents α and β cannot be predicted in advance, however the physical requirements lead to the conditions:

$$\alpha > 0; \quad \beta > 0{,}25\ \alpha$$

VII.6.3 Mass tranfer from vertical jets

The amount of entrained air logically effects the total mass transfer according to eq (VII.33). Because eq (VII.22), which predicts the bubble penetration depth of vertical jets, is valid for all entrainment regions, this criterion is also applicable to eq (VII.33).
In order to find the values α and β (eq. (VII.33)) regression methods were applied in which ϕ_A is calculated with the aid of eq (VI.9) and the model for high velocities derived in section V.2.

All the data obtained with vertical jets issuing from long nozzles are given in Appendix III with the values α and β 1 and 0.55 respectively. Hence eq (VII.33) becomes:

$$K_l A \sim v_j^{4/3} D_j \phi_A^{0.30}$$

The table in Appendix III shows the variation in the proportionality factor. The average value is $6.2.10^{-3}$. The values of ϕ_A used in preparing this table are those obtained by the use of the correlating equations given in chapter VI.6. Fig. VII.10 compares the data with the experimental relation obtained for the entrainment of vertical water jets:

$$K_l A = 6.2.10^{-3} v_j^{1.33} D_j^{1} \phi_A^{0.30} \qquad \text{(VII.34)}$$

As can be seen the lines fall within the accuracy of all the data. Because eq (VII.34) does not contain explicitely

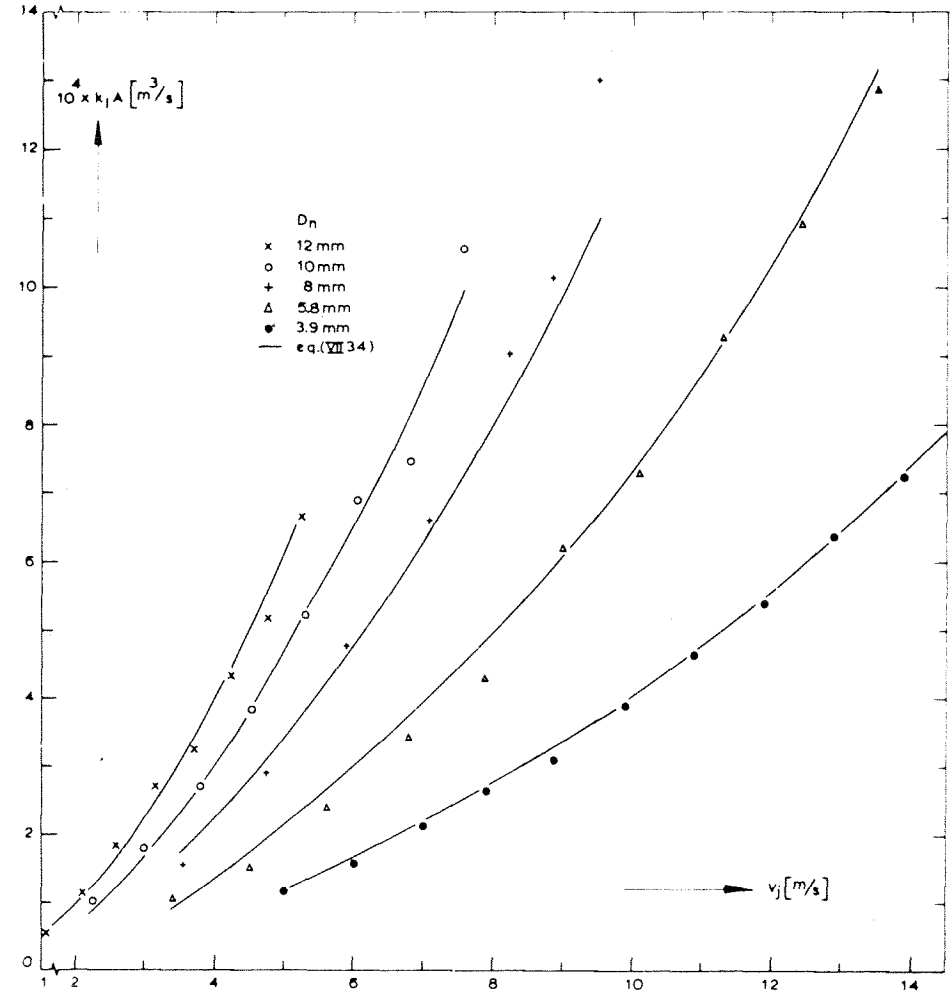

Fig. VII.10 Mass transfer as a function of jet velocity

a jet length dependence and the data of fig. VII.10 were obtained with a constant length, it is necessary to prove that any length dependency has been included in the δ_A term. Figure VII.11 shows that this is indeed so since the smooth curves relating jet length to mass transfer coefficient lie well within the spread of the experimental data.
When the nozzle length decreases the entrainment will be effected (chapter VI.6). For this reason mass transfer measurements were done with a fixed nozzle diameter, velocity

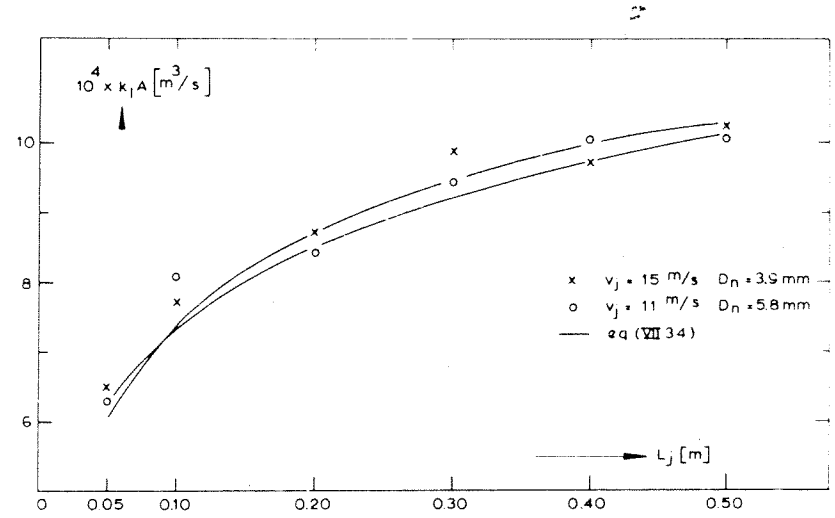

Fig. VII.11 Mass transfer dependence upon jet length

and length of the jet. Although no equations are available for the amount of entrained air, with the use of eq (VII.22) and (VII.34) an estimation of the mass transfer is possible. Combination of these two equations gives:

$$K_l A = \frac{0.22\ v^{2.93} D^{2.2}}{H^{1.2}} \qquad \text{(SI units)} \qquad \text{(VII.35)}$$

A single measurement of the penetration depth is therefore now sufficient to predict the mass transfer.

Fig. VII.12 shows the results. As can be seen the qualitative discussed expectations in chapter VI.6 agree with the data. $K_l A$ is not very sensitive to b_A because of the low value of the exponent in eq (VII.22), so the relative constancy of $K_l A$ for different nozzle is not surprising. The ease with which the penetration depth can embody the effects of all the other variables is both surprising and useful.

VII.6.4 The influence of the angle of impact.

The equations derived for vertical jets might in principle be applied to inclined jets because implicitely the influence of the angle is embodied in the amount of entrained air. With decreasing angle in general the entrainment in-

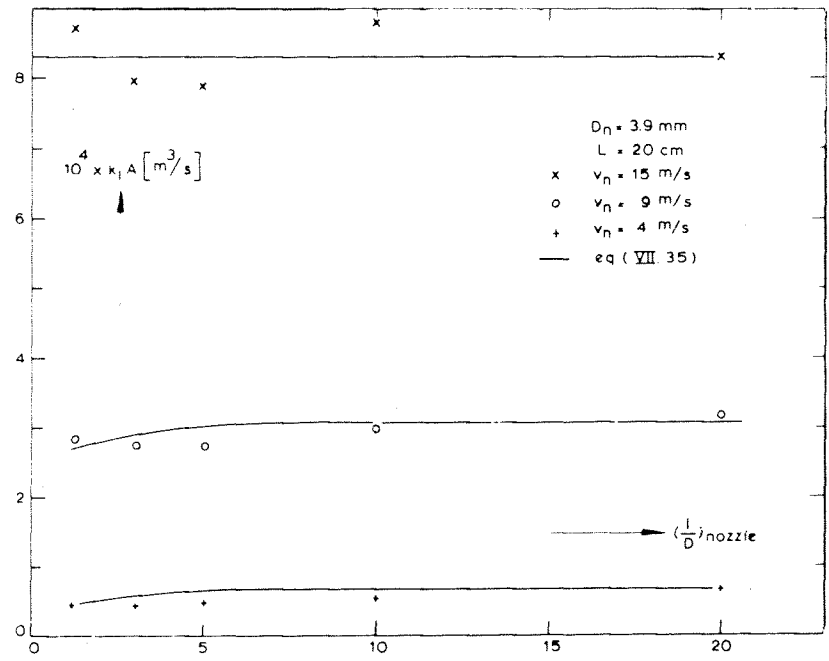

Fig. VII.12 Mass transfer dependence on nozzle geometry

creases. So more air is available to transport oxygen. Because the average residence time of the bubbles is of the same order of magnitude a better mass transfer might be expected.

Table VII.1 contains some data. Instead of an increase the mass transfer decreases slightly with diminishing angle. This result is however understandable if we consider the phenomena in more detail.
The bubbles inside the cone are somewhat larger in comparison with the vertical situation because of the decrease of turbulence. Besides, the cone itself is shorter. In contrast to vertical jets separate bubbles appear soon after the point of impact even in the cone. Because most oxygen transfer for vertical jets takes place inside the cone (small bubbles, high turbulence) and for inclined jets the conditions there are less severe, a slight decrease is possible. Even so, the total mass transfer does not change more than 30% with varying angle. For that reason a reasonable estimate for inclined jets can be given if the oxygen take-up of the vertical jet is known.

D_n	V_n	$K_1A(30^o)$	$K_1A(45^o)$	$K_1A(60^o)$	$K_1A(75^o)$	$K_1A(90^o)$
10 mm	7.5 m/s	$9.3.10^{-4}$	$9.4.10^{-4}$			$10.5.10^{-4}$
10	6.8	7.2	7.7	7.2		7.5
10	6.0	5.8			6.4	6.8
10	5.9			5.7		6.3
10	5.6		5.2			5.8
10	5.3	4.5			5.0	5.2
10	4.9			4.1		4.6
10	4.4	3.0	3.2		3.9	3.8
10	4.0			2.5		3.0
10	3.6	1.9			2.8	2.7
10	3.0	1.2			1.6	1.8
10	2.1	0.7	0.7	0.8	1.0	1.0

Table VII.1 The influence of the angle of impact. Jet length is 20 cm

VII.7 Comparison with other gas-liquid contactors

An absolute criterion which can test various contactors does not exist. For several problems practical and economical considerations can favour a certain equipment.Besides thermodynamical demands can be a determining factor.
Because some comparison must be made the oxygenation capacity is used. This criterion which is common in civil engineering for water treatment application, expresses the amount of oxygen take-up per kilowatt hour. The value of this ratio normally lies between 1 and 3 kgO_2/kwh (based on nett energy) for the conventional surface aerator systems. With this in mind the data of fig. VII.10 are recalculated on this basis and plotted in fig. VII.13.
The energy is based on the kinetic energy of the jet at the nozzle. The datapoints show that jet aeration is very efficient, especially for low jet velocities. The process even at higher velocities, is still attractive and the aeration capacity can be even further improved by the usage of longer jets. This interesting result emphasizes that this method of water aeration hitherto has received too little attention and that the practical use of jet aerators must be considered.

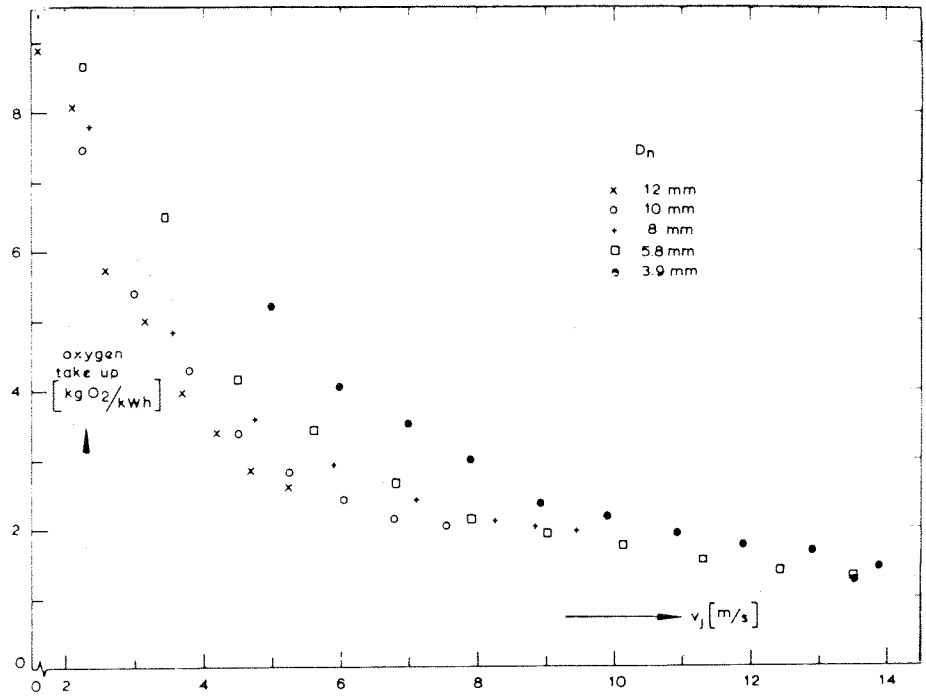

Fig. VII.13 Oxygen take-up plotted against jet velocity

All these experiments have been done on laboratory scale and therefore direct extrapolation to industrial applications is dangereous. From the data of the graph it appears that a slight diameter dependence exists and scale-up of the jet diameter does not appear favourable. It is probably better to use several jets instead of one because most mass transfer takes place inside the cone. An interacting effect between two neighbouring jets is therefore also not expected. Another point is that although the aeration efficiency at low jet velocities is incredibly high in practice these jets have limited value because of the small penetration depth. Especially this is disadvantageous when large amounts of pool liquid have to be aerated.
The specific contact aera inside the cone can scarcely be calculated. From the K_LA data the mass transfer coefficient is unknown but if one assumes a value of 10^{-4} m/s and only consider the volume of the bubble swarm the order of magnitude of the specific contact area is 10^3 m^2/m^3. In comparison with venturis, stirred vessels and bubble columns this is one order of magnitude higher. When the volume of the gas-liquid

equipment is equal to the bubble swarm volume a high mass transfer can be predicted. In many industrial processes the scale of mass transfer operations can be of the same order as the volume used in this work.

FINAL CONCLUSIONS

1. The study of entrainment by turbulent jets has enabled us to determine both qualitatively and quantitatively the parameters which affect the amount of induced air. The mechanism changes and so alters the parameter dependence. A single correlation describing the amount of entrained air over a wide jet velocity range is therefore unrealistic.
2. From the results it has been calculated that the initial disturbance level present in a turbulent jet must be at least three orders of magnitude greater than that present in a laminar jet. Evenso, in the absence of air friction, a modified version of the *Rayleigh* theory can be used to describe the disintegration process.
3. Jet surface deformations, which are the main cause of entrainment, are dependent on the developing flow in the nozzle and on air friction. With low velocity jets nozzle design can therefore influence the entrainment considerably. When air resistance is important however this has a dominant influence.
4. The impact of drops upon liquid surfaces shows that for low velocities the entrainment is energy controlled. This important fact has enabled us to establish the parameter groups which govern the process.
5. A model, based on the spreading of the jet and the induced air boundary layer, has been applied succesfully to the high velocity region.
6. A simple measurement of the bubble penetration depth for vertical jets, can be used to give direct information about the air entrainment rate and the potential mass transfer rate to the pool liquid.
7. The value of this system for gas-liquid contacting is proved. The very high efficiency achieved for oxygen take-up suggests its direct application as a system for waste water treatment with low operating and investments costs.
8. The phenomena are so complex that it is not surprising that there has been no satisfactory theoretical analysis. However by combining a theoretical background with observation it has been possible to build adequate models of the entrainment and mass transfer processes.
9. The present work has been limited in scale and in the fluids studied. In order to establish a more general understanding of the process and to formulate sound scale up rules further experimental work should be undertaken. Obvious factors to be considered include surface tension, fluid viscosity and the effects of dissolved or suspended materials.

Appendix I

THE INFLUENCE OF GRAVITY ON AN INCLINED JET

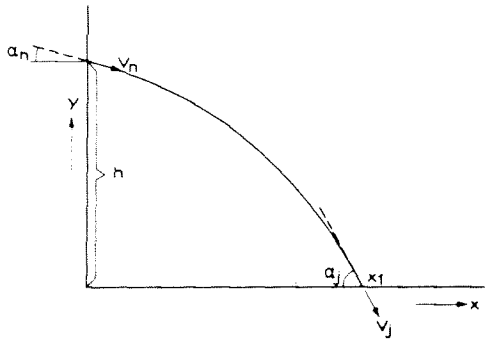

Fig.A1.1 The curved trajectory of a jet under the influence of gravity

The curve which describes the trajectory of the jet is a parabola. The influence of air friction is neglected because a change in the jet parameters at the impact point relative to those at the nozzle only occur with low jet velocities. The discharge velocity and angle of the jet are v_n and α_n (fig. A1.1). The parameters to be calculated at the impact point are v_j, d_j and the length of the jet. A simple calculation leads to the following equation for the parabola:

$$y = \frac{-g}{2v_n^2 \cos^2\alpha_n} x^2 - x \, tg\alpha_n + h \qquad (A1.1)$$

in which g is gravitational acceleration. With the aid of this equation α_j and v_j can be calculated:

$$tg\alpha_j = \frac{(v_n^2 \sin^2\alpha_n + 2gh)^{\frac{1}{2}}}{v_n \cos\alpha_n} \qquad (A1.2)$$

$$v_j = (v_n^2 + 2gh)^{\frac{1}{2}} \qquad (A1.3)$$

The length of the jet is:

$$L_j = \int_0^{x_1} (1 + (\frac{dy}{dx})^2)^{\frac{1}{2}} \qquad (A1.4)$$

Substitution of $z = |dy/dz|$ and making use of (A1.1) leads to:

$$L_j = \frac{v_n^2 \cos^2\alpha_n}{g} \int_{z_1}^{z_2} (1 + z^2)^{\frac{1}{2}} \, dz \qquad (A1.5)$$

z_1 and z_2 are tan α_n and tan α_j respectively. The complete solution of the integral in eq (A1.5) is now:

$$L_j = \frac{v_n^2 \cos^2 \alpha_n}{2g} \{ | z_2 (z_2^2 + 1)^{\frac{1}{2}} + {}^{10}\log (z_2 + (z_2^2 + 1)^{\frac{1}{2}}) | +$$

$$- | z_1 (z_1^2 + 1)^{\frac{1}{2}} + {}^{10}\log (z_1 + (z_1^2 + 1)^{\frac{1}{2}}) | \qquad \text{(A1.6)}$$

Appendix 2

ERROR SOURCES IN THE BUBBLE SIZE DETERMINATION

The bubble size determination is based upon length measurements of an elongated bubble drawn into a capillary tube. A constant pressure drop over the capillary assumes a constant velocity of the bubble if regular conditions exist. However a sample from a bubble swarm usually gives a fluctuating bubble velocity. For that reason two detectors were mounted on the capillary with a separation of 1 mm. A complete elimination of velocity fluctuation cannot be achieved however. In order to make an estimate of the wall shear stress fluctuations a calculation can be made for the case of fully developed flow which is only an approximation of the real situation . A typical velocity of the bubble inside the capillary is 3.2 m/s. The diameter of the capillary is 1 mm and, for the volume of bubbles present, slug flow conditions are satisfied (*Wallis (1969)*). The results presented by *Wallis* predict a thickness of the liquid layer that must exist between bubble and wall of 0.04 mm.

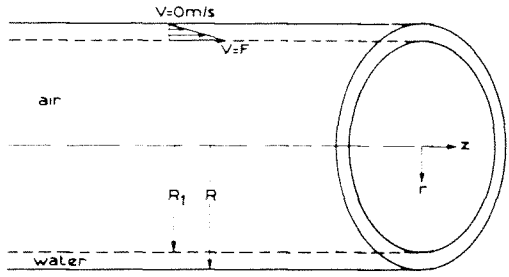

Fig. A2.1 Slug flow situation for completely air filled pipe

Assuming that a linear velocity gradient exists in the sublayer and the entire capillary is filled with air (fig. A.2.1). the *Navier-Stokes* equations for the layer reduce to:

$$\eta \left\{ \frac{1}{r} \frac{\partial}{\partial r} \left(r \frac{\partial v_z}{\partial r} \right) \right\} = 0 \qquad \text{(A2.1)}$$

with the boundary conditions:

$r = R_1$; v=fraction of bubble velocity because of slip and velocity profile consideration = F

$r = R$; $v = 0$ m/s

The wall shear stress is equal to:

$$\tau_{wall} = - \frac{F}{R \ln \frac{R_1}{R}} = 25\ F \qquad (A2.2)$$

The pressure drop used ($2.4.10^4$ N/m^2) gives an average velocity of the water when the capillary is completely filled with water, of approximately 3 m/s (entry lengths are neglected). The wall shear stress calculated with the familiar equations has a value of 45 N/m^2. Comparison between these evaluated shear stresses explains why velocity fluctuations must occur with constant pressure drop because F is a function of flow conditions and not equal to a constant value of 45/25 = 1.8 m/s. However the order of magnitude of F, which physically might be expected is in the same range so large velocity fluctuations are not expected. Measurements of the fluctuations (with an oscilloscope connected with the detection) show a maximal variation of 30%.

A calibration was thought to be necessary. A second capillary was used which produced a regular train of uniform bubbles. Because all the bubbles were drawn into the sampler, velocity fluctuations in the slug flow were hardly present. Fig. A2.2 shows a comparison between measured length and bubble volume. As can be seen, a straight line through the origin connects the data points implying the correctness of the measuring procedure for regular conditions.
A sucked sample of a bubble swarm must be representative for the swarm. This means that coalescence or break-up at the capillary mouth effects the measurement. Coalescence occur when there is no accelaration in the capillary mouth. In the mouth a contraction ratio of 6 over 1 cm gives the following conditions. Consider a rising bubble swarm with an absolute velocity of 0.5 m/s. When no resistance is present the residence time in the mouth is 2.10^{-2} sec. A bubble of 6 mm disappears in the capillary within $1.1.10^{-2}$ sec. Acceleration must exist, so further coalescence in the mouth is prevented.
Break-up or shearing of the bubbles is dependent upon the shape of the mouth. Streamlined surface and rounded edges can avoid destruction of the bubble but complete elimination is impossible.
For this reason a comparison has been made between the total bubble distribution measured with photographs and the above described procedure. A rising swarm produced by an inclined jet was used. Fig. A2.3 shows the result. 1000 bubbles were

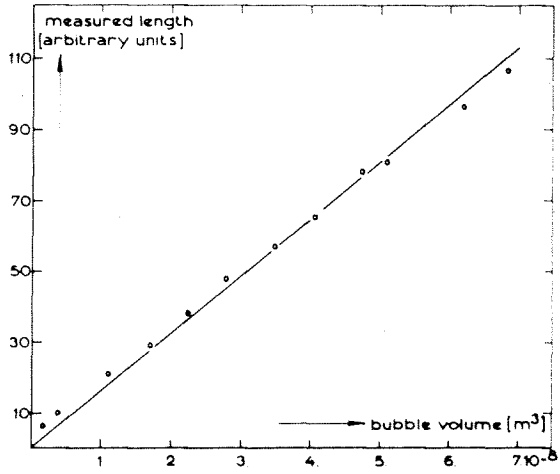

Fig.A2.2 Calibration curve in order to determine the bubble volume

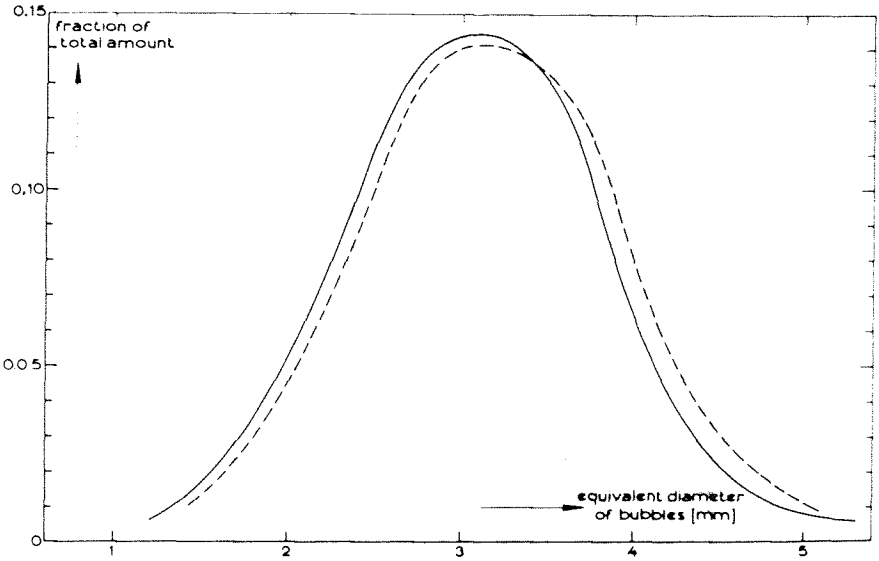

——— photographic method
- - - - - - - - measured with capillary

Fig. A2.3 Comparison between two methods of bubble size determination

measured from the photographs. The capillary measured 5000 bubbles within 5 minutes. A satisfactory comparison can be made however larger bubbles obtained from the photographs are rather difficult to determine because of their ill defined shape. Agreement between both curves, particularly when considering this last argument, confirms the correctness of the procedure used.
The measurements presented in section VII.4 were mostly done in the quiet part of the swarm and not in the bubble cone. For that reason the size distribution is rather accurate and directly the sauter mean diameters are presented.
The measuring procedure will possibly not be applicable for situations in which a strong flow field is present near the mouth. Coalescence and distortion probably occur in the capillary mouth and representative sampling is doubtful. The measurements done in the bubble cone are probably not trustworthy therefore.

Appendix 3

Data of vertical jets with a length of 0.2 m. Determination of the numerical factor in eq (VII.36).

D_n	v_j	K_1A	$\frac{K_1A}{\phi_A^{0.3} v_j^{4/3} D_j}$
12 mm	5.25 m/s	$6.6.10^{-4}$	$6.1.10^{-2}$
12	4.72	5.2	5.9
12	4.2	4.3	6.0
12	3.68	3.4	6.2
12	3.15	2.7	6.8
12	2.62	1.9	7.1
12	2.10	1.3	7.3
12	1.58	0.6	6.1
10	7.57	10.6	6.6
10	6.82	7.5	6.3
10	6.06	6.8	6.0
10	5.30	5.2	6.0
10	4.54	3.8	6.1
10	3.78	2.7	6.5
10	3.02	1.8	6.5
10	2.27	1.1	7.3
8	9.46	13.0	7.4
8	8.86	10.1	7.1
8	8.27	9.1	6.7
8	7.09	6.6	6.5
8	5.92	4.8	6.3
8	4.73	2.9	6.1
8	3.55	1.6	6.0
5.8	13.5	12.9	6.1

D_n	v_j	$K_1 A$	$\frac{K_1 A}{\phi_A^{0.3} v_j^{4/3} D_j}$
5.8 mm	12.4 m/s	$11.0.10^{-4}$	$6.1.10^{-2}$
5.8	11.3	9.3	6.2
5.8	10.1	7.3	6.2
5.8	9.0	6.2	6.0
5.8	7.9	4.3	5.6
5.8	6.8	3.4	5.6
5.8	5.6	2.4	5.7
5.8	4.5	1.5	5.6
5.8	3.4	1.1	6.7
3.9	14.9	8.0	6.0
3.9	13.9	7.3	6.2
3.9	12.9	6.4	6.2
3.9	11.9	5.4	6.1
3.9	10.9	4.6	6.1
3.9	9.9	3.9	6.1
3.9	8.9	3.1	5.8
3.9	7.9	2.7	6.1
3.9	7.0	2.2	6.2
3.9	6.0	1.6	6.0
3.9	5.0	1.2	6.2

REFERENCES

Abelson, H.I. (1971), J. Basic. Eng. 93D, 501

Allen, H.S. (1900), Phil. Mag. 50, 323

Anderson, J.L. and Quin, J.A. (1970), Chem. Eng. Sci. 25, 338

Badische Anilin und Soda Fabrik (1970), Patent 1923446, Deutches Patentamt

Barbin, A.R. and Jones, J.B. (1963), J. Basic.Eng. 85D, 29

Benedek, A. and Heideger, W.J. (1971), Biotechn.Bioeng. 13, 663

Birkhoff, G. and Isaacs, R. (1951), Naval Report 1490, White Oak.

Borisenko, A.I. (1953),J. Techn. Phys. USSR 23, 195

Bowlus, D.A. and Brighton, J.A. (1968), J. Basic. Eng. 90D, 431

Burchard, C.H. (1968), Ph. D. Thesis Stuttgart

Burgess, J.M., Molloy, N.A. and McCarthy, M.J. (1972), Chem. Eng. Sci. 27, 442

Calderbank, P.H. (1967), Mixing II page 2-111, V.W. Uhl, J.B. Gray, Academic Press, New York

Chandrasekhar, S. (1961), Hydrodynamic and Hydromagnetic Stability, Oxford

Ciborowski, J. and Bin, A. (1972), Inzynieria Chemiczna II, 4, 557

Crane, L., Birck, S. and McCormack, P.D. (1964), Brit. J.Appl. Phys. 15, 743

Crane, L., McCormack, P.D. and Birck, S. (1965), Brit.J.Appl. Phys. 16, 395

Davies, J.T., Kilmer, A.A. and Ratcliff, G.A. (1964), Chem. Eng. Sci. 19,583

De Frate, L. and Rush, F.(1969) Selected Papers Symposium - Part II 64th National Meeting A.I.Ch.E. New Orleans, Louisiana, March

Van Dierendonck, L.L. (1970), Ph.D. Thesis, Twente

Donnelly, R.J. and Glaberson, W. (1966), Proc. Roy. Soc. (London) Ser. A.S. 547

Engel, O.G. (1962), WADD-TR-60-475. Part II, Aeronautical Systems Div., Ohio

Engel, O.G. (1966), J. Appl. Phys. 37, 1798

Engel, O.G. (1967), J. Appl. Phys. 38, 3935

Fenn, R.W. and Middleman, S. (1969), A.I.Ch.E.J. 15, 379

Fillippov, G.V. (1958), Sov. Phys. 32, 1681

Frössling, N. (1938), Beitr. Geophys. 32, 170

Gal-OR, B. and Hoelscher, H.E. (1966), A.I.Ch.E.J. 12, 499

Goedde, E.F. and Yuen, M.C. (1970), J. Fluid Mechn. 40, 495

Grant, P.G. and Middleman, S. (1966), A.I.Ch.E.J. 12, 669

Griffith, R.M. (1960), Chem. Eng. Sci. 12, 198

Haenlein, A. (1931), Forschung 2. Heft 4, 139

Hanratty, T.J. (1956), A.I.Ch.E.J. 2, 359
Haüsler, E. (1961), Ph. D. Thesis, München
Henderson, J.B., McCarthy, M.J. and Molloy, N.A. (1970), Proc. Chemeca 1970, Australia,Sec. 2 pp 86-100, Butterworths
Higbie, L. (1935), Trans. A.I.Ch.E. 31, 365
Hinze, J.O. (1959),'Turbulence',McGraw-Hill,New York
Hobbs, P.V. and Kezweeny, A.J. (1967), Science 155, 1112
Hobbs, P.V. and Osheroff, T. (1967), Science 158, 1184
Houghton, G., McLean, A.M. and Ritchie, P.D. (1957), Chem. Eng. Sci. 7, 40
Hyman, D. (1962),'Advances in Chemical Engineering', Academic Press, New York
Ivanov, V.A. (1966), J.Appl.Mech. and Techn. Phys. 7, 30
Jagusch, L. and Schönherr, W. (1972), Chem. Techn. 24, 68
Jenkins, D.C. (1967), Ingenieur-Archiv 36,280
Von Kârmân, T. (1939), Trans. Am. Soc. Mech. Engrs. 61, 705
Kleinstein, G. (1971), A.I.A.A.J. 9, 1626
Koetsier, W.T. (1973), Ph. D. Thesis Twente
Van de Kroon, G.T.M. and Schram, A.H. (1969), H_2O (2) 22,528
Kurzweg, H. (1933),Annalen der Phys. 18, 193
Laufer, J. (1954), NACA Report 1174
Lin, T.J. and Donnelly, H.G. (1966), A.I.Ch.E.J. 12, 563
Lindgren, E.R. and Chao, J. (1969), Phys. of Fluids 12, 1364
Macklin, W.C. and Hobbs, P.V. (1969), Science, 166,107
Marucci, G. and Nicodema, L. (1967), Chem. Eng. Sci. 22,1257
May, A. (1951), Naval Report 2240
May, A. (1970), J. Hydronautics 4, 140
McCarthy, M.J., Kirchner, W.G., Molloy, N.A. and Henderson, J.B. (1969), Trans. Inst. Min. Metall. 78, C 239
Mertes, A.T. (1938), Patent 2,128,311 United States Patent Office
Miesse, C.C. (1955), Ind. Eng. Chem. 47, 1690
Nayfeh, A.H. (1970), Phys. of Fluids 13, 841
Nikuradse, J. (1932), Forschungsheft No. 356
Ohyama, Y., Takashima, Y. and Idemura, H. (1953), Kagaku Kenkyusho Hohoku 29, 344
Pennell, W.T., Sparrow, E.M. and Eckert, E.R.G. (1973), Int. J. Heat Mass Transf. 15, 1067
Phinney, R.E. (1972), A.I.Ch.E.J. 18, 432
Phinney, R.E. and Humphries, W. (1973), A.I.Ch.E.J. 19, 655
Prandl, L. (1910), Phys. Z. 11, 1072
Prasher, B.D. and Wills, G.B. (1973), Ind. Eng. Chem. Proc. Des. Develop 12, 351
Rayleigh, Lord (1945), 'Theory of sound', Dover
Reith, T. (1968), Ph. D. Thesis, Delft
Richardson, E.G. (1954), Appl. Sci. Res. A4, 374
Robertson, D.G.C., O'Shaughnessy, D.P. and Molloy, N.A. (1973), Chem. Eng. Sci. 28, 1635

Rotta, J. (1956), Ing. Arch. 24, 258
Rotte, J.W. (1969), Ph.D. Thesis, Delft
Rutland, D.F, and Jameson, G.J. (1970), Chem. Eng. Sci. 25, 1689
Sakiadis, B.C. (1961), A.I.Ch.E.J. 7, 467
Van de Sande, E. and Cordemans, W. (1973), Trans. Inst. Chem. Eng. 51, 247
Schlichting, H. (1965), 'Grenzschicht-Theorie' Karlsruhe
Shirley, R.W. (1950), M.Sc. Thesis, Univ. Iowa, Ames
Siemes, W. and Borchers, E. (1960), Chem. Eng. Sci. 12, 77
Siscoe, G.L. and Levin, Z. (1971), J. Geophys. Res. 76, 5112
Swiggett, G.E. (1969), Ph. D. Thesis no. 69-463 Univ. Microfilms Ann Arbor, Mich.
Szekely, J. (1969), Trans. Metall Soc. A.I.M.E. 245, 341
Todtenhaupt, E.K. (1971), Chem. Ing. Techn. 43, 536
Tsou, R.K., Sparrow, E.M. and Goldstein, R.J. (1967), Int. J. Heat Mass Transf. 10, 219
Voncken, R.M. (1966), Ph. D. Thesis, Delft
Wallis, G.B. (1969), 'One dimensional Two-phase Flow' McGraw Hill, Inc. U.S.A.
Wang, D.P. (1968), J. Fluid Mech. 34, 299
Weber, C. (1931), Z. Angew. Math. Mech. 11, 136
Worthington, A.M. (1882), Proc. Roy. Soc. (London), 34, 217
Worthington, A.M. (1908), 'A study of Splashes' New York (Longmans Green and Compagny)
Yoshida, F. and Miura, Y. (1963), Ind. Eng. Chem. Proc. Des. Develop 2, 263
Yuen, M.C. (1968), J. Fluid Mech. 33,151

SAMENVATTING

Een plonsende vloeistofstraal op een vloeistofoppervlak is in staat bellen te kreeëren. Dit welbekende verschijnsel heeft tot nu toe te weinig aandacht gekregen, ondanks dat het veelvuldig voorkomt in de natuur (watervallen enz.) en in tal van industriële processen. De invloed op produktkwaliteit en de toepassing op (afval)waterbehandeling is pas in de laatste jaren onderkent hetgeen resulteerde in een toenemende belangstelling voor dit onderwerp.
Dit proefschrift beperkt zich tot de studie van waterstralen die luchtbellen veroorzaken onder het wateroppervlak. De resultaten hiervan zijn algemeen toepasbaar op vloeistoffen met een vergelijkbare viskositeit.
Na een algemene inleiding wordt bij het gebruik van turbulente waterstralen het luchtmeename-mechanisme beschreven. Met toenemende straalsnelheid verandert het karakter van de bellenvorming van diskontinue naar kontinue luchtmeename. Dit feit verklaart waarom onderscheid moet worden gemaakt tussen stralen met een lage- ($v<5$ m/s) en een hoge snelheid ($v>\sqrt{10\,\sigma/\rho_A D}$). Bij lage snelheden wordt de hoeveelheid lucht bepaald door de aanwezigheid en de grootte van verstoringen op de straal en de wisselwerking daarvan met het wateroppervlak. Bij hoge snelheden daarentegen is het aantal luchtbellen afhankelijk van de dikte van de bijbehorende luchtgrenslaag en van de hoeveelheid lucht in de straal. Deze gegevens leidden tot de konklusie dat grondiger onderzoek naar zowel de oorzaak en het ontstaan van de straalverstoringen, als het gedrag van gedeformeerde vloeistofoppervlakken gewenst was.
Gedurende de afgelopen 100 jaar is veel wetenschappelijk onderzoek verricht naar de faktoren, die de instabiliteit van vloeistofstralen veroorzaken. De invloed van straalpijpgeometrie, turbulentie en luchtwrijving is echter totaal onbekend. Straalpijpgeometrie en zijn invloed op het ontstaan van turbulentie bepalen direkt de grootte van de oppervlakte verstoringen. Hiervoor zijn kriteria vastgesteld.
Luchtwrijving veroorzaakt een breder worden van de straal en een relatie wordt gegeven die de toename van de straaldiameter korreleert met de gebruikte variabelen.
Een heel hoofdstuk is gewijd aan de kraterdiepte in wateroppervlakken veroorzaakt na de inslag van druppels. Een theoretisch model beschrijft deze diepte als funktie van de tijd na de inslag van één enkele druppel. Indien meerdere druppels na elkaar het vloeistofoppervlak treffen is dit model niet meer toepasbaar. Deze situatie is meer kwalitatief beschreven.
De resultaten van de luchtmeename metingen, tezamen met de meest belangrijke data van andere auteurs, zijn vergeleken

met de theoretische verwachtingen. Een aantal relaties zijn vastgesteld waarmee deze luchthoeveelheid berekend kan worden. Stofoverdrachtsaspekten worden eveneens beschouwd. Menging in het waterbad zelf en de grootte van de bellen in de bellenzwerm zijn hierbij belangrijke faktoren. Een onderzoek gaf aanwijzingen omtrent de belangrijkste straalparameters die een rol spelen bij het zuurstofoverdrachtsproces. Het geheel resulteerde in hanteerbare vergelijkingen die de zuurstotopname in een waterstraalsysteem bepalen.
De indringdiepte van de bellenzwerm is ook bestudeert. Hiermee werd een opmerkelijk resultaat bereikt. Een simpele meting van deze diepte verschaft informatie over de hoeveelheid meegesleurde lucht en de zuurstofopnamekapaciteit wordt bekend.
De voornaamste konklusie die uit het onderzoek getrokken kan worden is, dat waterstraalbeluchting,onder zekere omstandigheden, erg efficiënt is en de toepassing op (afval)waterbehandeling meer gestimuleerd moet worden.